The Abdus Salam
International Centre for Theoretical Physics

United Nations
Educational, Scientific and
Cultural Organization

IAEA
International Atomic Energy Agency

2292-20

School and Conference on Analytical and Computational Astrophysics

14 - 25 November, 2011

Active Galactic Nuclei – Observations and Interpretations

Silvano Massaglia
Universita' degli Studi di Torino
Italy

Astrophysical Outflows: Observations, Theories and Simulations

Silvano Massaglia
Università di Torino

ICTP 2011

Overview

- AGNs: Observations and interpretations
  (Constraining the physical parameters)

- MHD simulations of AGN jets:
  propagation and morphologies

- MHD simulations of AGN jets:
  Jet instabilities

- MHD acceleration of jets

AGNs: Observations and interpretations
(Constraining the physical parameters)

Normal Galaxies

Normal Galaxies

Normal Galaxies

- Stars and interstellar gas contribute to the radiation emission, predominantly in the optical band.
- The spectrum shows absorption lines by stars and emission by HII regions.

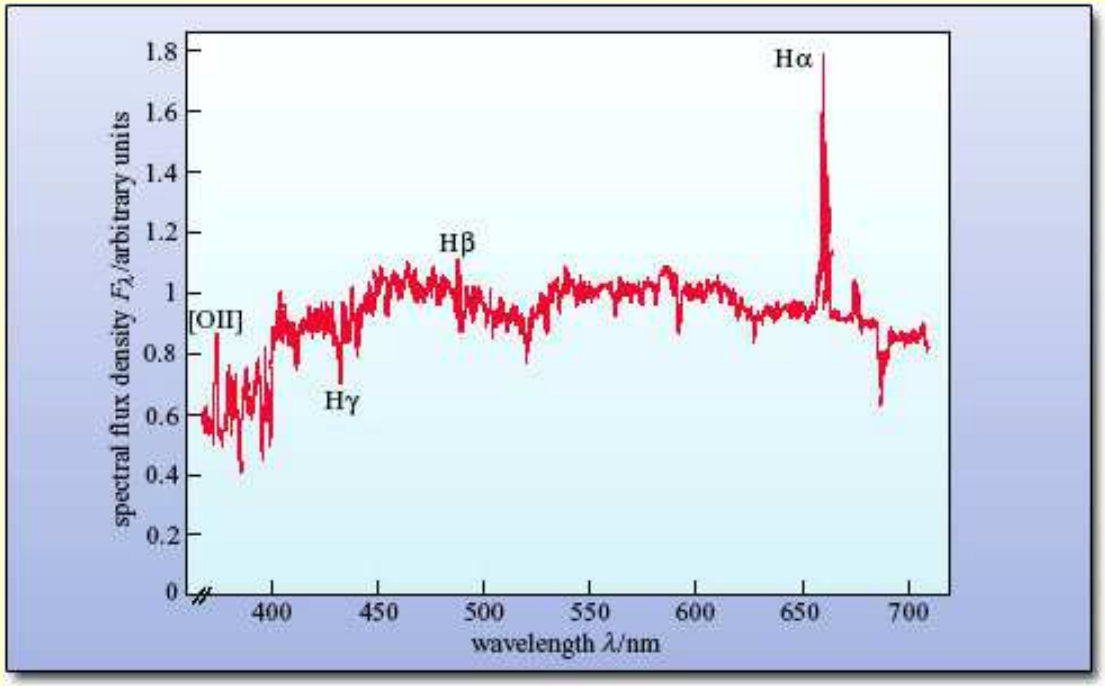

NGC 4750
(Kennicut 1992)

Normal Galaxies

- Typically, ~10^{11} stars of a galaxy like the Milky Way emit a luminosity of ~10^{44} ergs s^{-1}

- About 99% of the galaxies of the Local Universe are normal galaxies

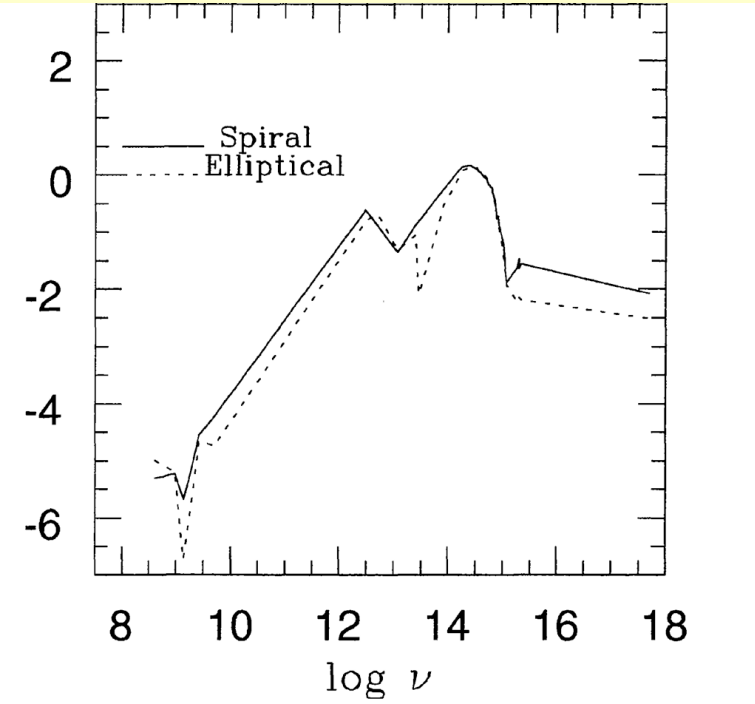

Spectral Energy Distribution (SED) of a normal galaxies

Active Galaxies

About 1% of the galaxies of the Local Universe show:

- Strong and broad emission lines, consistent with velocity dispersion of several thousand kilometers per second for the emitting gas

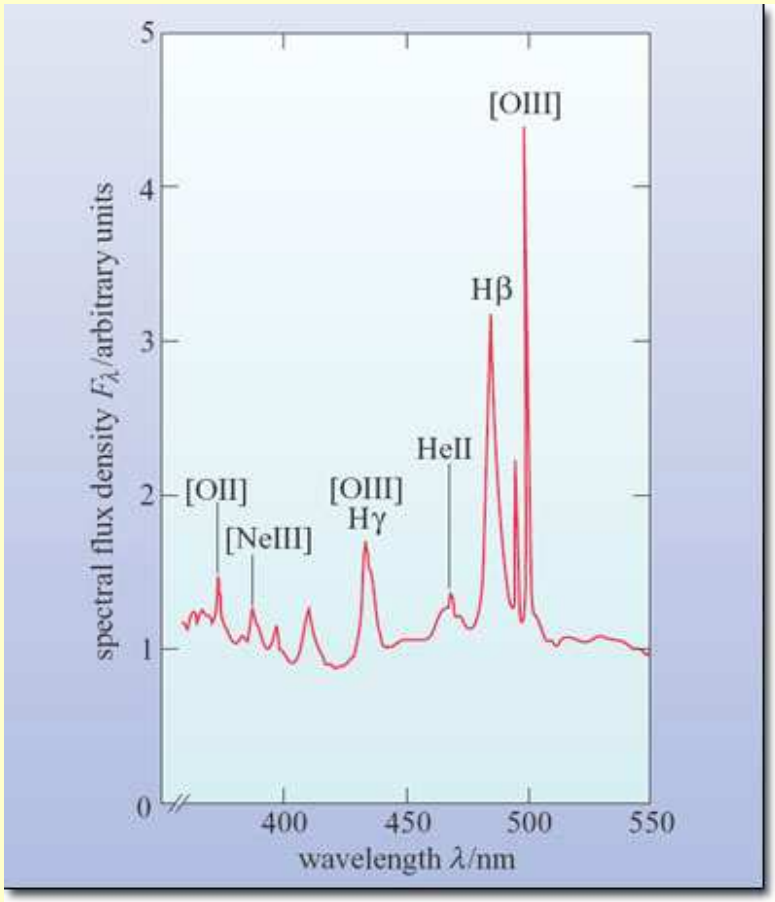

Active Galaxies

- **Non-thermal emission extending from the radio to the X-rays and gamma bands**

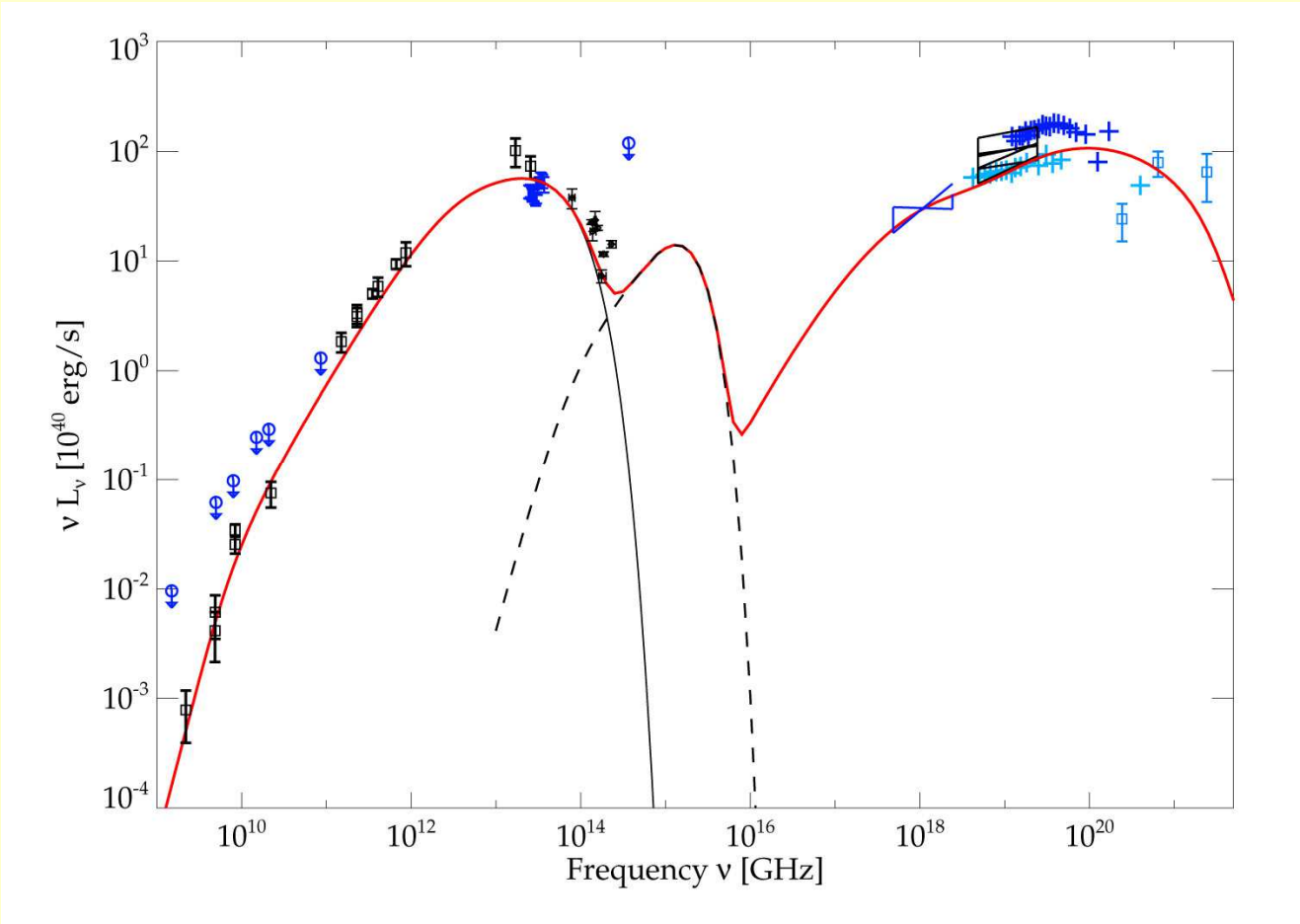

SED of Cen A
(Prieto et al. 2007)

Normal vs Active Galaxies

Spectral Energy Distributions

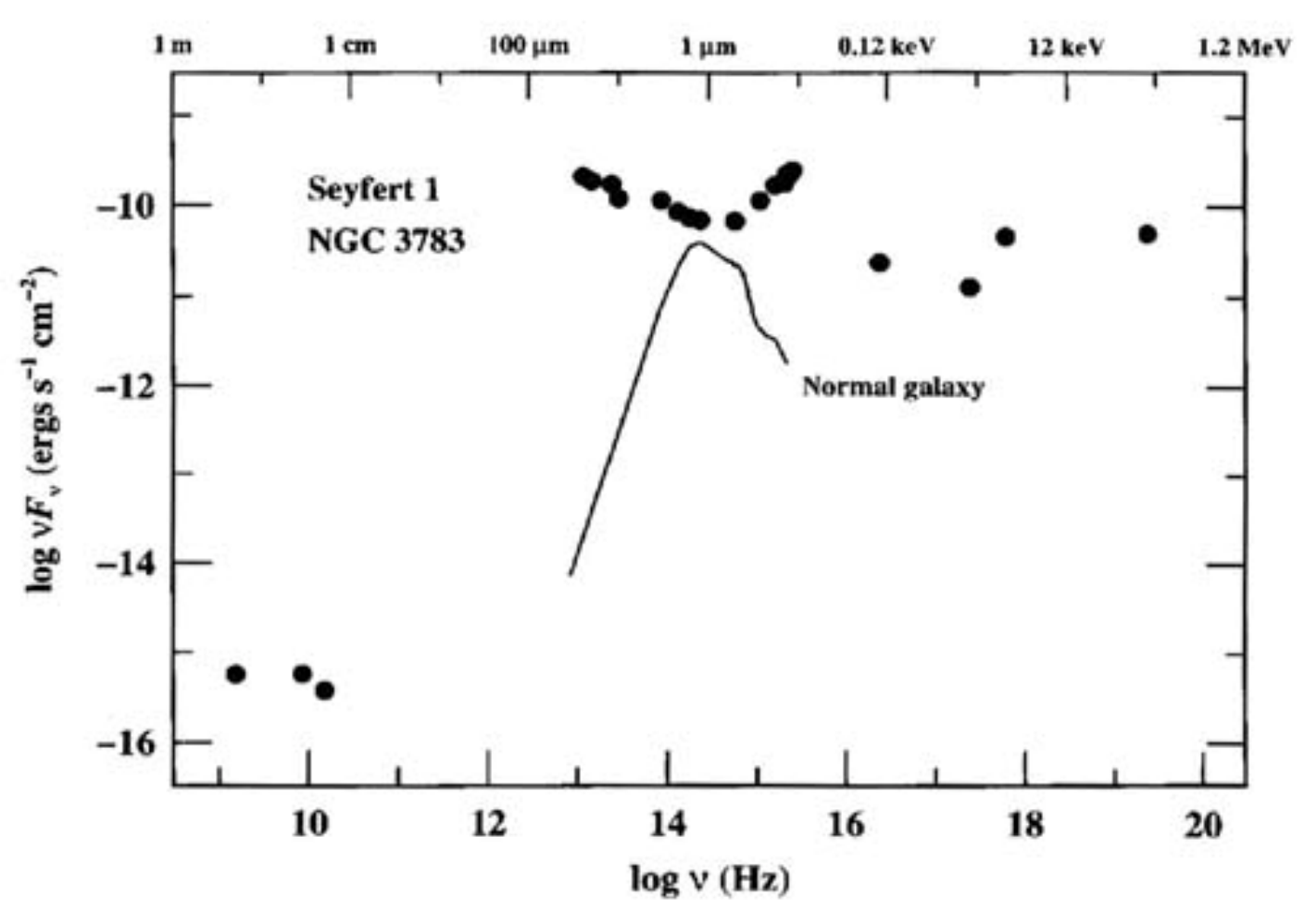

Active Galaxies

The dominant contribution to the total luminosity is not from stars but from an Active Nucleus

R ~ 30 kpc

R ~ 2 kpc

R ~ 10^{-5} kpc

M87

AGN Zoology

~90% Radio quiet AGNs: No jets

- Seyfert 1 galaxies (Sey 1) (BLR, ~ 10^4 km/s)
- Seyfert 2 galaxies (Sey 2) (NLR, $\leq 10^3$ km/s)
- Radio Quiet Quasars (QSOs)

~10% Radio loud AGNs: Jets

- Radio galaxies
- Radio Quasars
- BL Lac Objects
- Optically Violent Variables (OVV's)

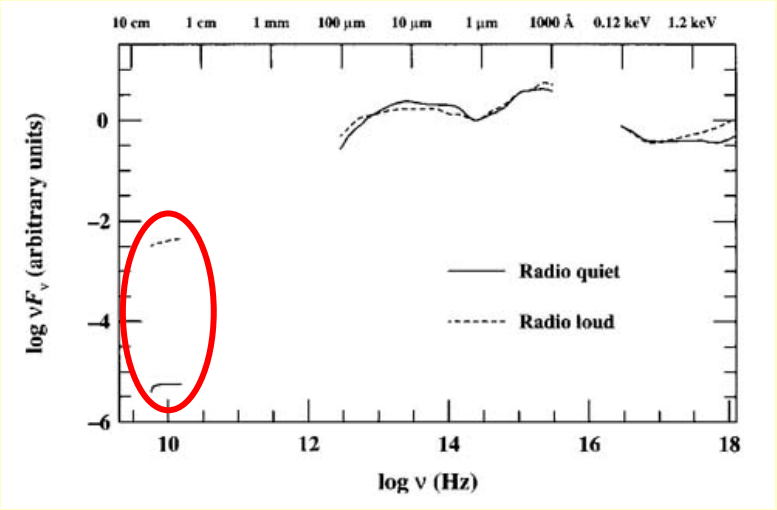

Radio loudness parameter: $R=L_{5GHz}/L_{B(nuclear)}>10$

The AGN Unified Model

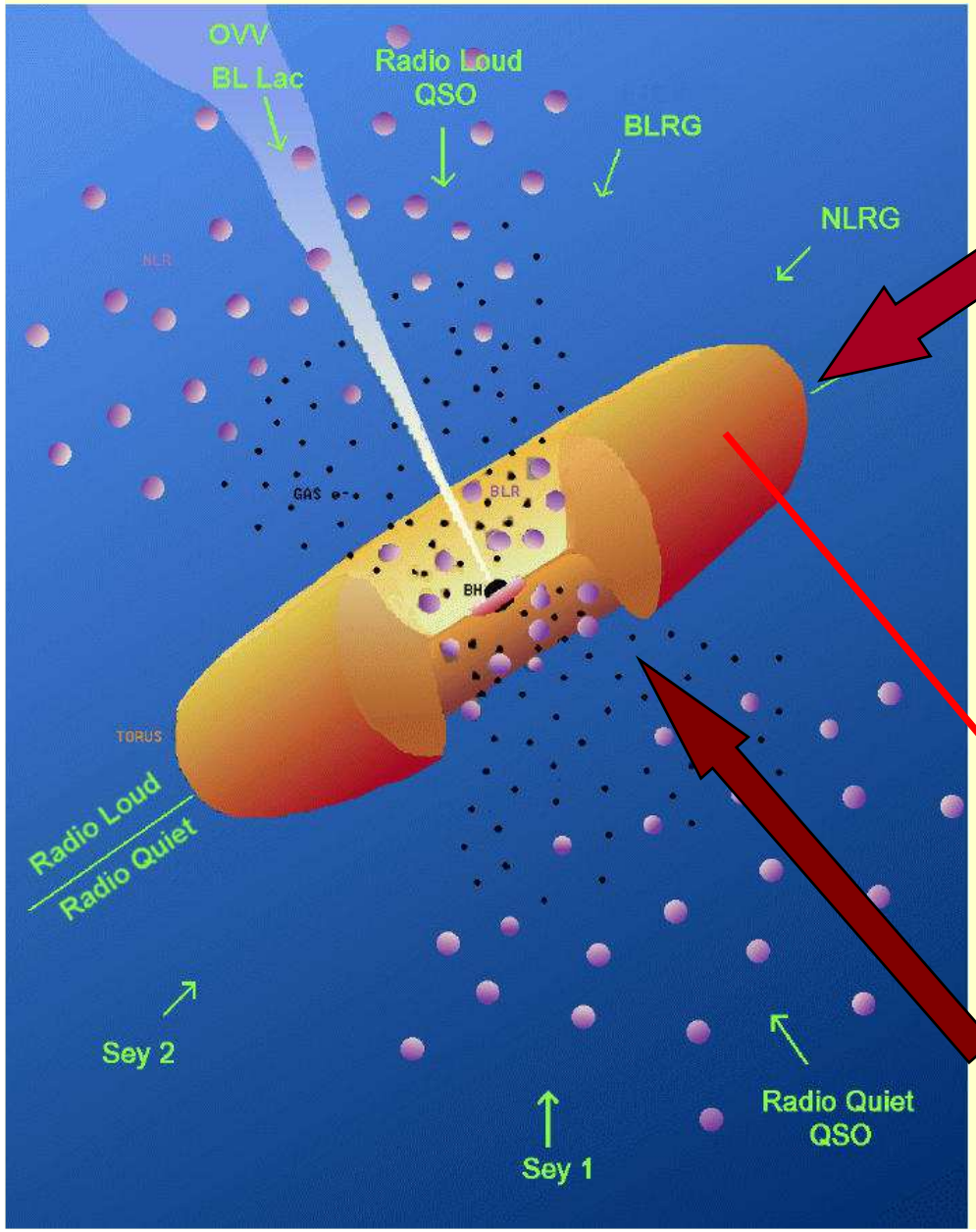

narrow lines
NLR, L~0.1kpc

Accretion onto a SMBH through an accretion disk, with possible jet ejection seen at differen angles

(Urry & Padovani, 1995)

Obscuring torus

broad lines

Astrophysical Jets

Collimated outflows in form of jets are ubiquitous in the Universe:

1. Jets from AGNs in Radio Galaxies;
2. binary systems;
3. from Young Stellar Objects;
4. in SS433;
5. from the Crab Pulsar;
6. in the sources of Gamma Ray Bursts

About Radio Galaxies and Jets

Synchrotron Radio to X-rays

Radio emission
Synchrotron:
$F(\nu) \propto \nu^{-\alpha}$
$\alpha \sim 0.5$

Electron power law distribution
$n(E) \propto E^{-p}$
$p=2\alpha+1$

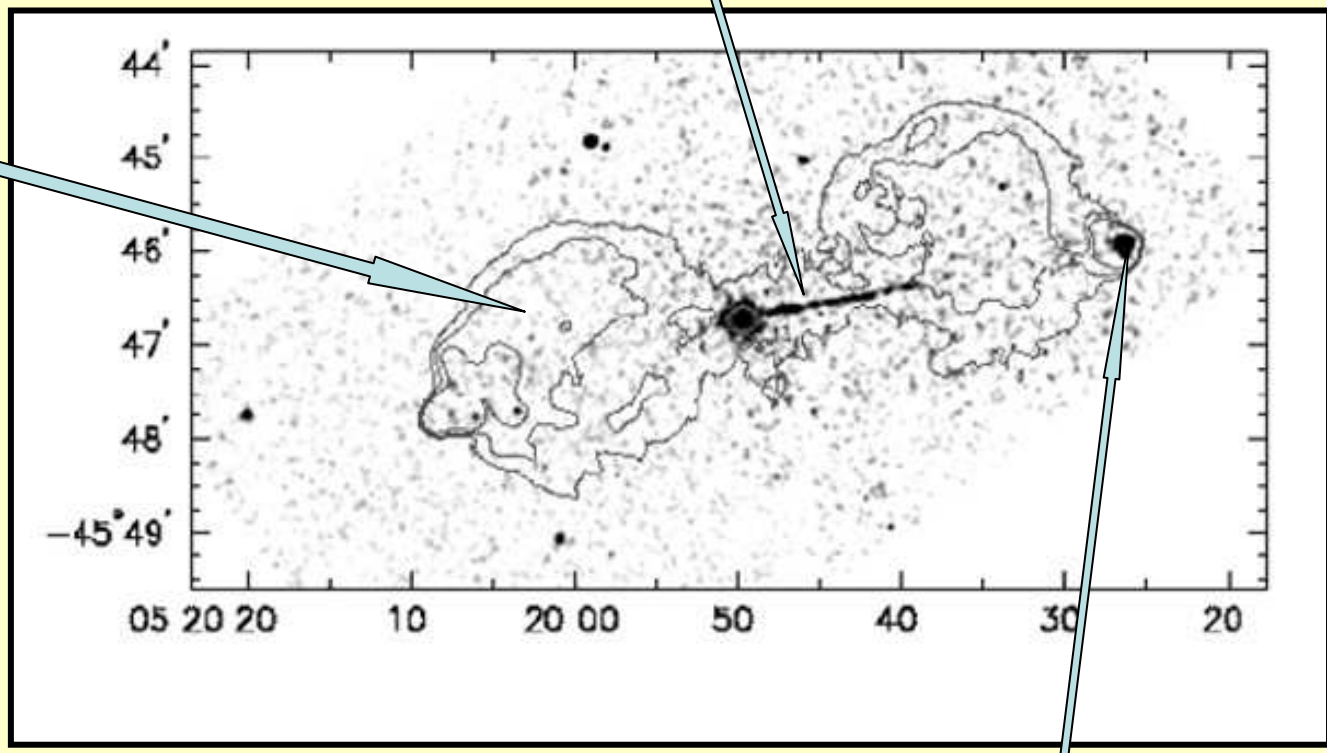

Pictor A (z=0.035)
Nucleus to hot-spot ~ 270 kpc
jet ~ 120 kpc

Radio: synchrotron X-rays: synchrotron+SSC

Radio Galaxies: Main facts

What we know:

- Radio luminosity: 10^{41}-10^{44} ergs s^{-1}
- Size: a few kpc – some Mpc
- Morphologies: brightness distributions
- Polarization degree: about 1%-30%

What we derive from hypotheses and models:

- Life timescale: 10^{7}-10^{8} ys
- Magnetic field: 10 – 10^{3} μG
- Kinetic power: 10^{44}-10^{47} ergs s^{-1}
- Jet Mach number: M>1
- Jet velocity: possibly relativistic
- Jet density: 10^{-5}-10^{-4} cm^{-3}

Radio Galaxies: Main facts

Why these uncertainties in constraining the basic parameters?:

Absence of any line in the radiation spectrum!

Parameters are constrained by indirect means:

- **Magnetic field: by minimum energy condition (equipartition)**
- **Kinetic power: energy requirements**
- **Jet Mach number: indication of shocks**
- **Jet velocity: jet one-sidedness**
- **Jet density: jet numerical modelling**

Observed morphologies:
The Fanaroff-Riley classification

FR I or jet dominated

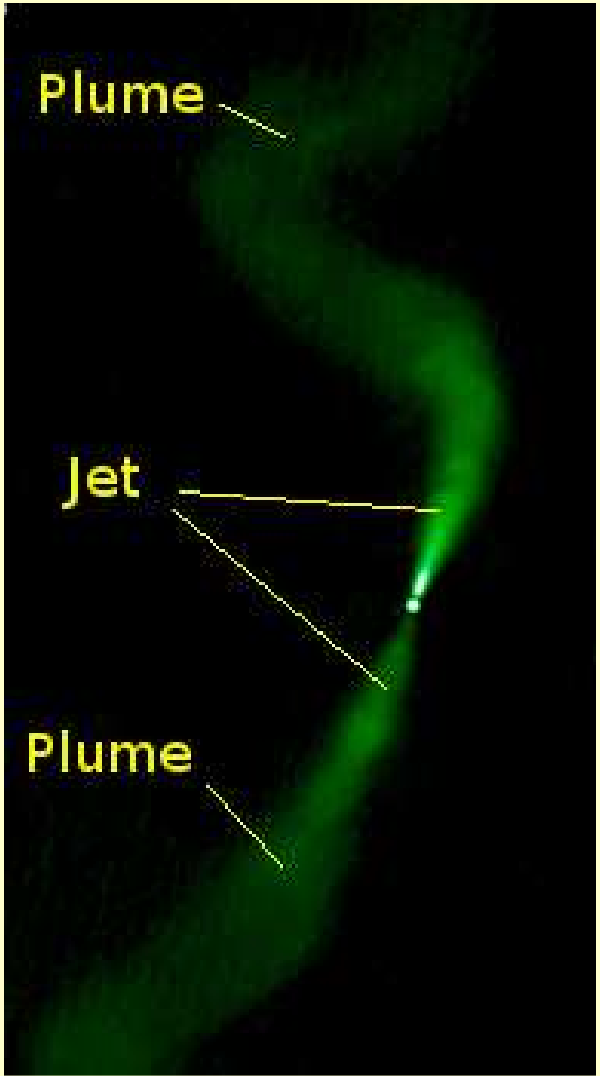

3C 31
VLA

FR II or lobe dominated (classical doubles)

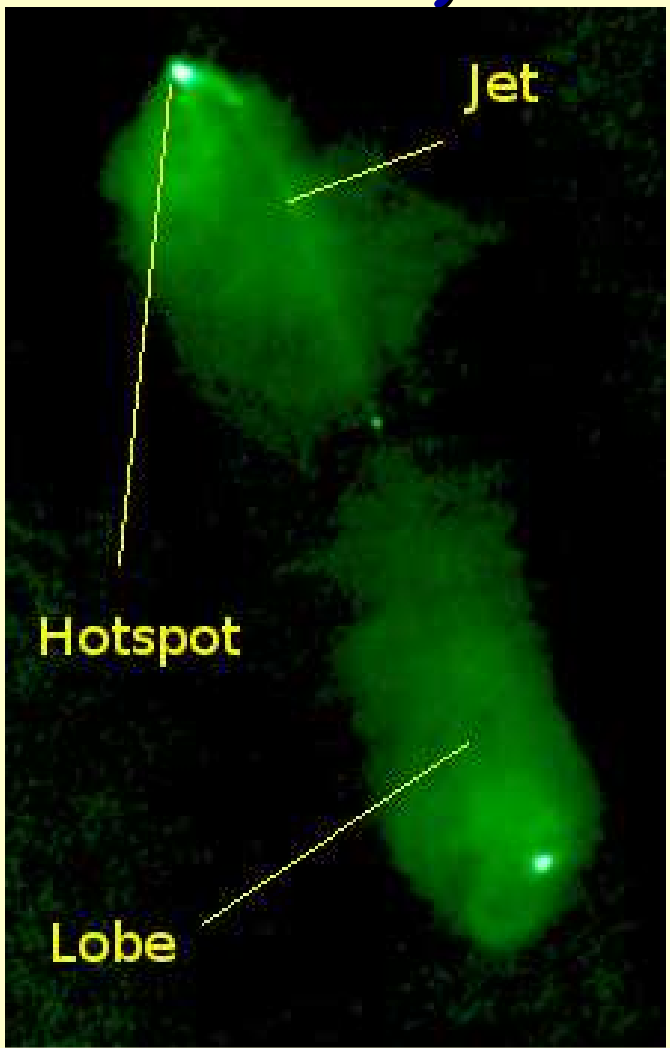

3C 98
VLA

FR II only have Hot-spots!

- **FR I**: Jet dominated emission, two-sided jets, found in rich clusters, weak-lined galaxies, less powerful
- **FR II**: Lobe dominated emission, one-sided jets, isolated or in poor groups, strong emission lines galaxies, more powerful

Radio vs optical luminosities:

$$L_R \propto L_{opt}^{1.7}$$

(Owen & Ledlow 1994)
Environment plays a role?

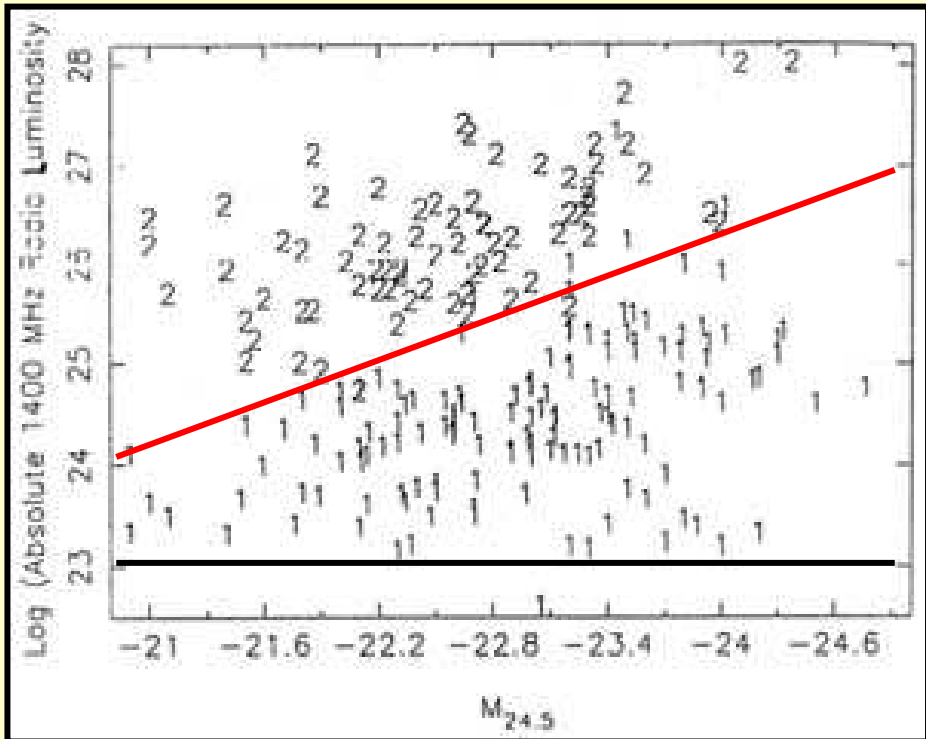

Jet composition

Different possibilities:

1. ordinary proton-electron plasma;
2. e^--e^+ dominated plasma;
3. Poynting flux jets.

Jet composition

The work done by the jets against the ambient to inflate lobes and cocoon favors the electron/proton jets interpretation (Shankar et al. 2008):

- e^--e^+ jets suffer strong inverse Compton losses off the CMB (e.g. Harris & Krawczynski 2006)
- Jets can be Poynting-dominated up to ~1000 r_g but become kinetically-dominated further away (Sikora et al. 2005, Giannios and Spruit 2008: kink instability?

How can we model jets?

These are some of the main questions concerning radio galaxies and jets. To understand the physics of these systems one must start from basic principles, i.e. can jets be considered as fluids in motion?

The particle-particle collision m.f.p. is much larger than the size of the system:

does a fluid description apply?

On the Validity of the (M)HD Equations

(Poedts talks)

Consider a system made of identical particles of mass m and assume that we can write a statistical distribution function (i.e. $N >> \sqrt{N}$) in the 6th-dimensional space (x,y,z,v_x,v_y,v_z) can be defined for these particles:

$$f[\mathbf{r(t)},\mathbf{v(t)},t]$$

and the number of particles in the hyper-volume $d^3r\ d^3v$ at the time t is:

$$f(\mathbf{r},\mathbf{v},t)\ d^3r\ d^3v$$

If we neglect collisions, i.e. sudden changes in the particle velocity coordinates, and if velocity and acceleration of each particle are finite the distribution function obeys

an equation of continuity (*Liouville's theorem*):

$$\frac{\partial f}{\partial t} + \nabla_{\mathbf{r},\mathbf{v}} \cdot [f \cdot (\dot{\mathbf{r}}, \dot{\mathbf{v}})] = 0$$

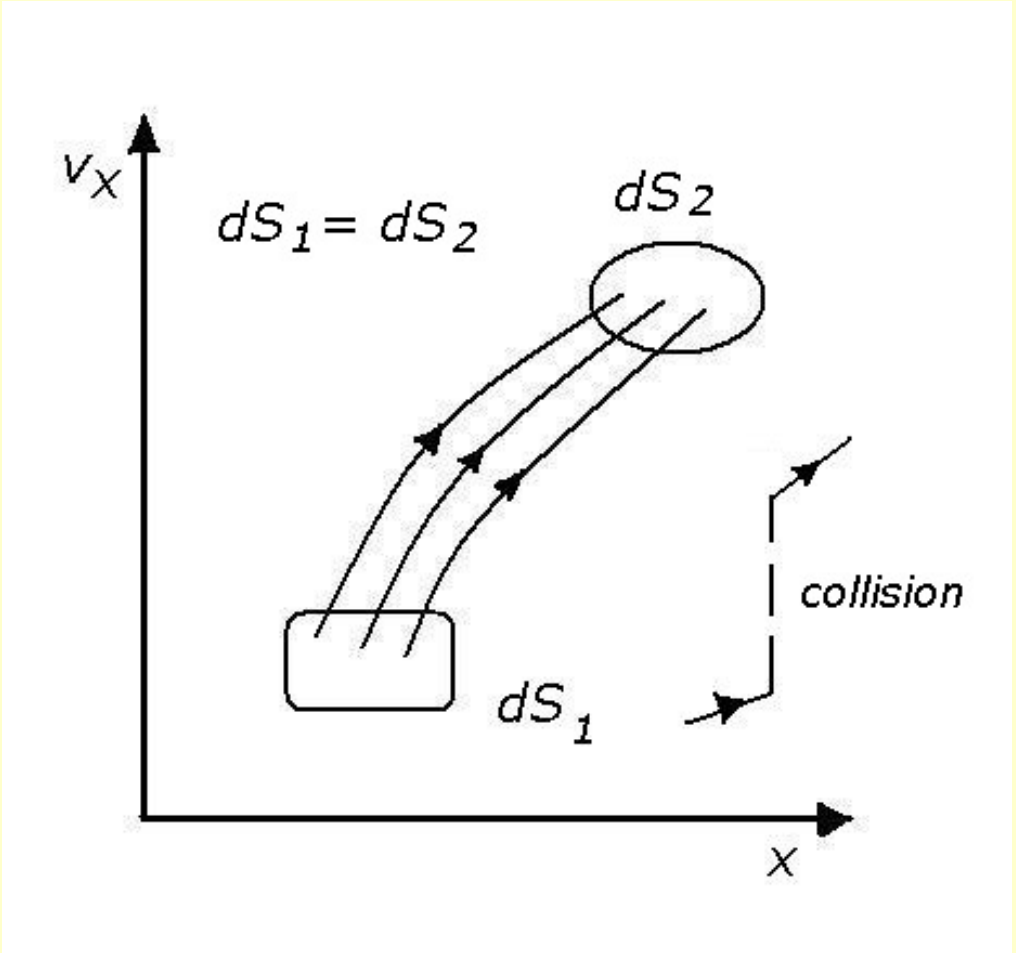

(collisionless) ***BOLTZMANN EQUATION*** :

$$\frac{\partial f}{\partial t} + \frac{\partial f}{\partial x_i}\dot{x}_i + \frac{\partial f}{\partial v_i}\dot{v}_i = 0$$

or:

$$\boxed{\frac{\partial f}{\partial t} + \frac{\partial f}{\partial x_i}\dot{x}_i + \frac{F_i}{m}\frac{\partial f}{\partial v_i} = 0}$$

with:

$$f = f(\mathbf{r}(t), \mathbf{v}(t), t)$$

$$\frac{df}{dt} = 0$$

Points in the hyper-space $(\boldsymbol{r}, \boldsymbol{v})$ behave as an incompressible fluid.

No hypotheses made on the distribution function.

The 1st-order moment of the Boltzmann Equation is the equation of motion:

$$mn\left(\frac{\partial u_k}{\partial t}+u_i\frac{\partial u_k}{\partial x_i}\right)=-\frac{\partial p_{ik}}{\partial x_i}+n\langle F_k\rangle$$

$$mn\frac{du_k}{dt}=-\frac{\partial p_{ik}}{\partial x_i}+n\langle F_k\rangle$$

The pressure p_{ik} is a tensor for an arbitrary distribution function of the velocities.

Collisions: yes or no

Fluid equations are a correct description of the system even without the intervention of collisions, for a general distribution function in the hyperspace;
BUT the pressure is a *tensor*.

Typically, we do not know the local physical parameters enough for beeing able to write down the pressure tensor.

For adopting the classical scalar form of the pressure for a perfect gas we need collisions ⟶ M-B distribution ⟶ *Eulerian fluid*
Hypothesis: particle distribution becomes a thermal Maxwell-Boltzmann distribution by collisions with magnetic inhomogeneities (Alfvén waves)

When is bremsstrahlung important?

Bremsstrahlung loss rate increases with temperature
Atomic processes become less important as the gas becomes fully ionized

} high T

Example: gas in the Coma cluster of galaxies

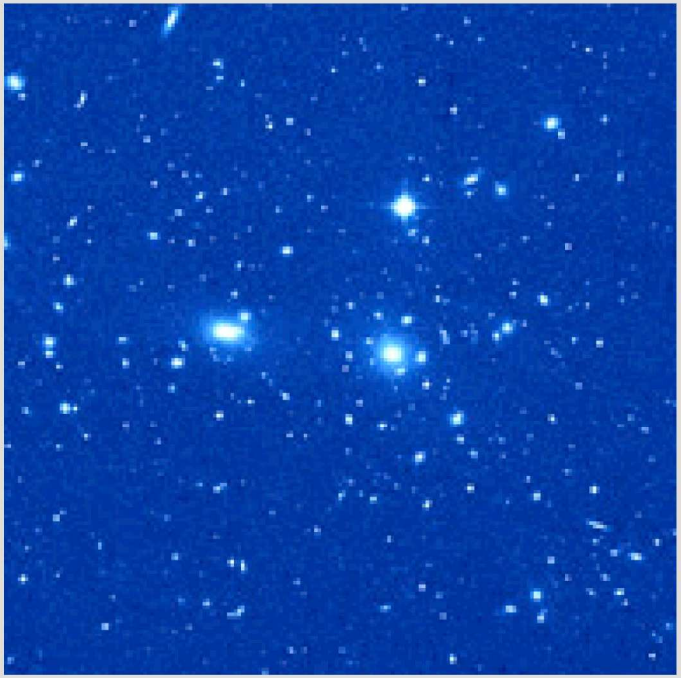

Optical

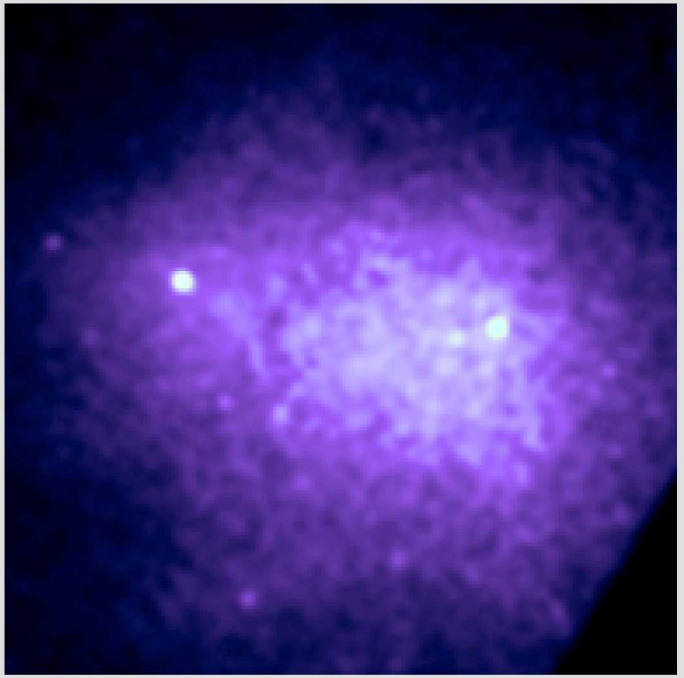

X-ray

X-ray spectrum of Coma

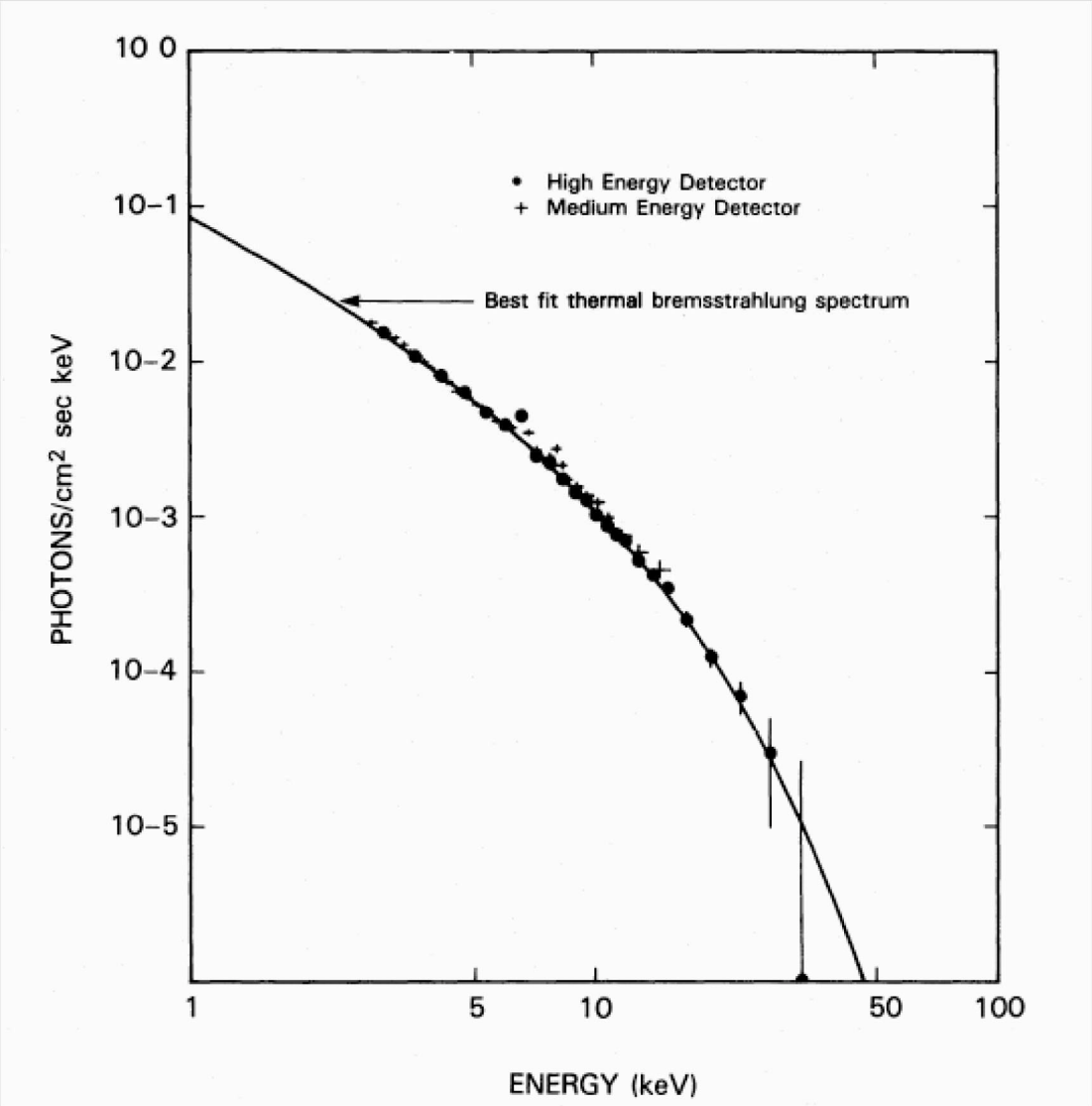

Shape of spectrum gives the temperature.

Intensity (for a known distance) gives the density of the gas.

Galaxy cluster: find T = 10 - 100 million K.

Radio jets in the galaxy cluster Abell 400

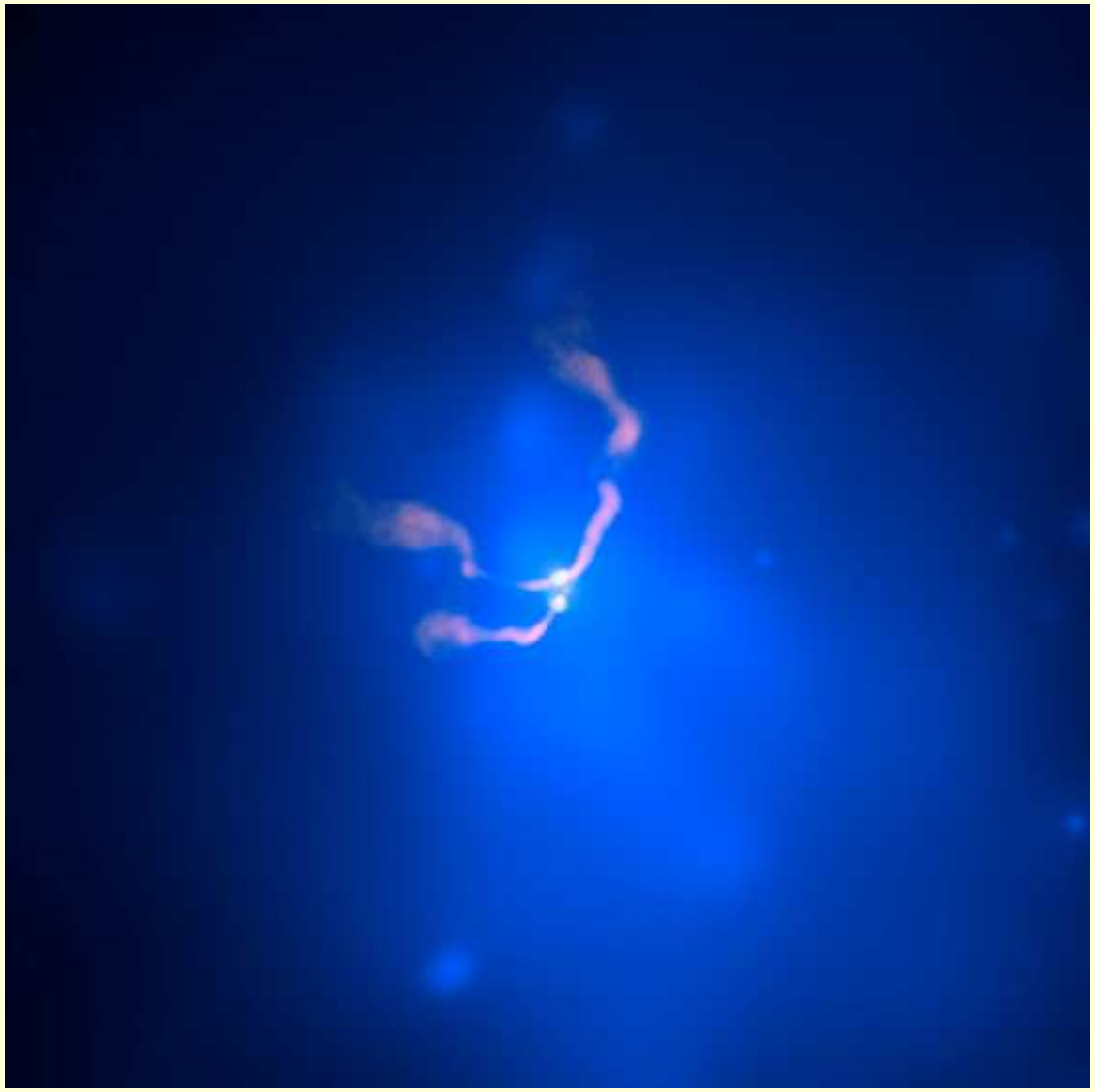

Ideal MHD Equations

(Mignone, Poedts lectures)

$$\frac{\partial \rho}{\partial t} + \nabla \cdot (\rho \vec{u}) = 0$$ **Continuity**

$$\rho \frac{d\vec{u}}{dt} = -\nabla p + \frac{1}{4\pi}(\nabla \times \vec{B}) \times \vec{B}$$ **Motion**

$$\frac{dp}{dt} - \Gamma \frac{p}{\rho} \frac{d\rho}{dt} = 0$$ **Energy**

$$\frac{\partial \vec{B}}{\partial t} = \nabla \times (\vec{u} \times \vec{B})$$ **Induction**

$$\nabla \cdot \vec{B} = 0$$

Solution of (M)HD Equations

(M)HD equations can be solved by analytical means in a limited set of cases (e.g. linear stability analyses, Parker's solar wind, etc.)

In general, one has to employ numerical methods for the solution.

Numerical modelling: basic physical parameters

Theoretical modelling and numerical simulations of AGN jets on large scale require a *minimum* set of parameters:

1. Lorentz factor (γ)
2. Jet Mach number (M)
3. Jet-ambient density ratio (η)

How to constrain these parameters?

Velocity: jet one-sidedness

Flux ratio of the approaching (isotropic) jet to the receding one (*Doppler boosting*):

$$\frac{F_a}{F_r} = \left(\frac{1+\beta_j \cos\theta}{1-\beta_j \cos\theta}\right)^{2+\alpha}$$

With $F \propto \nu^{-\alpha}$.

Apparent *vs* intrinsic speed:

$$\beta_{app} = \frac{\beta_j \sin\theta}{1-\beta_j \cos\theta}$$

In principle, one can solve for β_j and θ.

NGC 4261

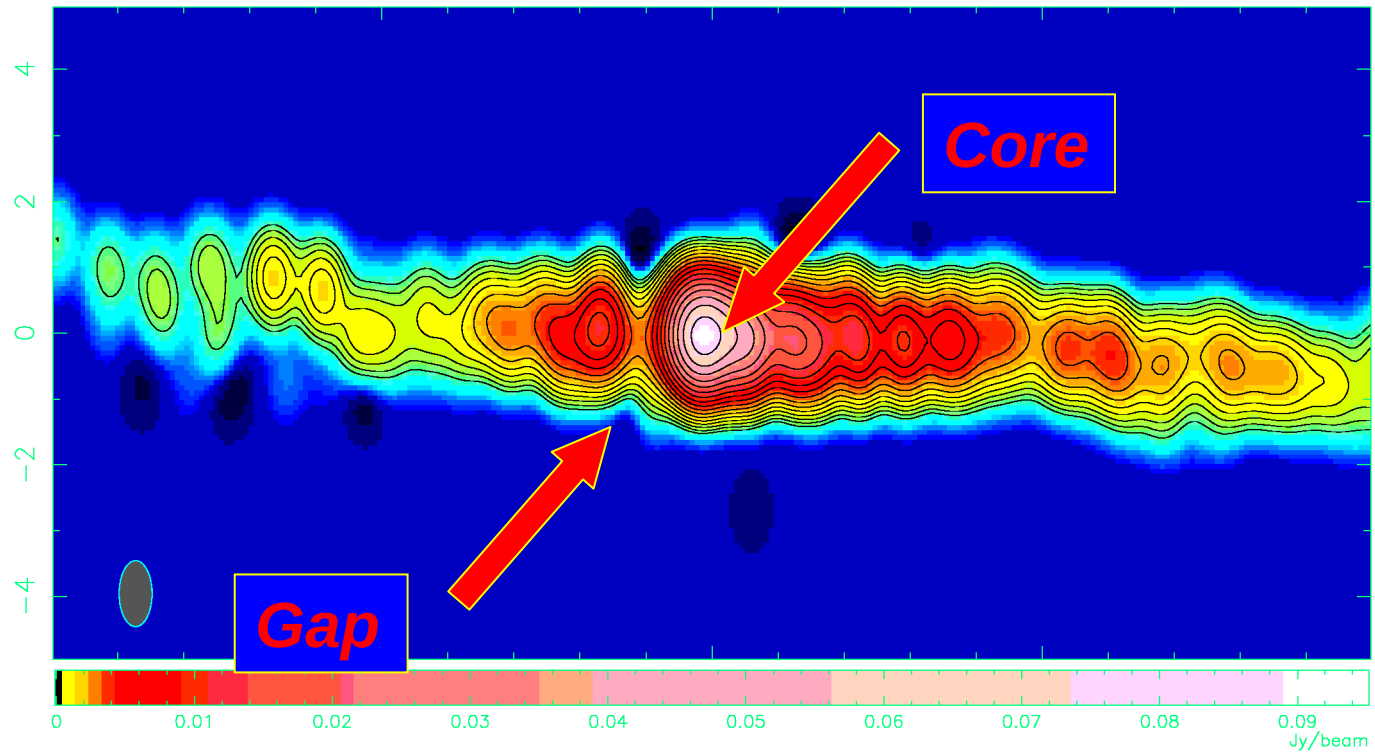

FIG. 2.— Super-resolved false color CLEAN image of NGC 4261 from the 8.4 GHz VLBA observation on 1999 October 21. The displayed region extends to ±10 mas from the presumed core in right ascension, and ±5 mas in declination. The gap in emission is clearly visible 1 mas east of the core. The restoring beam has a FWHM of 1.0 × 0.5 mas. The lowest contour represents a flux density of 0.3 mJy beam^{-1}, and successive contours are each a factor of $\sqrt{2}$ higher.

Jet and counterjet are both visible and proper motions detected: β=0.46±0.02, θ=63±3°

(Piner et al. 2002)

Difficulties...

1. The counterjet is not visible in most cases
2. Proper motions observed in few objects only

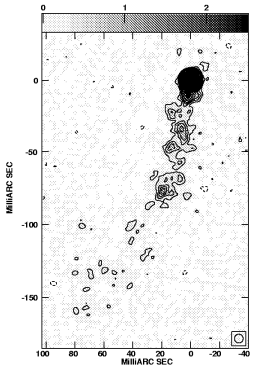

Fig. 9.— VLBA image of 0331+39 with natural weight at 5 GHz. The HPBW is 6 mas. The noise level is 0.08 mJy/beam and levels are: -0.25, 0.25, 0.5, 0.75, 1, 1.5, 3, 5, 10, 20, 30, 50, 70 and 100 mJy/beam.

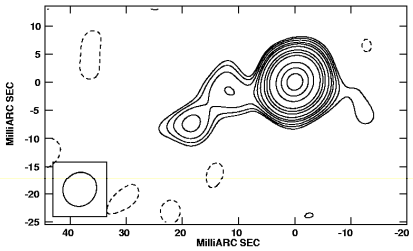

Fig. 11.— VLBA image of 0648+27 at 5 GHz. The HPBW is 6.4 × 5.9 mas (PA -30°). The noise level is 0.2 mJy/beam and levels are: -0.5, 0.5, 0.7, 1, 1.5, 2, 3, 5, 7, 10, 20, 30 and 40 mJy/beam.

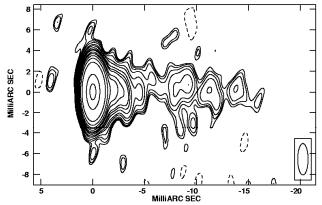

Fig. 15.— Global VLBI image of 1441+52 (3C303) at 5 GHz. The HPBW is 3 × 1 mas in PA 0°. The noise level is 0.05 mJy/beam and levels are: -0.1, 0.1, 0.12, 0.15, 0.2, 0.3, 0.4, 0.6, 0.8, 1, 1.5, 2, 3, 5, 10, 50, and 100 mJy/beam.

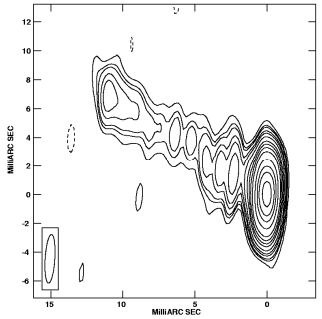

Fig. 16.— Global VLBI image of 1833+32 (3C382) at 5 GHz. The HPBW is 3.4 × 0.7 mas in PA = -4°. The noise level is 0.15 mJy/beam and levels are: -0.5, 0.5, 0.8, 1, 1.5, 2, 3, 5, 7, 10, 15, 30, 50, 70, and 100 mJy/beam.

Jet Mach number: indication of shocks

Pictor A

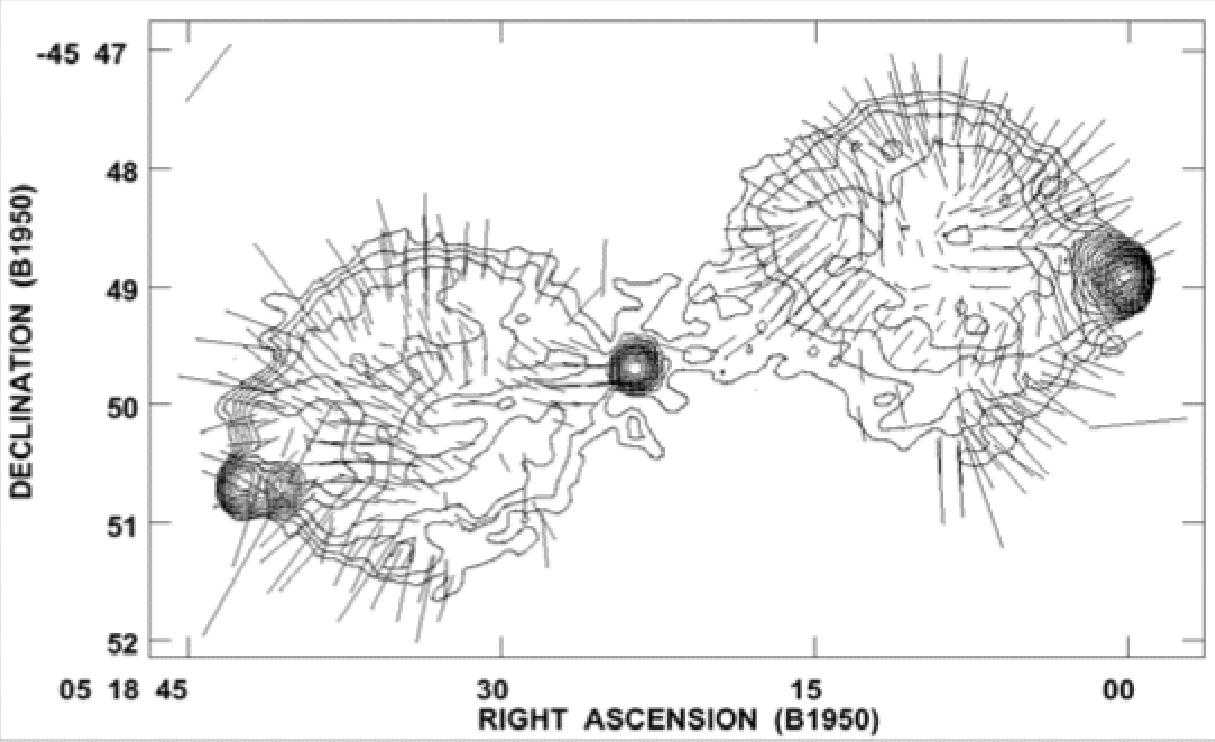

The implied direction of the magnetic field in this image is perpendicular to the straight lines. That is, the magnetic field has a circumferential direction with respect to the plasma in the lobe.

Jet Mach number: indication of shocks

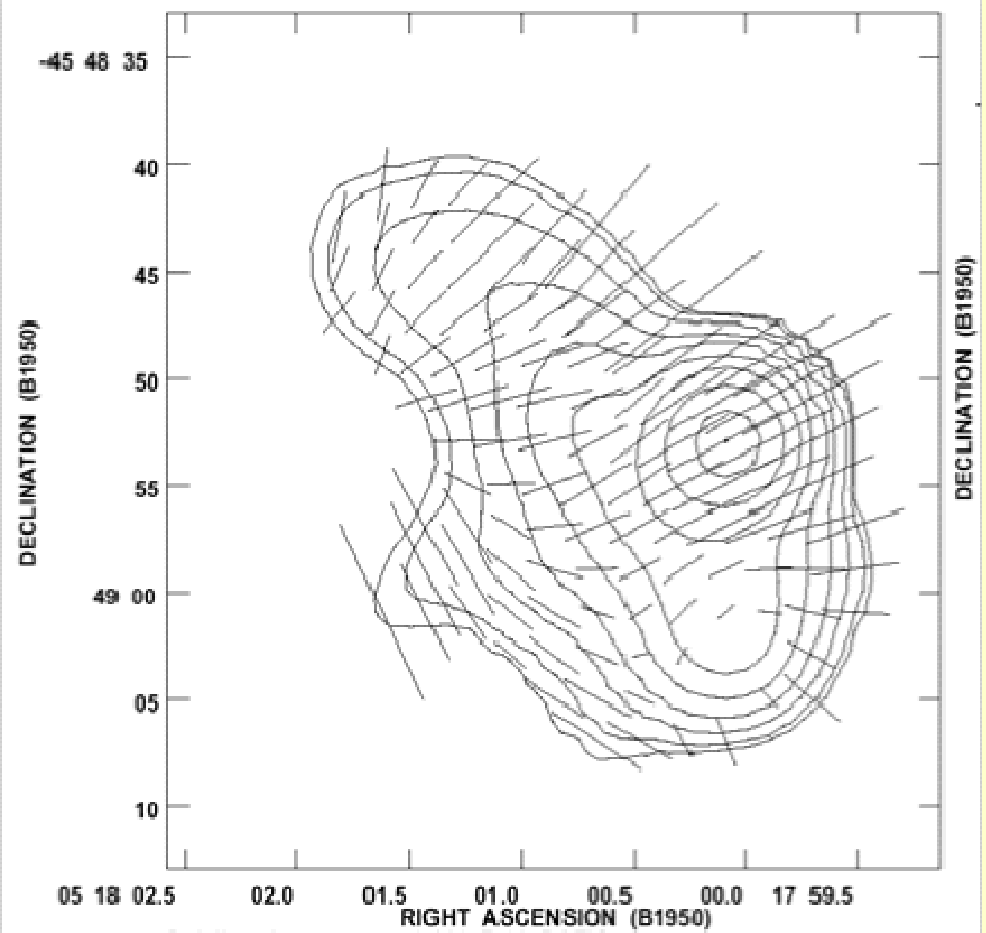

Polarization of the western hot spot of Pictor A, at 3.6 cm wavelength with 400 resolution (left), and at 0.77 by 0.17 resolution (right). The lower resolution map shows the general features of this region, and is contoured at 0.391% and then with a spacing of a factor of 2 between 0.552 and 70.71% of the maximum intensity of 1.55 Jy/beam. The dashed lines again indicate the plane of the electric vector. Their lengths are proportional to the degree of polarization, with 100 equal to 6.67%.

The western hot spot of Pictor A

$B_{eq}=4.6\times10^{-4}$ G

Jet Mach number: indication of shocks

The polarisation of the hot spot in Pictor A reveals magnetic field structure that is consistent with that produced by a shock wave.

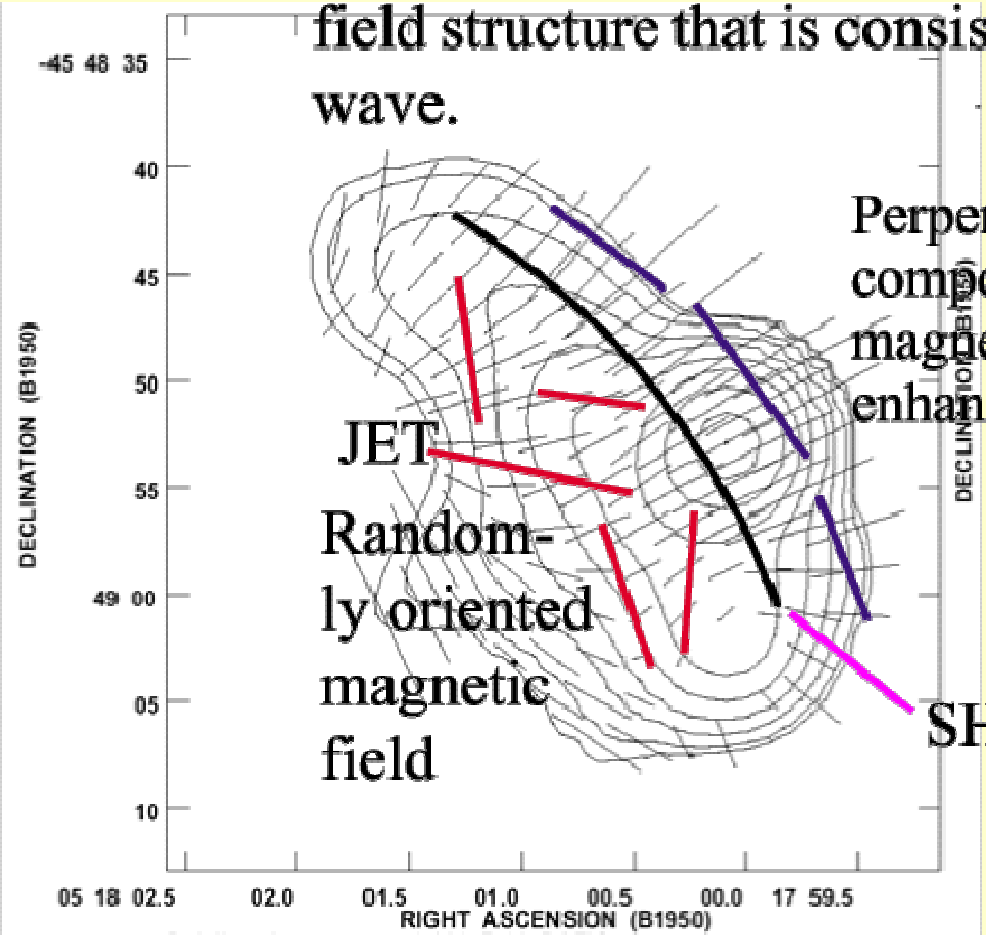

At the terminal shock of the jet, the compo-nent of the magnetic field perpendicular to the shock is amplified, whilst leaving the par-allel component un-changed. This lines the field up with the shock as shown

Observations of FR II hot-spots

3C445 at the VLT I-band (0.9 μm) (Prieto et al. 2003)

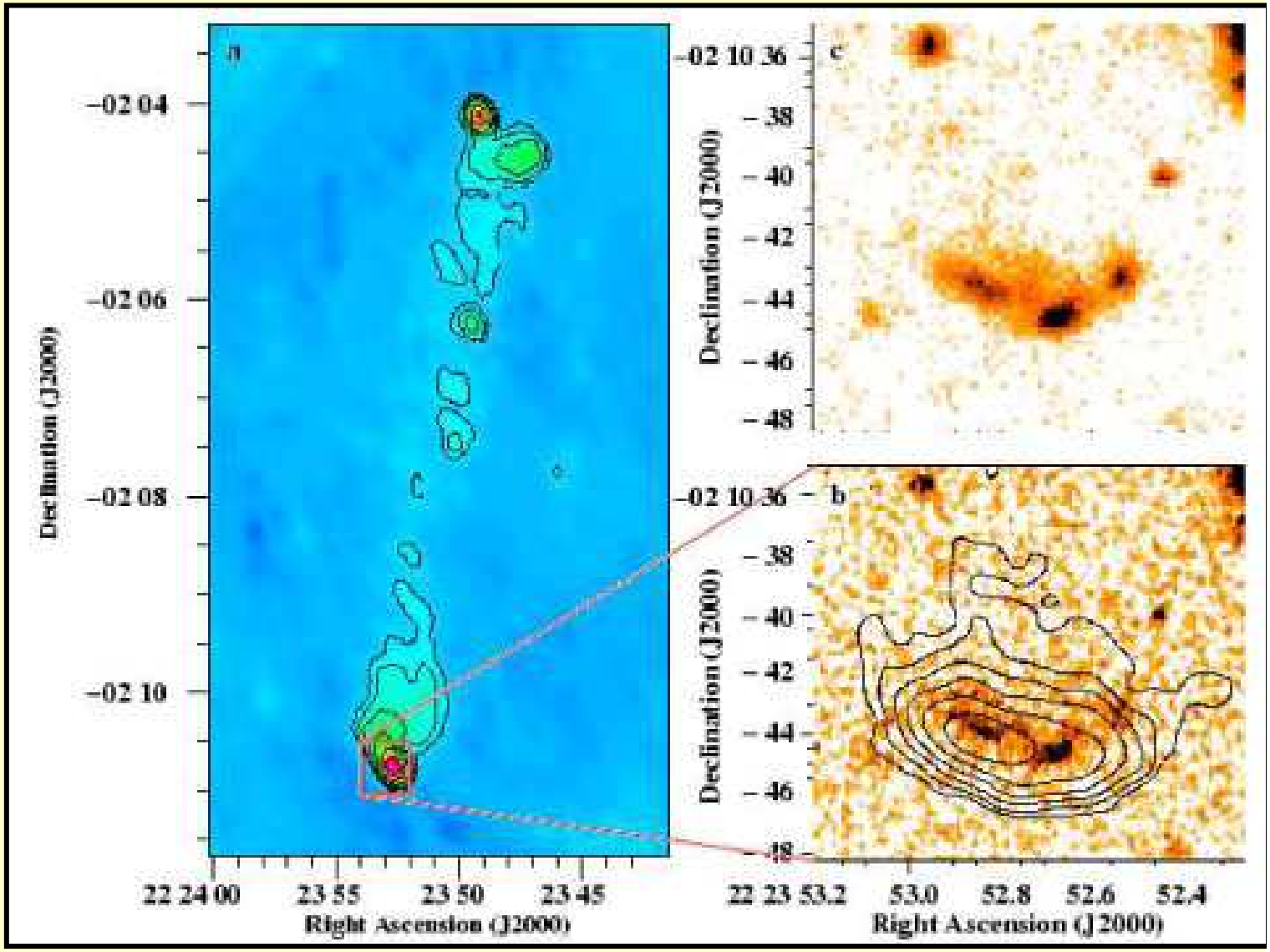

FR II hot-spots

Synchrotron models

K, H, J and I bands and radio flux at 8.4GHz

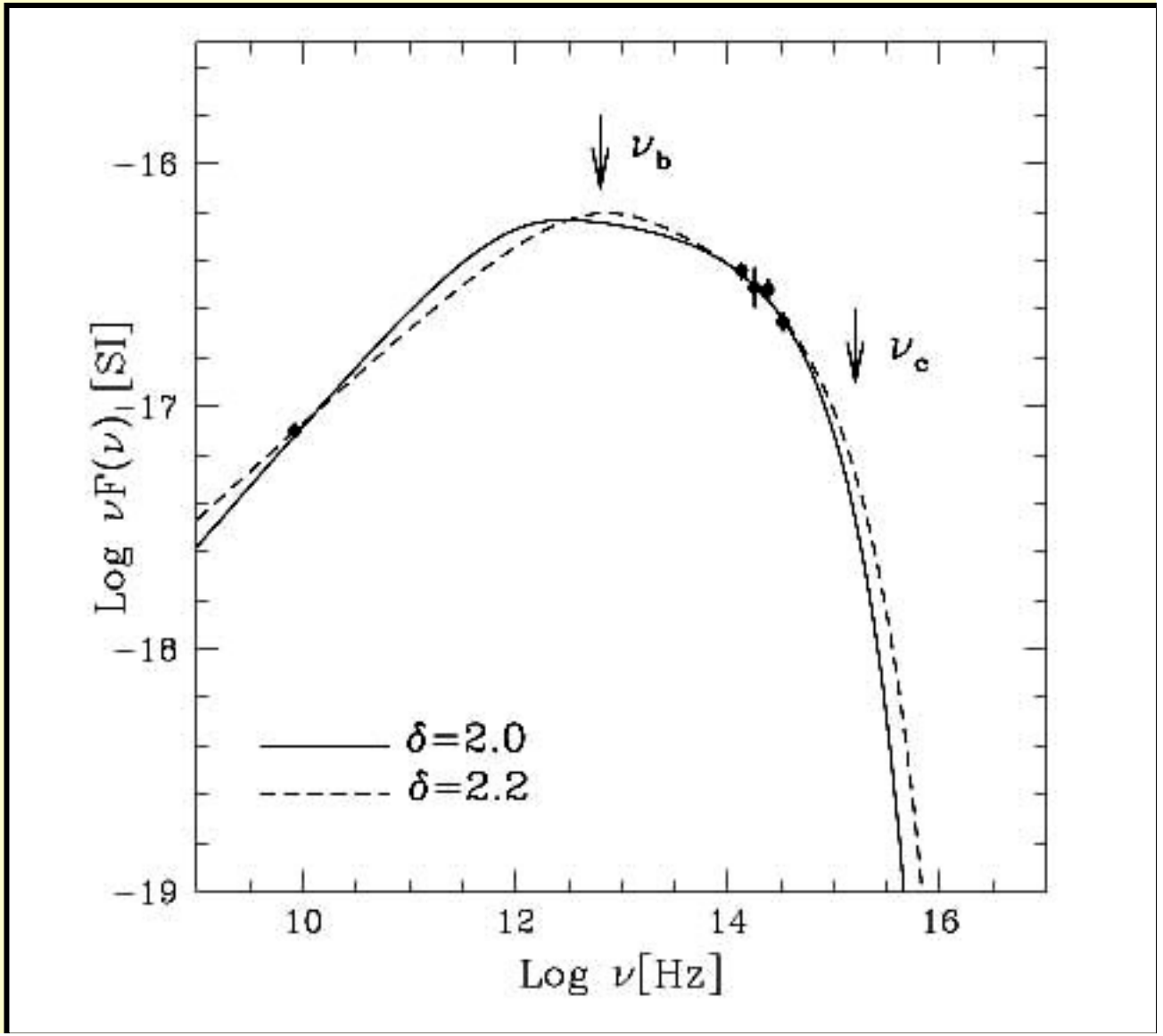

Modelling the jet termination in FR II sources

Bow-shock

Mach disk: possible cosmic ray acceleration site

Contact discontinuity

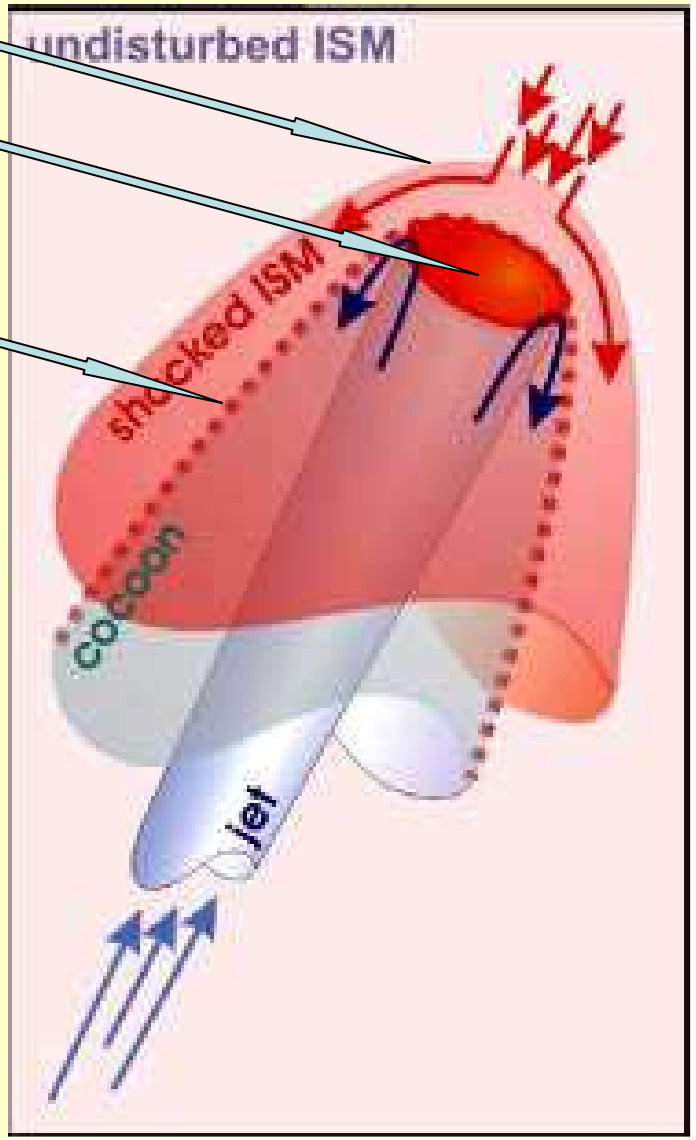

- AGN (FRII) jets are supersonic (M>1)
- Emission non-thermal
- Comparison of model B with B_{eq}

Modelling the jet termination in FR II sources (Mignone's lecture)

Terminal shock

jet

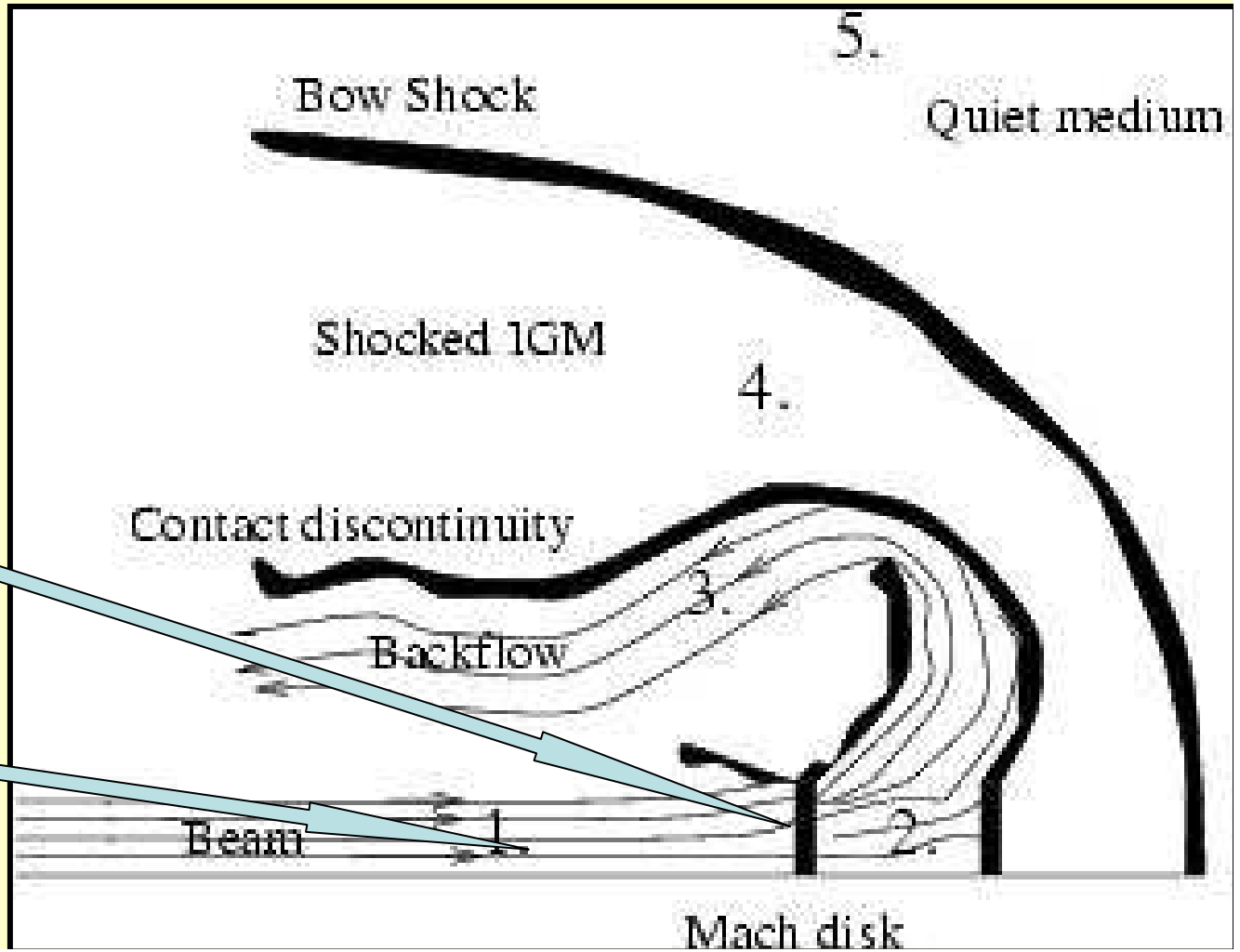

Jet density from FRII morphologies

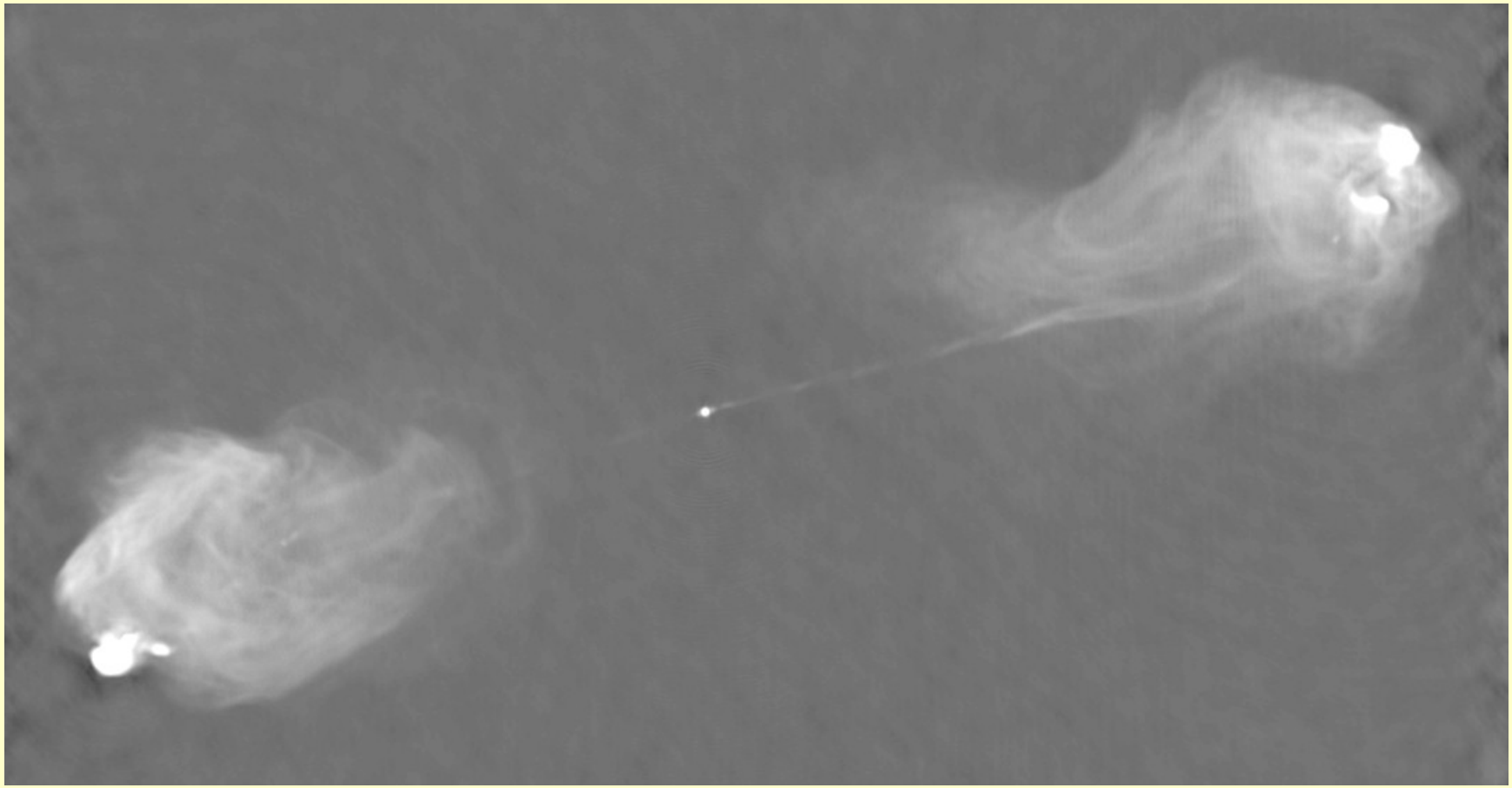

Cygnus A (FR II) - VLA, 6cm

Jet density from FRII morphologies

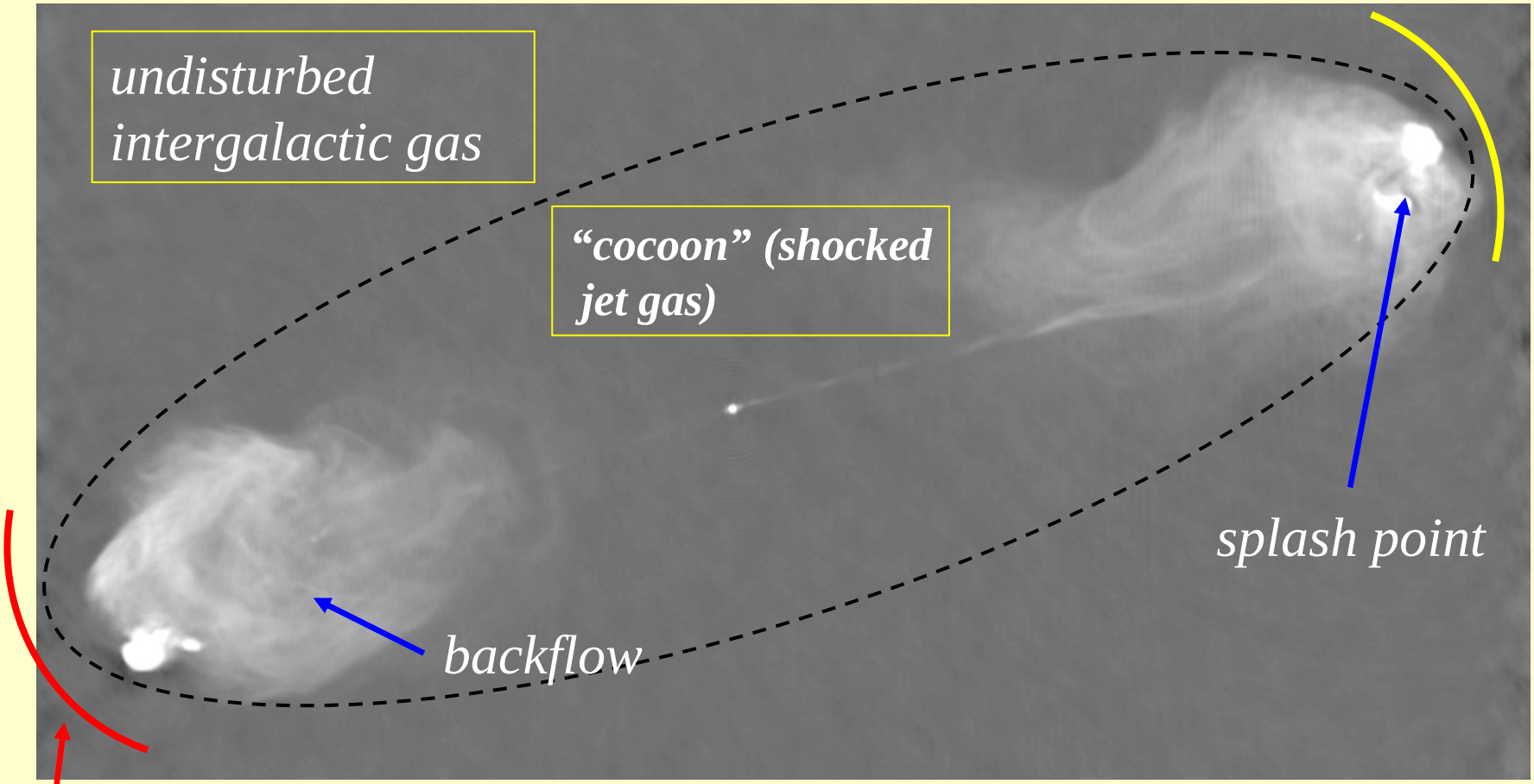

Cygnus A (FR II) - VLA, 6cm

- **MHD simulations of AGN jets: propagation and morphologies**

Numerical simulations of FR II

Supersonic jet ($M=10$), weakly relativistic ($\gamma=2$) with different density jet-ambient ratios η
(classical case by Mignone)

$$\eta=10$$

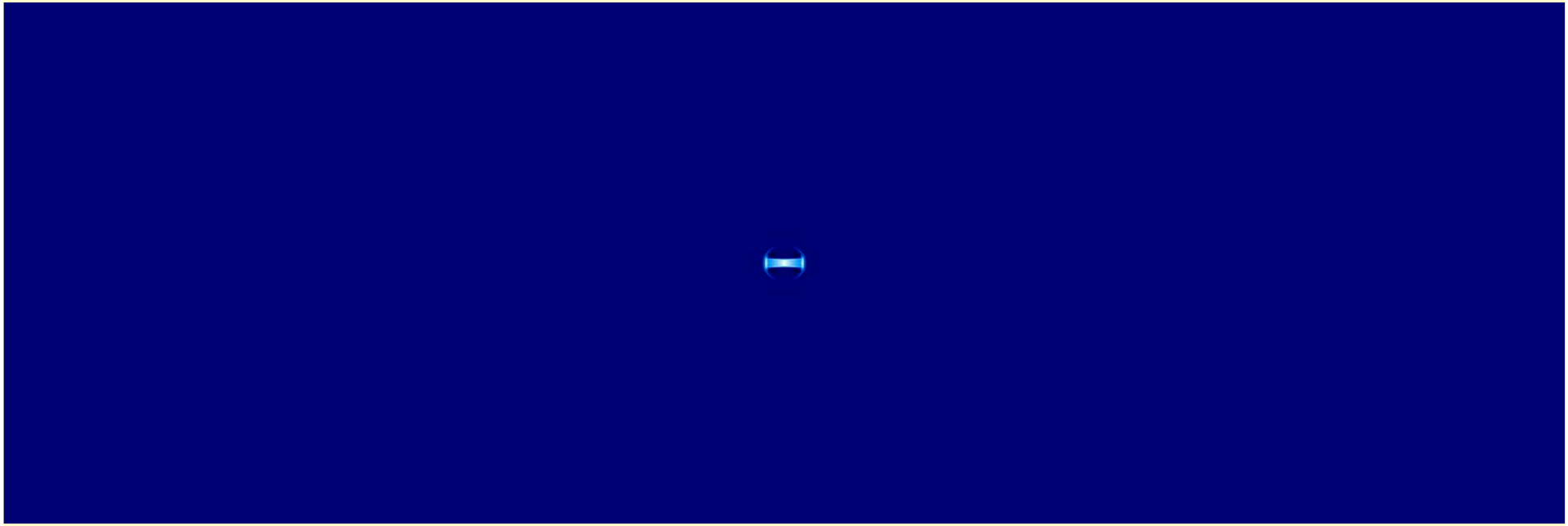

(M)HD code PLUTO, based on high resolution shock-capturing schemes.
(http://plutocode.ph.unito.it)

Numerical simulations of FR II

$\eta=0.1$

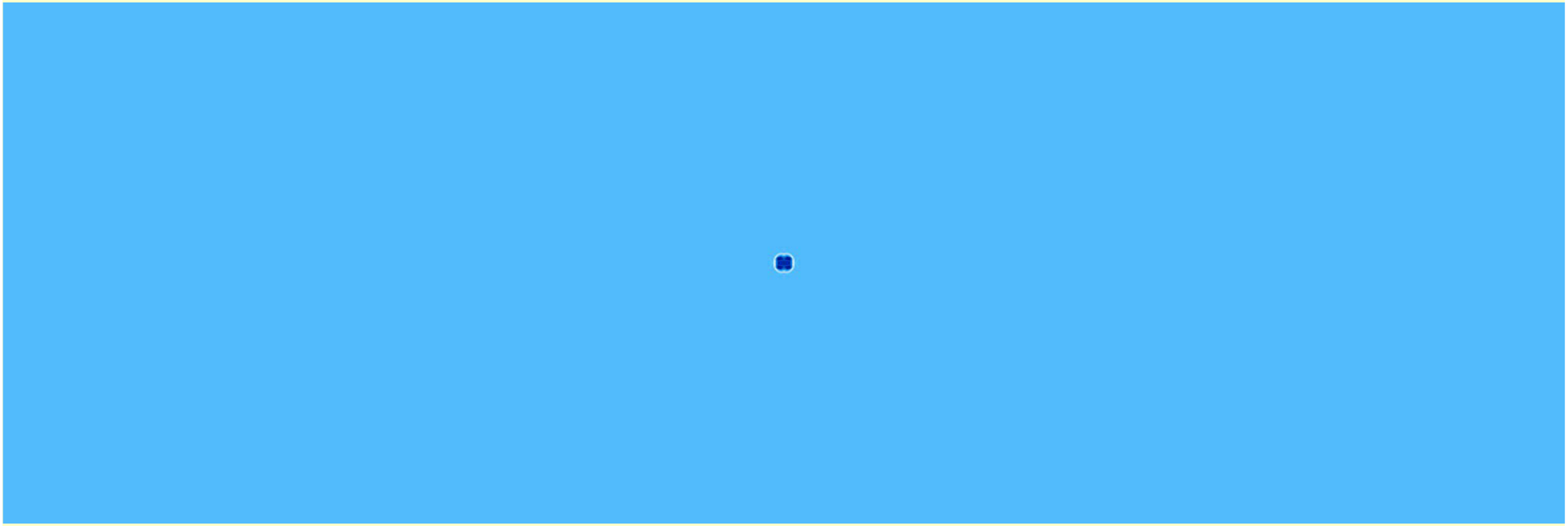

Numerical simulations of FR II

η=0.001

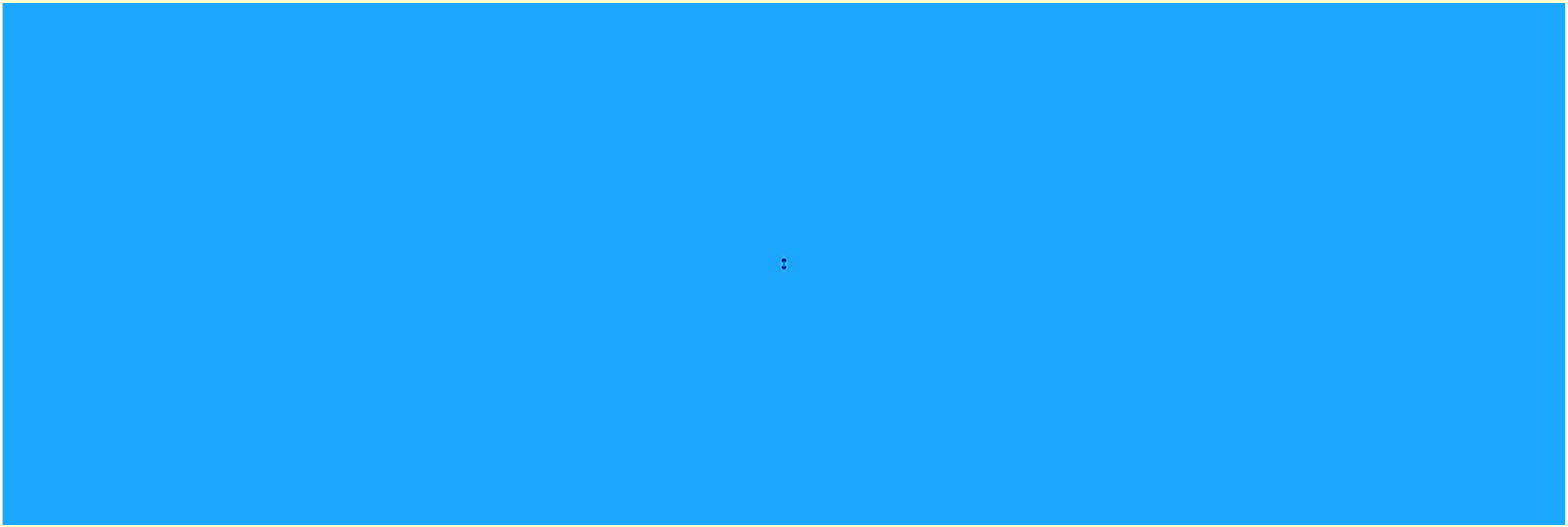

$$v_{head} = \frac{\sqrt{\eta}}{\sqrt{\eta}+1} v_j \,,\; \eta = \frac{\rho_j h_j}{\rho_a h_a} \gamma^2 \,,\; h = 1 + \varepsilon + \frac{p}{\rho}$$

Chandra X-ray Observatory

Cygnus A **Wilson et al. (2001)**

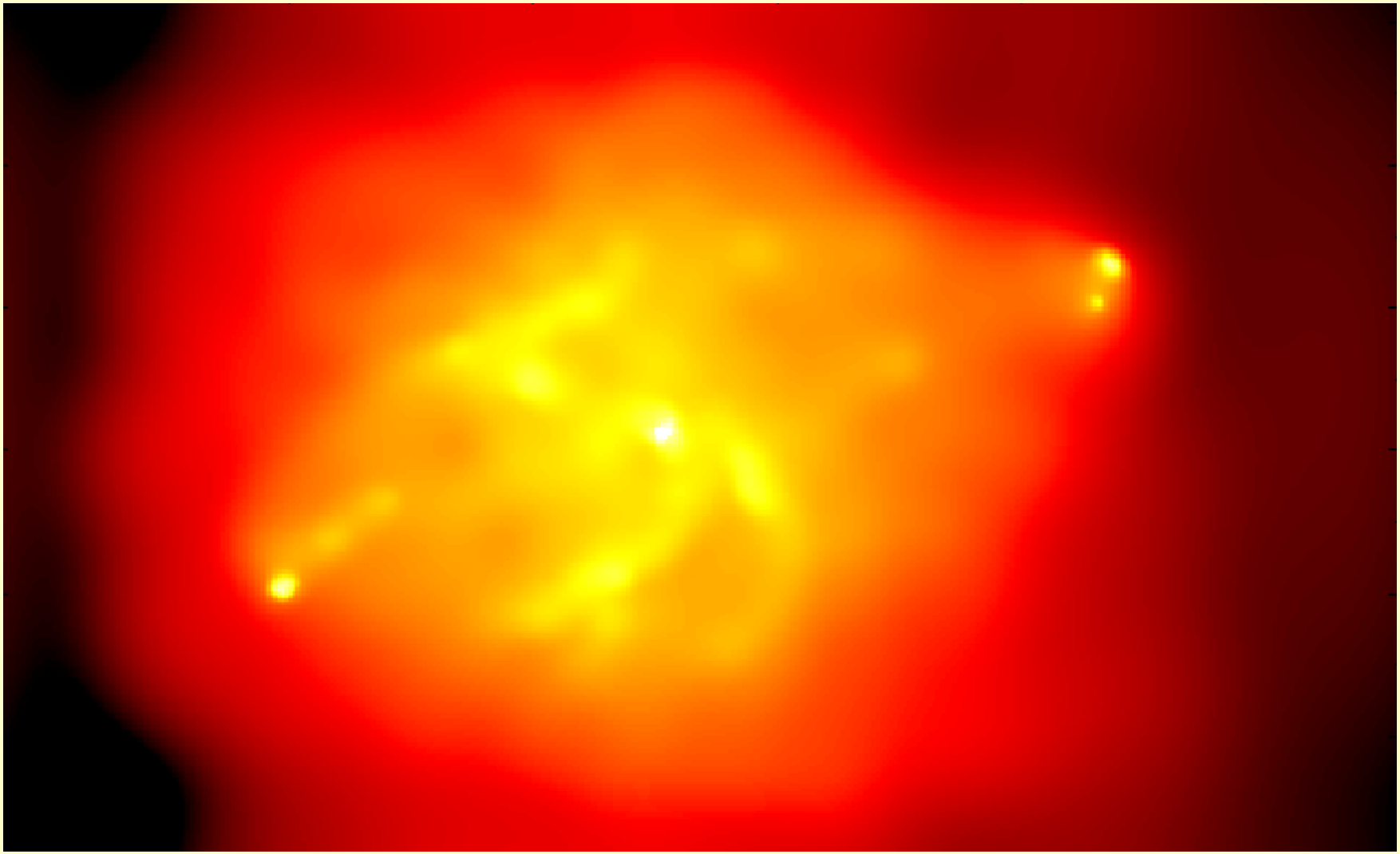

Numerical simulations of FR II

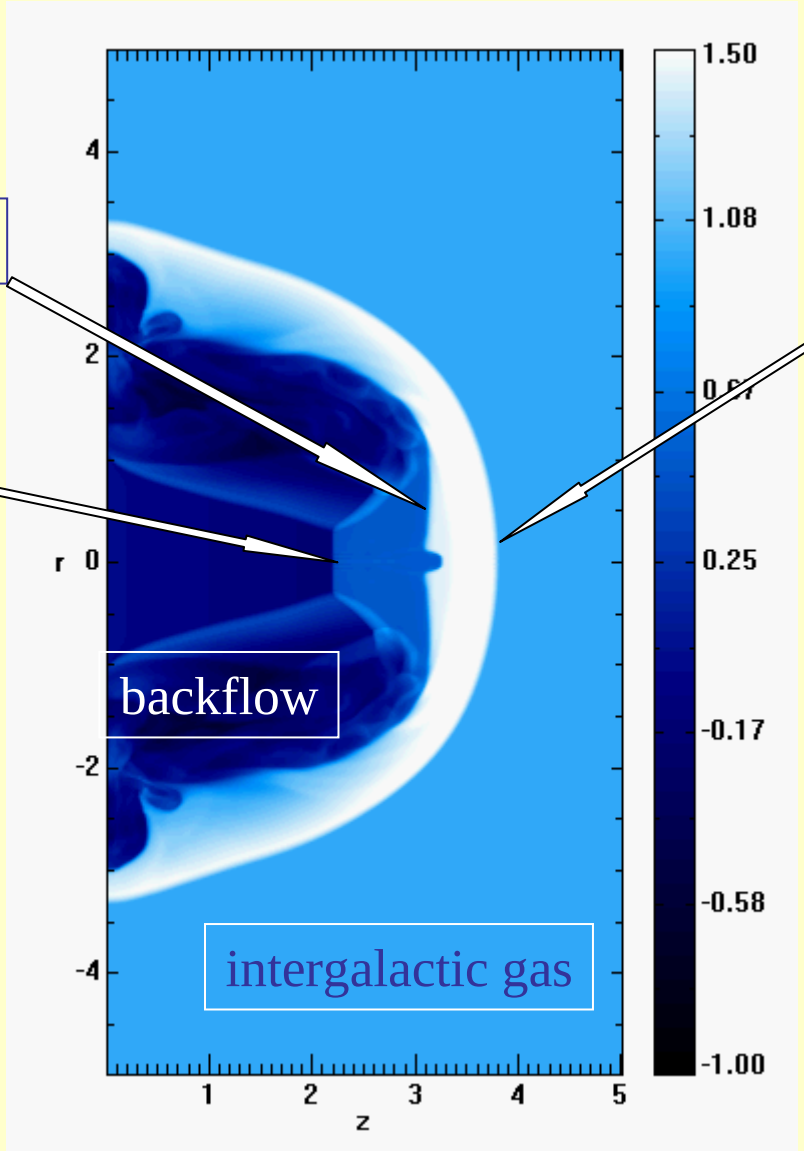

Numerical simulations of FR II

Comparison of observed and simulated morphologies

1. Relativistic (one-sidedness), $\gamma>1$
2. Supersonic (presence hot-spots), $M>1$
3. Underdense (presence of cocoons), $\eta<1$ (simulations)

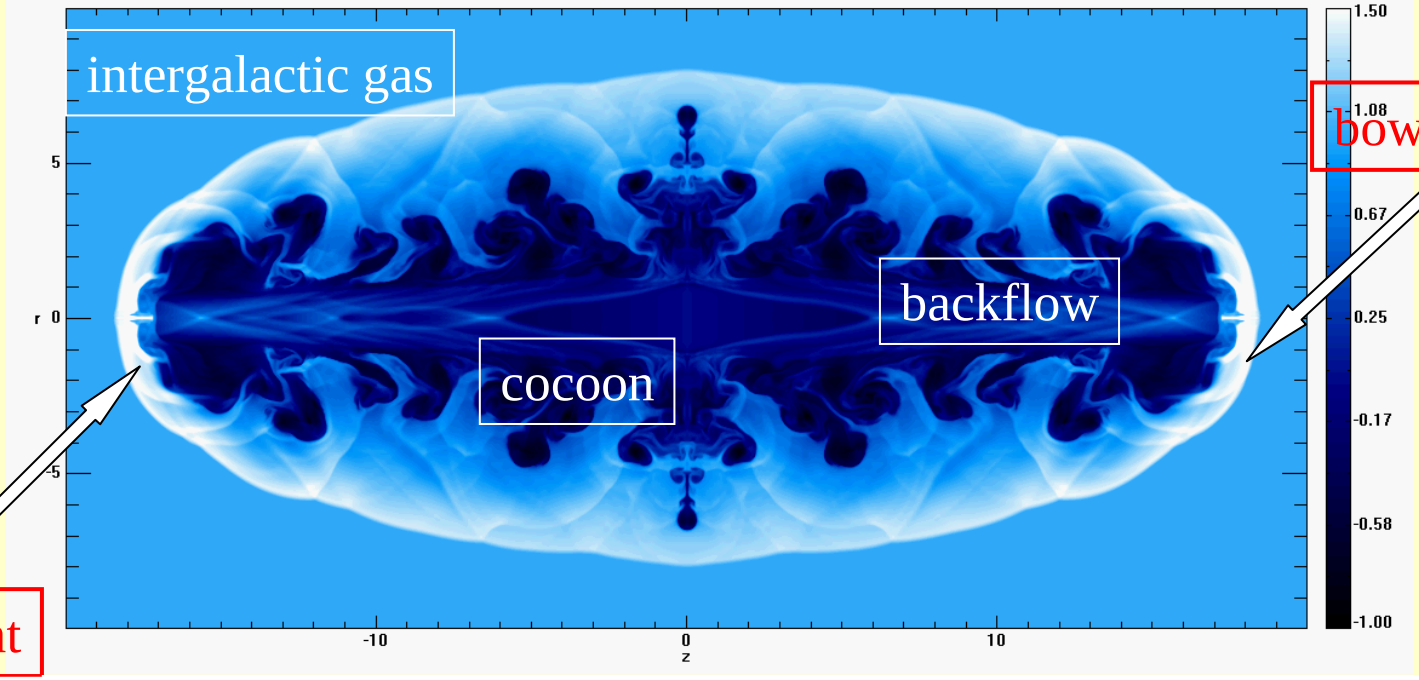

On Kinematical Models for FRIs

Jet models through conservation laws can obtain jet density, pressure, Mach number, etc. along the jet compatible with observations (Bicknell 1994, Laing & Bridle 2002)

They rely upon assumptions concerning the geometry and kinematics of the jet.

These assumptions are hard to reproduce by dynamical models based on the solution of (M)HD equations.

FR I source 3C31, VLA observations:

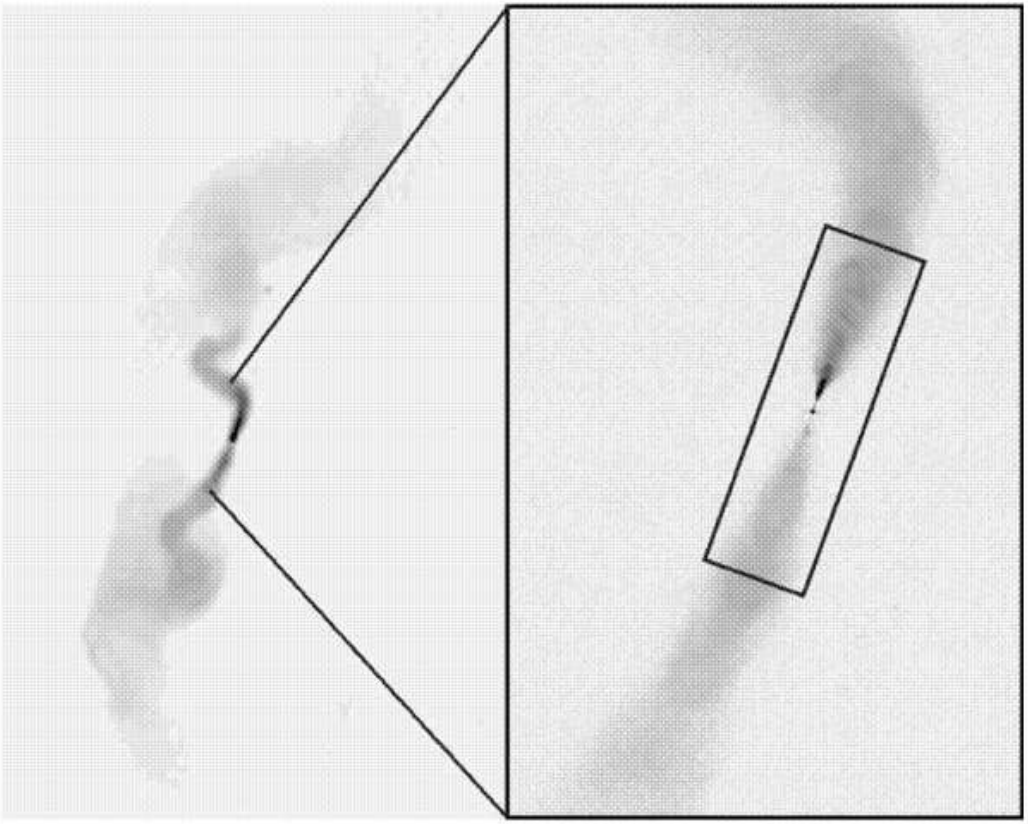

Figure 1. Montage showing the large-scale structure and jets of 3C 31. Left-hand panel: VLA 1.4-GHz image of a 15-arcmin (300 kpc) north–south field at 5.5 arcsec (1.9 kpc) resolution. Right-hand panel: VLA 8.4-GHz image of an approximately 2-arcmin (40 kpc) north–south field at 0.25 arcsec (85 pc) resolution. The rectangle within the right-hand panel shows the relatively straight segment of the jets that we have chosen to model.

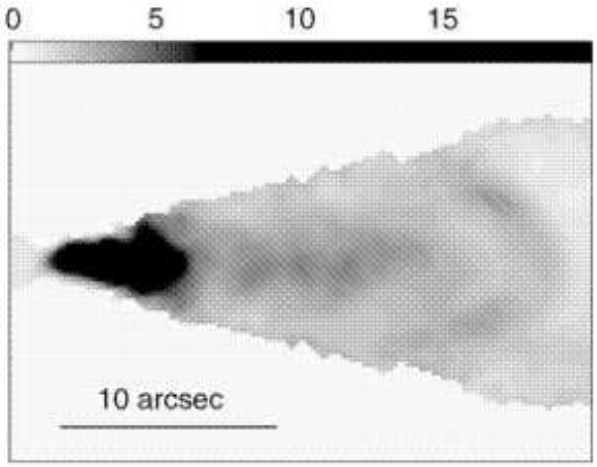

Figure 2. The observed jet/counter-jet brightness ratio (sidedness) at a resolution of 0.75 arcsec, from the 8.4-GHz observations. This was constructed by dividing the *I* image by a copy of itself rotated through 180° and is in the sense main jet/counter-jet.

This configuration can hardly be reproduced by numerical simulations

Lateral shocks necessarily form by the jet expansion and recollimate the jet

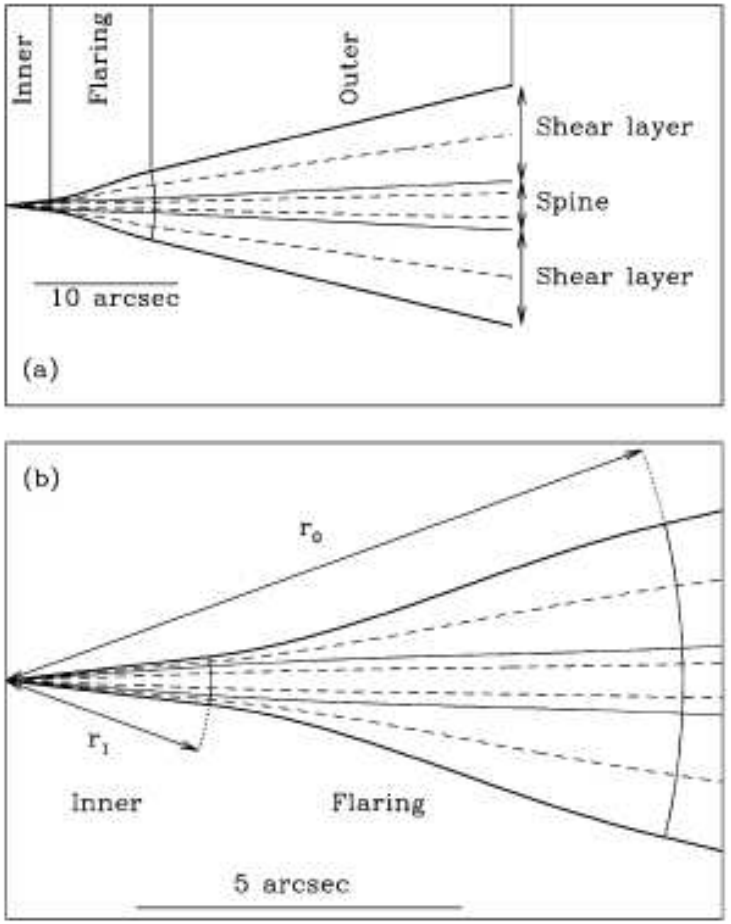

Figure 4. Geometry of the spine/shear-layer model, showing the inner, flaring and outer regions in the plane containing the jet axis. The thick full curves represent the edge of the jet, the boundaries between regions are represented by thin full curves and the $s = 0.5$ streamlines for the spine and shear layer are drawn as dashed curves. (a) The entire modelled region; (b) the base of the jet on a larger scale, showing the boundary surfaces at distances of r_1 and r_0 from the nucleus. The Gaussian model is essentially the same, but with the spine component removed.

FRI 3C31, Laing 2002

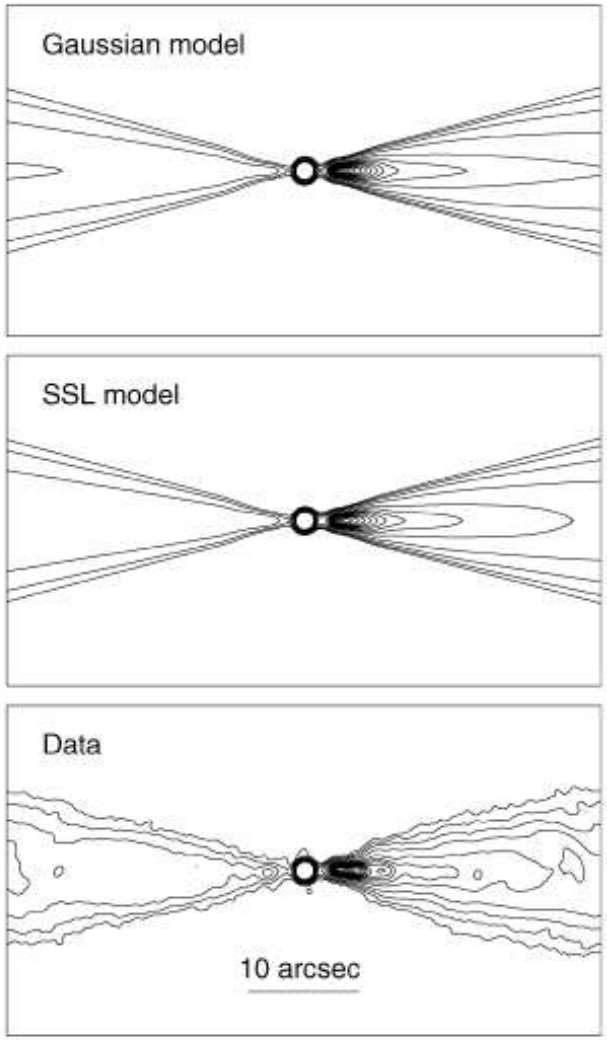

Figure 6. Contours of total intensity at a resolution of 0.75 arcsec, covering ±27 arcsec from the nucleus. The contour levels are: −1, 1, 2, 4, 8, 16, 24, 32, 40, 48, 56, 64, 72, 80, 88, 96, 104 ×40 μJy (beam area)$^{-1}$. From the top panel down: model with Gaussian profile, model with spine/shear layer, VLA data.

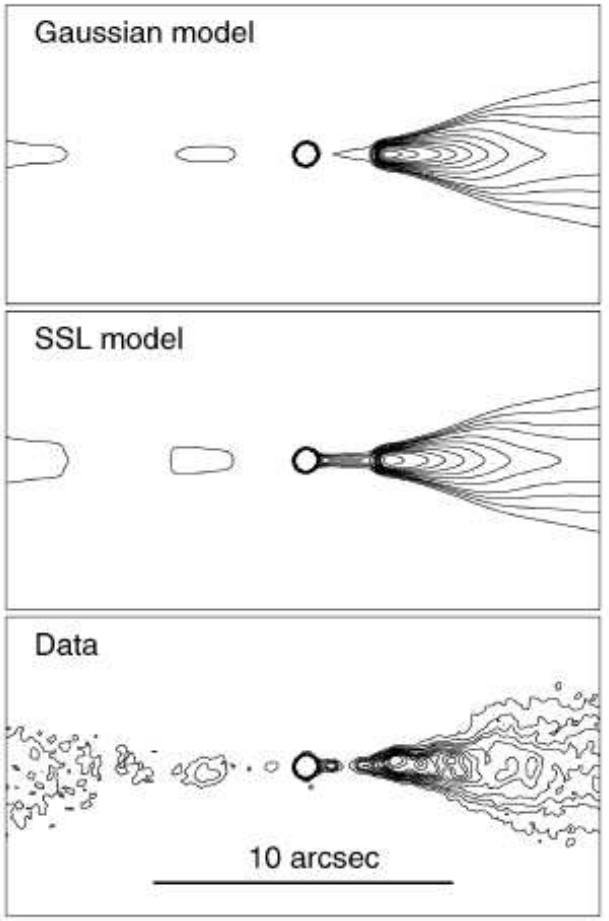

Figure 7. Contours of total intensity at a resolution of 0.25 arcsec. The plot covers ±10 arcsec from the nucleus. The contour levels are −1, 1, 2, 3, 4, 6, 8, 10, 12, 14, 16, 20, 24 ×30 μJy (beam area)$^{-1}$. From the top panel down: model with Gaussian profile, model with spine/shear layer, VLA data.

Velocity β = v/c: deceleration and transverse gradients

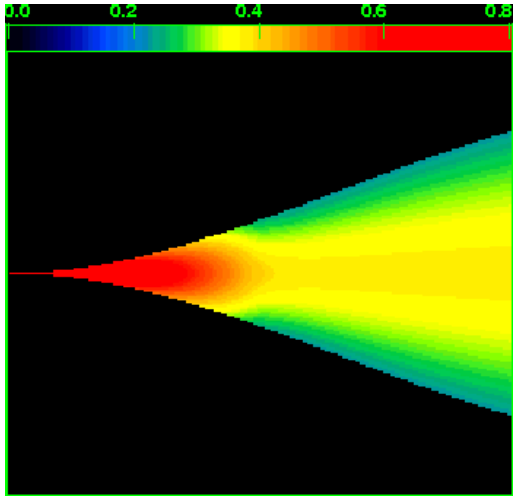

NGC 315

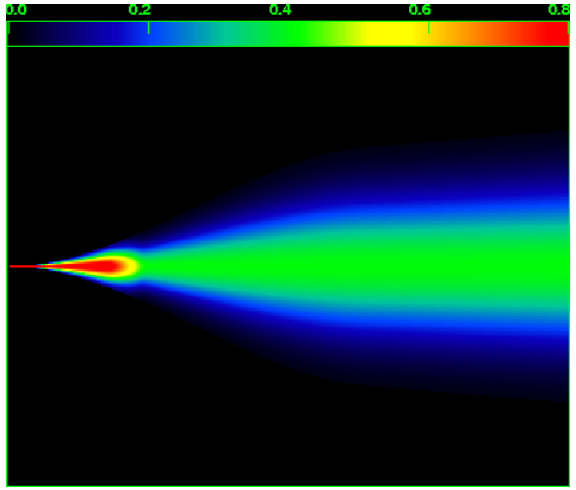

3C296

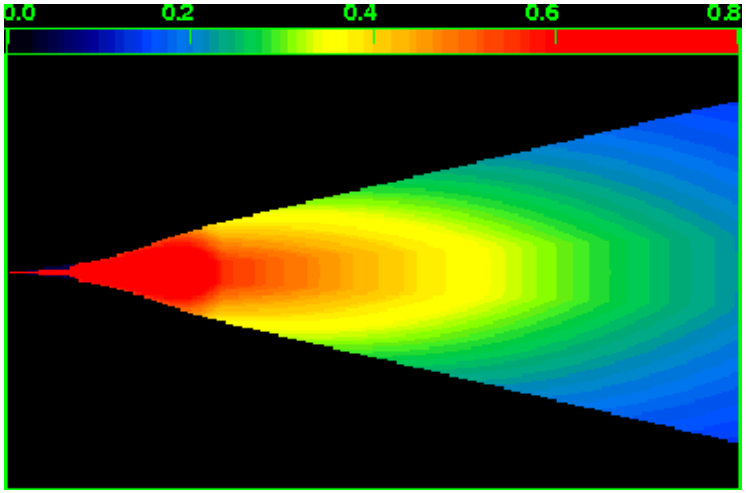

3C 31

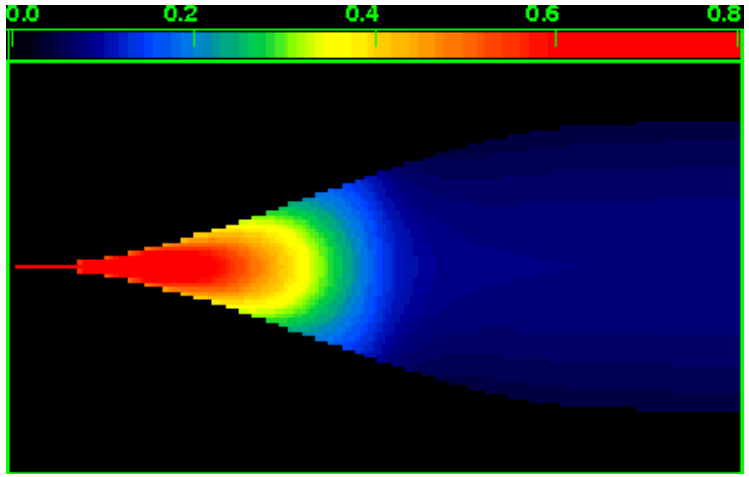

B2 0326+39

Pressure ratio=10, η=0.1, M_r=10, γ=2

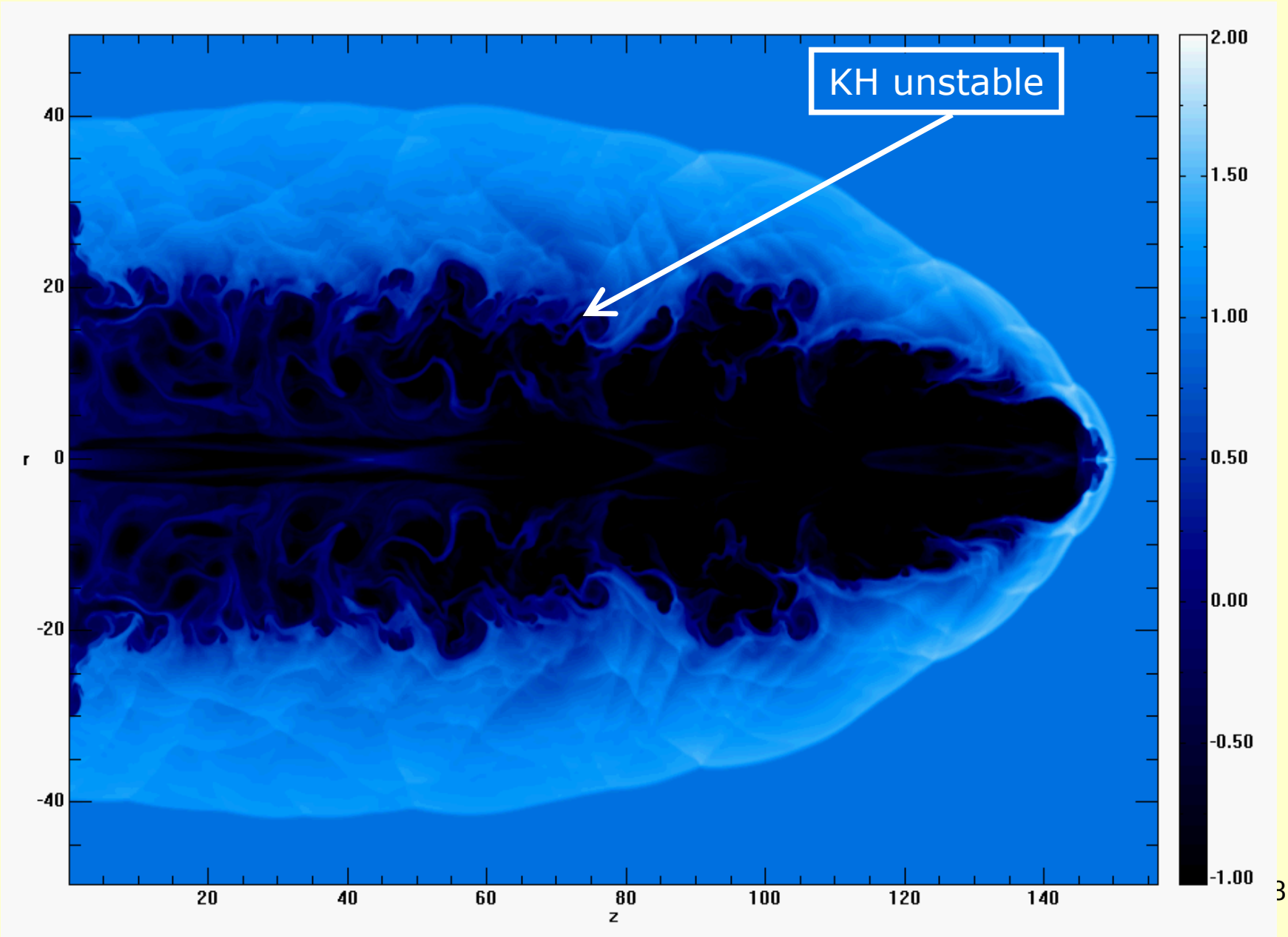

Over-pressured jets do not flare as invoked by empirical models. FRI morphologies remain difficult to reproduce.

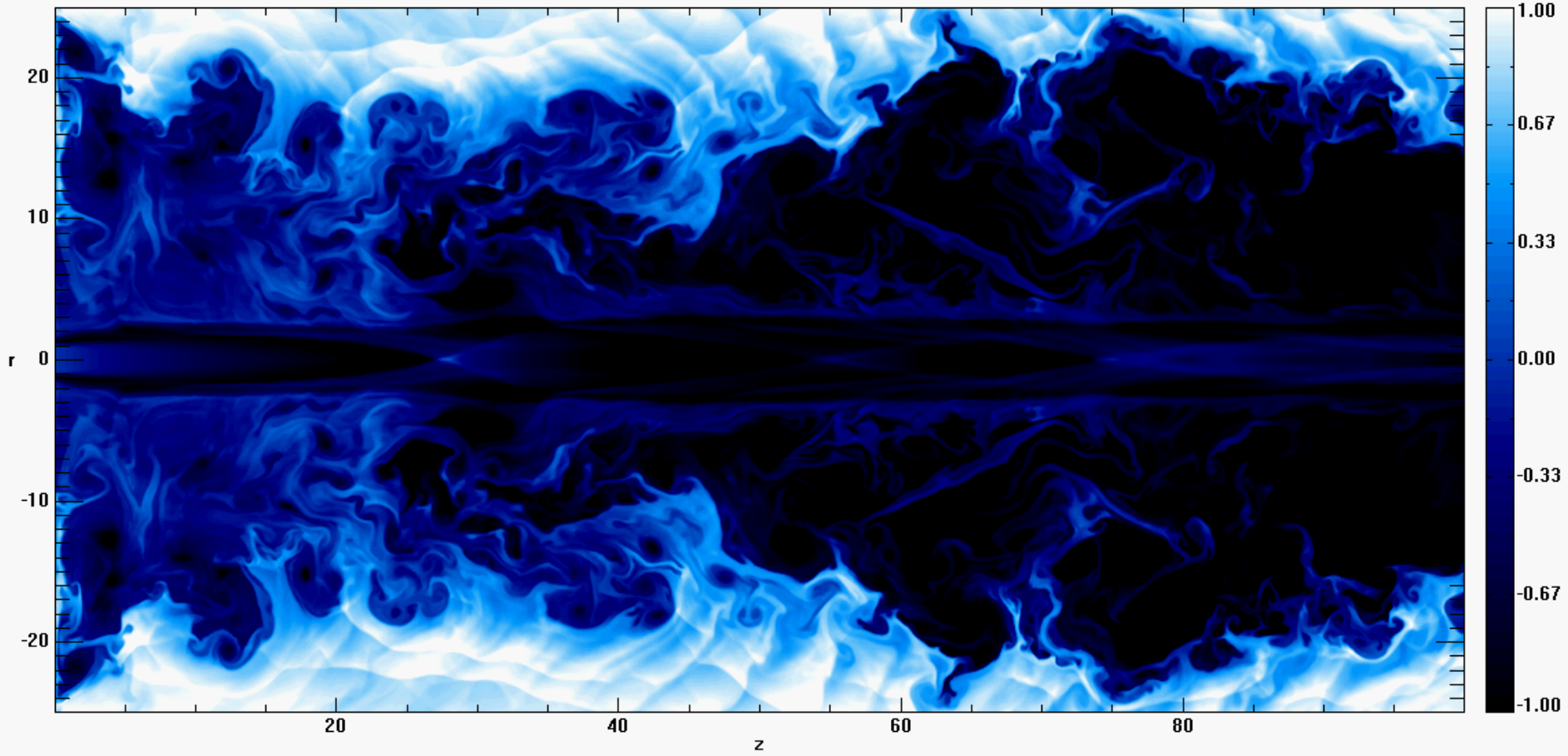

About FRI/FRII Dichotomy

Assumptions:

- AGN jet acceleration is governed by the accretion rate through an accretion disk in a relativistic regime (e.g. Camenzind 1998 in steady state, Koide et al. 1999 simulations GRMHD).
- AGN jets can be Poynting dominated in the sub-parsec region, but are matter-dominated beyond

Question:

- Why are radio jets dichotomic? (YSO jets are not)

Radio Galaxies: More facts

- FR I and FR II have different kpc-scale morphologies and radio power but are similar on the parsec scale, where the jet bulk Lorentz factor is in the range $\gamma = 3\text{-}10$ (e.g. Giovannini et al. 2001)
- FR I sources are weakly or non-relativistic at kpc scales
- FR I radiogalaxies, about 10 VLBI sources, show limb-brightened radio emission at parsec scales

Limb-brightening

B2 1144+35

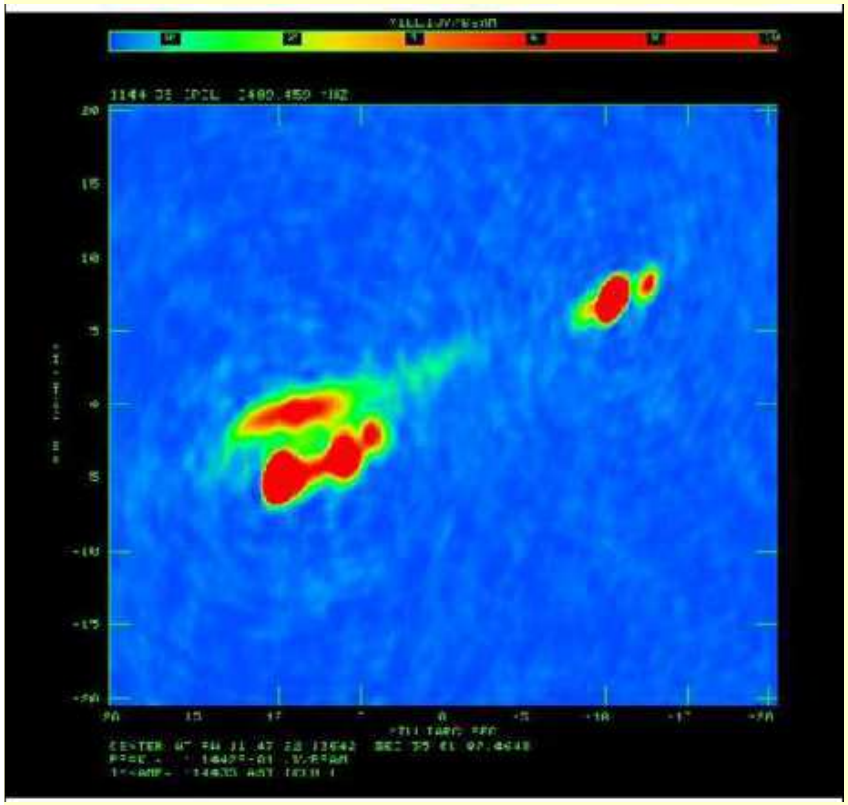

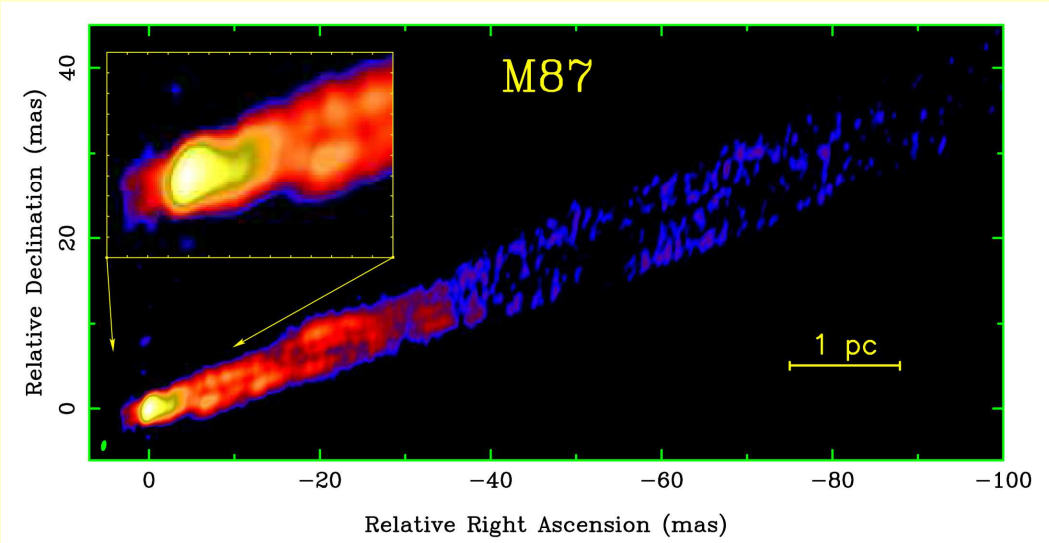

About FR I / FR II Dichotomy

- **Intrinsic explanations:**

1. Differences in jet composition (e^+-e^- for FR I sources, Reynolds et al. 1996a);
2. Difference in the central engine (a fast spinning BH yields FR II jets, Meier 1999)
3. ADAF produce FR I (and BL Lacs), while 'standard' accretion discs FR II (and quasars) (Reynolds et al. 1996b).

- **Extrinsic explanation:**

1. Jets are similar close to the source (apart from power); weaker jets are decelerated by instabilities and/or entrainment to produce FR Is, stronger jets remain stable to form FR IIs (Komissarov 1990, Bicknell 1995, Bowman et al. 1996, Laing 1996, Rossi et al. 2008).

FRI jets braking

Problem: jet deceleration from the VLBI to VLA scale (Bowman et al. 1996, Laing et al. 2003)

VLBI

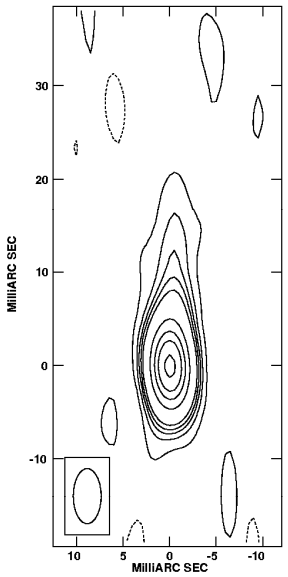

Fig. 13.— Global VLBI image of 1222+13 (3C272.1) at 1.7 GHz. The HPBW is 6 × 3 mas in PA 0°. The noise level is 0.5 mJy/beam and levels are: -1, 1, 3, 5, 7, 10, 30, 50, 70, and 100 mJy/beam.

VLA

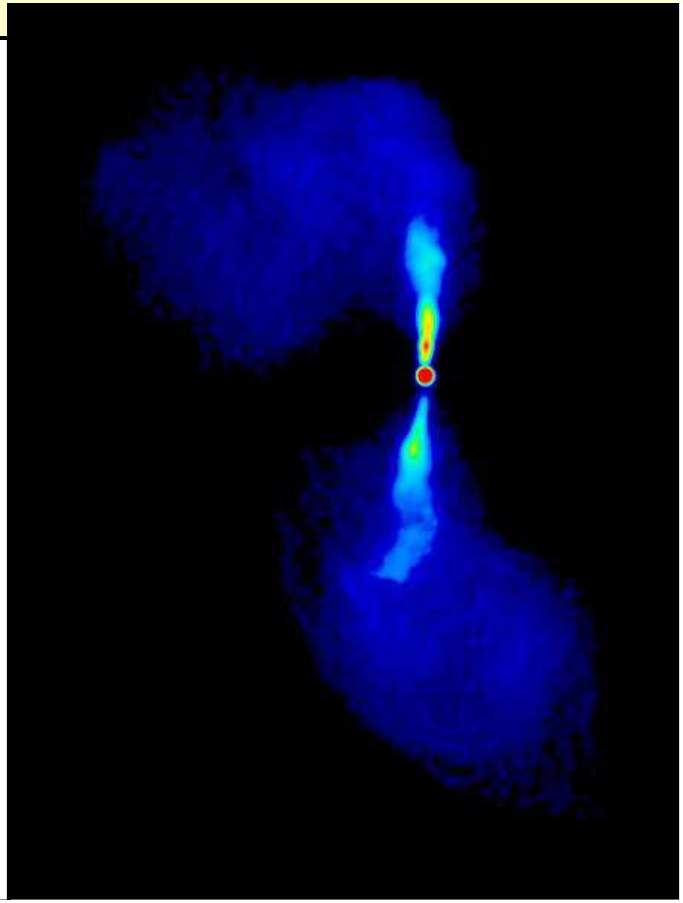

FRI jets limb-brightening

"Spine-layer" velocity structure of the jet: inner core with high Lorentz factor surrounded by a slower external layer (e.g. Chiaberge et al. 2000, Piner & Edwards 2004)

$$P_{observed} = P_{emitted} \times \left[\gamma\left(1-\beta\cos\theta\right)\right]^{-(2+\alpha)} = P_{emitted} \times \delta^{-(2+\alpha)}$$

For θ (angle jet to line-of-sight) large enough the spine emission is "de-boosted". Possibilities:

1) The jet has a spine-layer structure from its origin;
2) this structure results from interaction with the ambient medium via instabilities.

- **MHD simulations of AGN jets: Jet instabilities**

Jet instability and braking in FRIs

Jet instabilities: linear growth $\tau_{KH} \sim 2\pi M_J R_J / c_s$

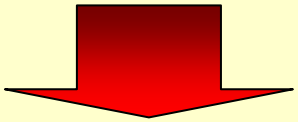

Nonlinear growth: $\tau_{KH} \leq 10 R_J / c_s$

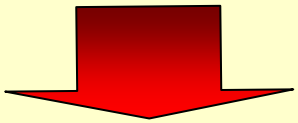

Mixing and mass entrainment

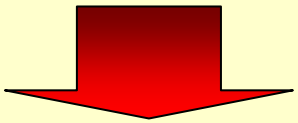

Jet braking

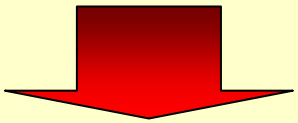

Limb-brightening

About shear-layer instabilities

Shear-layer (or Kelvin-Helmholtz) instabilities arise at the interface of two fluid in pressure equilibrium and in relative motion.

They are relevant for astrophysical flows where geometrical, magnetic and relativistic effects govern their behavior and evolution.

In the case of jets, these instabilities are invoked to interpret the observed morphologies, relativistic particle acceleration and entrainment processes.

The linear stability analysis

1. to classify the unstable modes;
2. to limit the instability regions in the parameter space;
3. to obtain the spatial or temporal growth rate.

Advantages:

1. possibility to study the stability for a wide field of physical parameters and spatial and temporal scales;
2. derive a guideline for a physical understanding of the nonlinear development of the instability.

BUT the reality is nonlinear…

The linear stability analysis

The interface between the two fluids is displaced by a small amount:

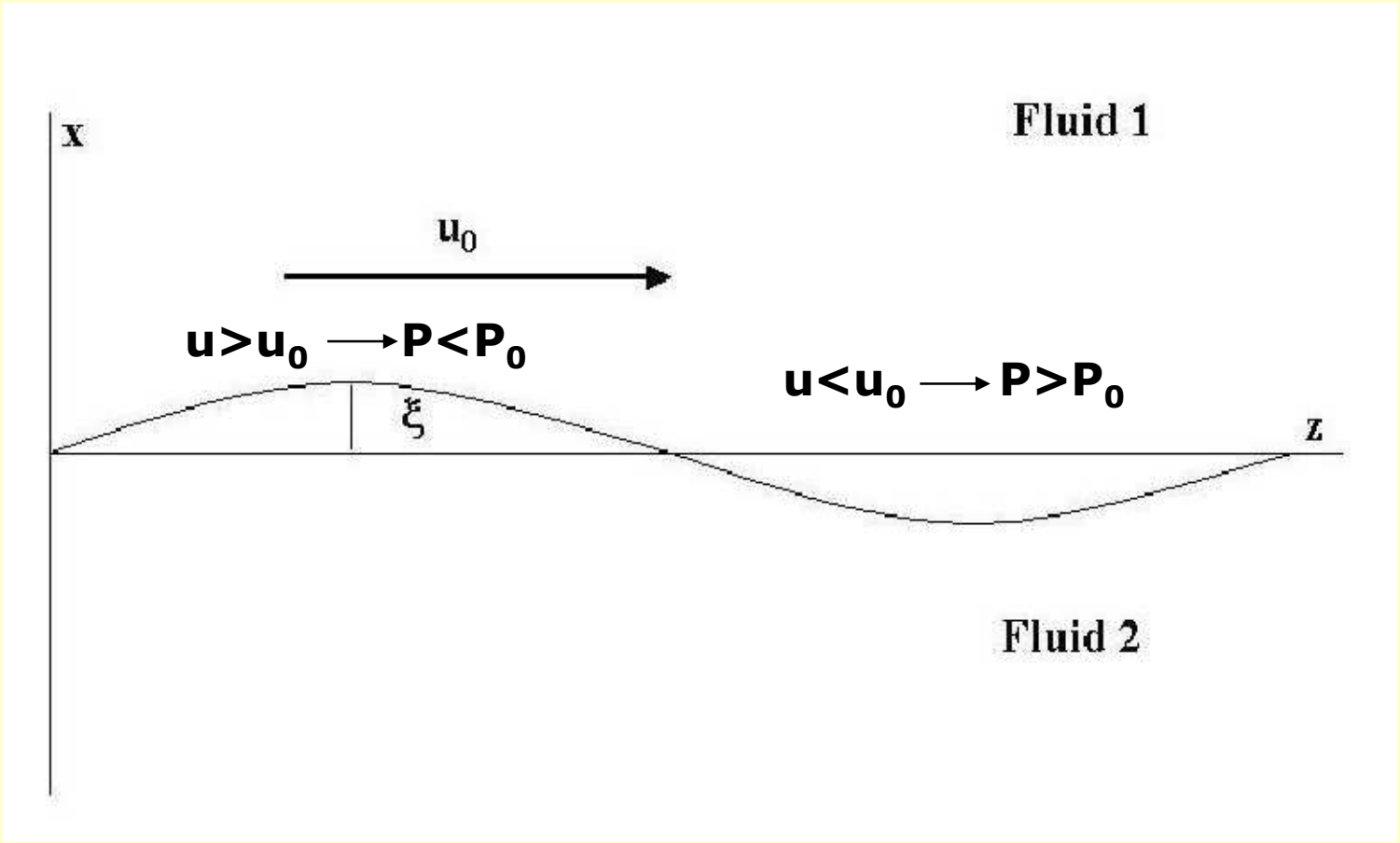

The linear stability analysis

Qualitative interpretation:

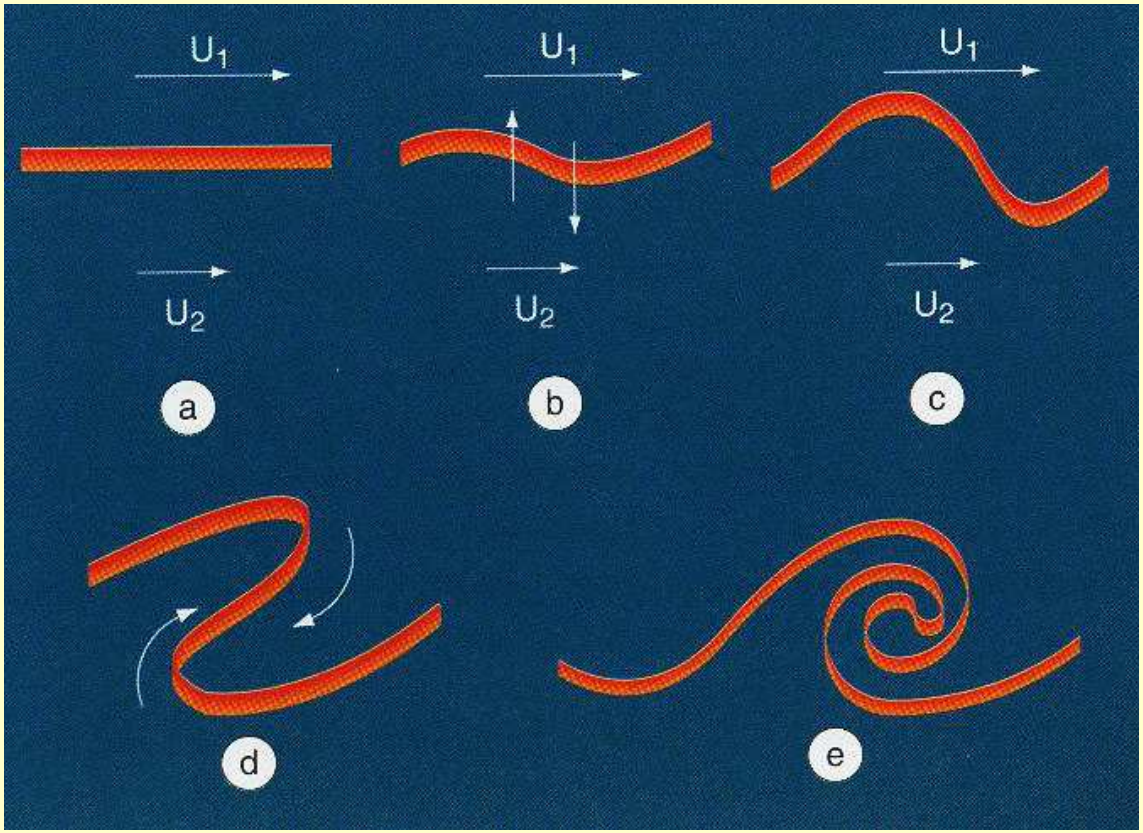

The linear stability analysis

Linearize the HD equations:

$$\frac{\partial \rho_1}{\partial t} + \rho_0 \nabla \cdot \vec{u}_1 + \vec{u}_0 \cdot \nabla \rho_1 = 0$$

$$\rho_0 \frac{\partial \vec{u}_1}{\partial t} = -\nabla p_1$$

$$\frac{\partial p_1}{\partial t} + (\vec{u}_0 \cdot \nabla) p_1 - \Gamma \frac{p_0}{\rho_0} \left[\frac{\partial \rho_1}{\partial t} + (\vec{u}_0 \cdot \nabla) \rho_1 \right] = 0$$

$$c_s^2 = \Gamma \frac{p_0}{\rho_0}$$

The linear stability analysis

Plane-wave analysis:

$$\left|\vec{u}_1\right|, \rho_1, p_1 \propto \exp\left\{ i\left(\vec{k}\cdot\vec{r} - \omega t\right)\right\}$$

Temporal analysis: ω complex and k real
Temporal analysis: ω real and k complex

After imposing the pressure equilibrium across the interface and the continuity of the displacement of the surface separating the two fluids one obtains the:

Dispersion relation $D(\omega, k)=0$

The linear stability analysis

Planar flow ⟶ algebraic DR (temporal)

$$\Omega = k_z u_0 - \omega, \quad q_1 = \pm\left(k_z^2 - \frac{\Omega^2}{c_s^2}\right)^{\frac{1}{2}}, \quad q_2 = \pm\left(k_z^2 - \frac{\omega^2}{c_s^2}\right)^{\frac{1}{2}}$$

$$D(\omega, k_z) = \Omega^2 q_2 - \omega^2 q_1 = 0$$

Unstable solutions are:

$$\phi = \frac{M}{2} + i\left[\left(M^2+1\right)^{\frac{1}{2}} - \left(\frac{M^2}{4}+1\right)\right]^{\frac{1}{2}}$$

with $\phi = \dfrac{\omega}{k_z c_s}$, $M = \dfrac{u_0}{c_s}$

The linear stability analysis (planar)

Growth rate behaviour:

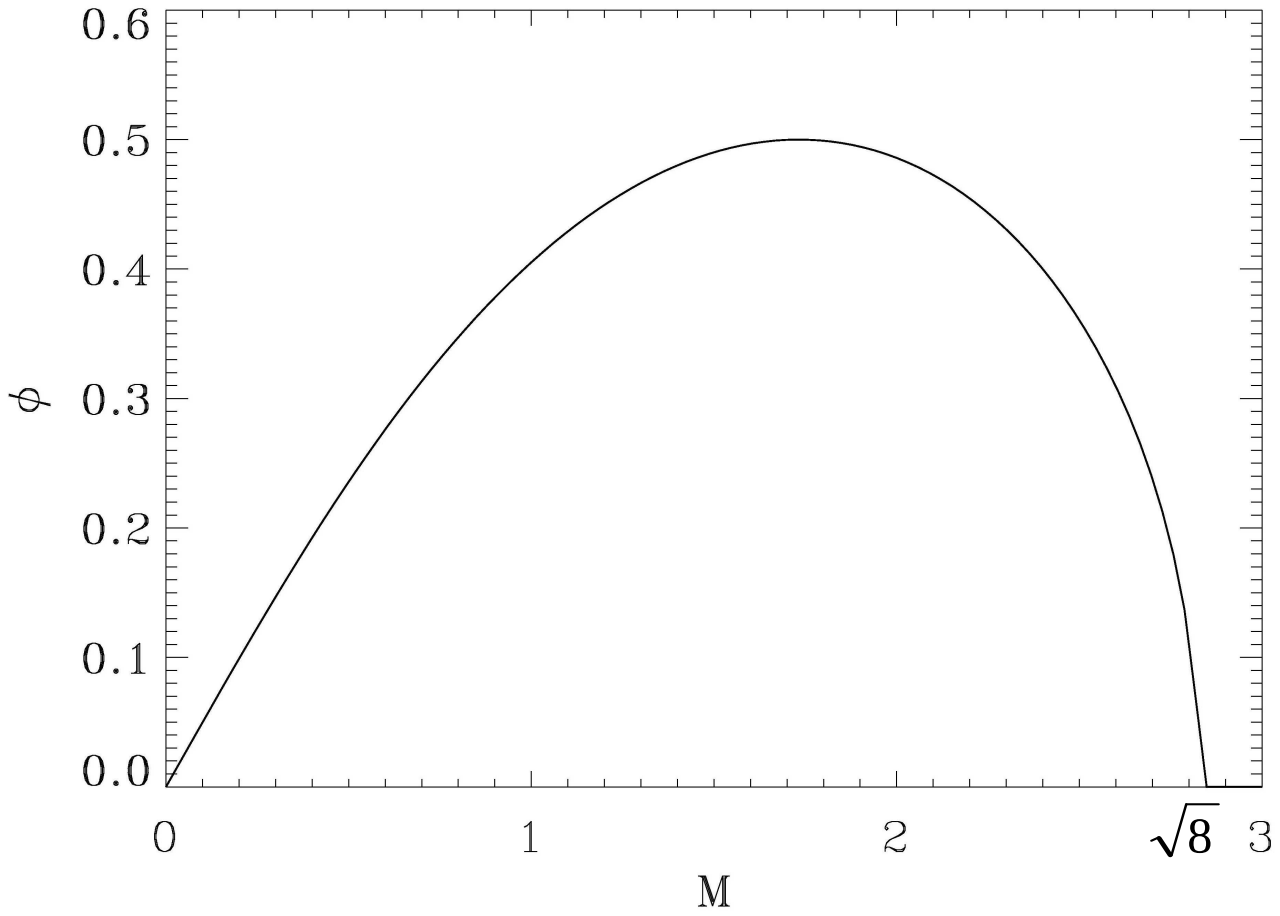

The linear stability analysis (planar)

The limit $M \ll 1$, incompressible flow:

$$\phi = \frac{M}{2}\left(1 \pm i\right)$$

Always unstable against KHI.

For $M > \sqrt{8}$ the two roots become real and the perturbations become travelling sound waves.

Effect of a magnetic field

Longitudinal:decrease in the growth rates (Fig.)
Transverse: no effect if $M \rightarrow u_0 / \sqrt{\left(c_s^2 + v_A^2\right)}$
(Trussoni 2007)

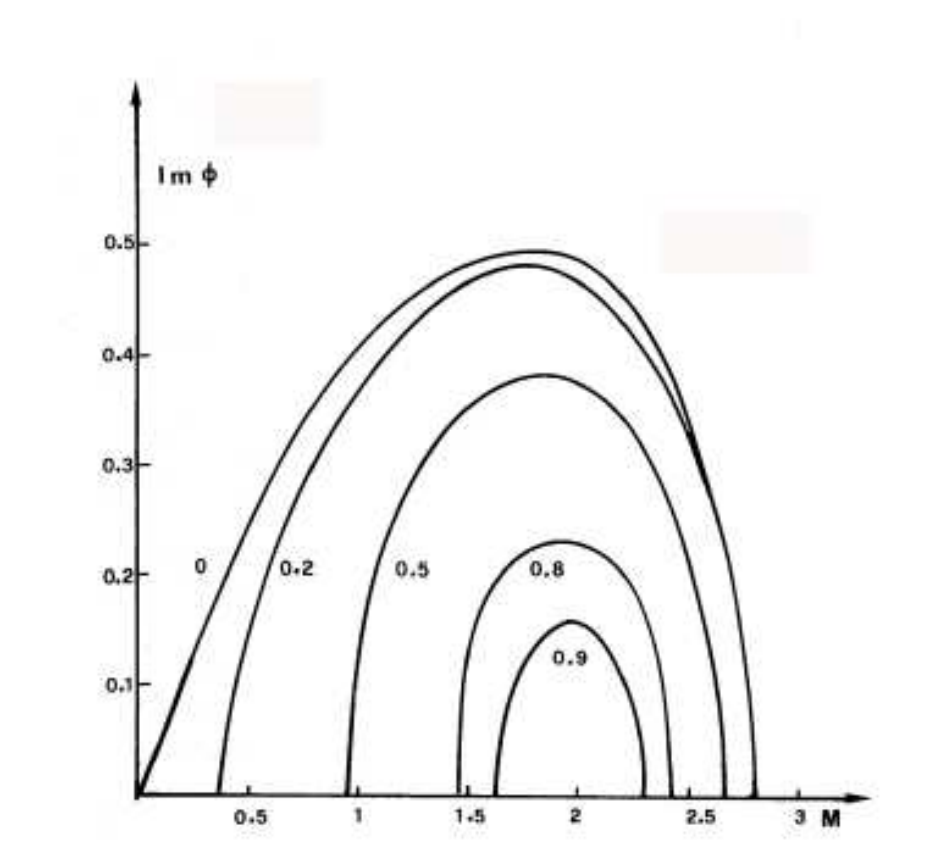

In cylindrical geometry the DR is:

$$(\phi - M)\Delta_e \frac{H_n'^{(1)}(ka\Delta_e)}{H_n^{(1)}(ka\Delta_e)} - \phi\Delta_i \frac{J_n'(ka\Delta_i)}{J_n(ka\Delta_i)} = 0$$

$$\Delta_i^2 = (\phi - M)^2 - 1, \quad \Delta_e^2 = (\phi^2 - \nu) - \nu, \quad \nu = \frac{\rho_i}{\rho_e}$$

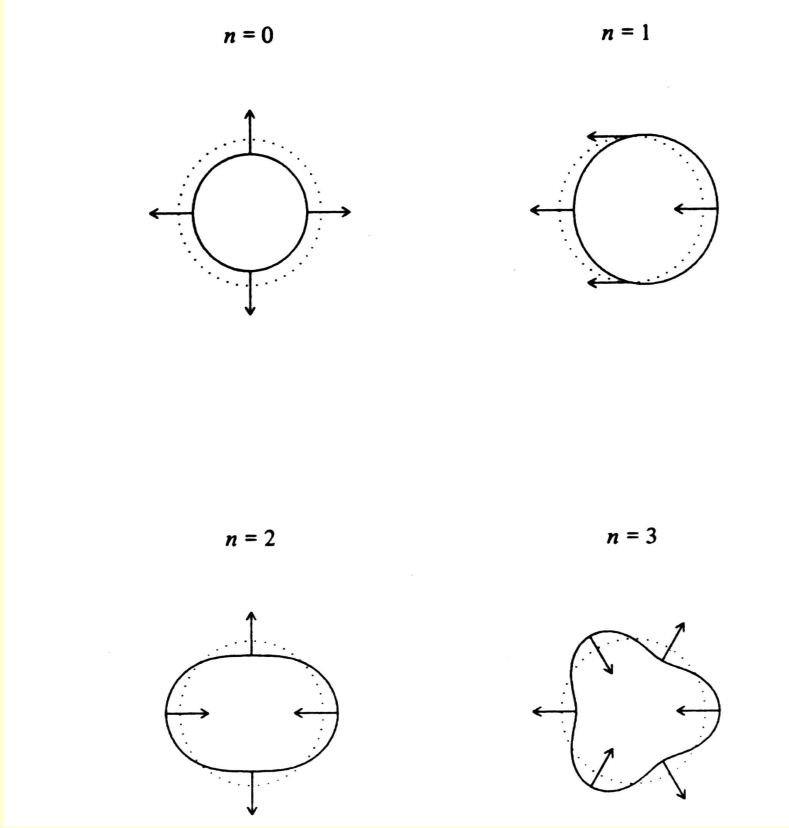

The linear stability analysis

Ordinary (surface) modes:

1. decay with distance from the shear
2. non propagating

Reflected (body) modes:

1. unstable for $M \gtrsim 2$
2. propagating as sound waves or MHD waves
3. interest the whole space

The linear stability analysis

Growth times of the most unstable modes:

$$\tau_{KH} = \psi_1 \tau_c \frac{\lambda_0}{R_j} \qquad \left(\lambda_0 \approx 2\pi R_j M_j \,, \quad \tau_c = \frac{2R_j}{c_{si,A}} \right)$$

Growth lengths of the most unstable modes:

$$\lambda_{KH} = \psi_2 c_{si,A} M_j \tau_{KH}$$

$\psi_1, \psi_2 \geq 1$ **(depend on theoretical details)**

The nonlinear evolution

Ordinary (surface) modes ($M=1$):

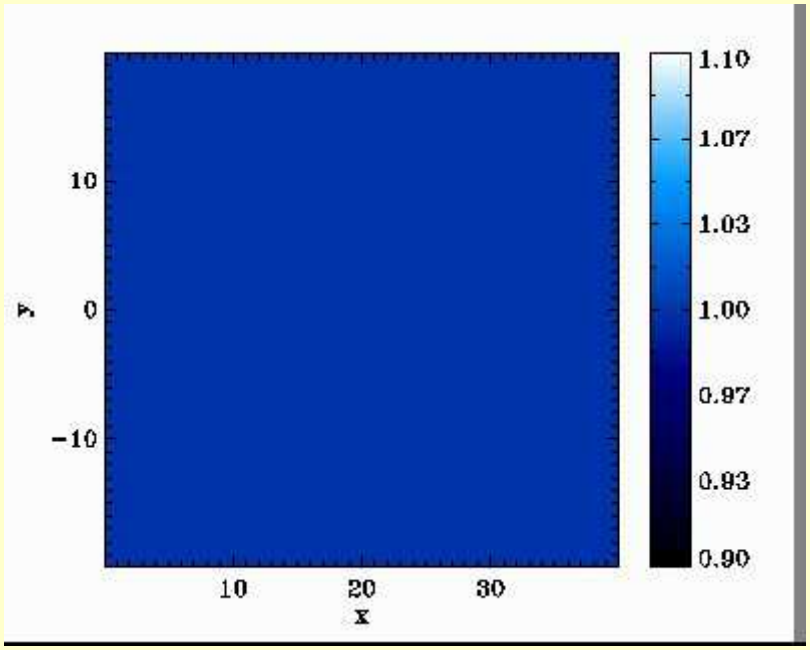

The nonlinear evolution

Reflected (body) modes ($M=3$):

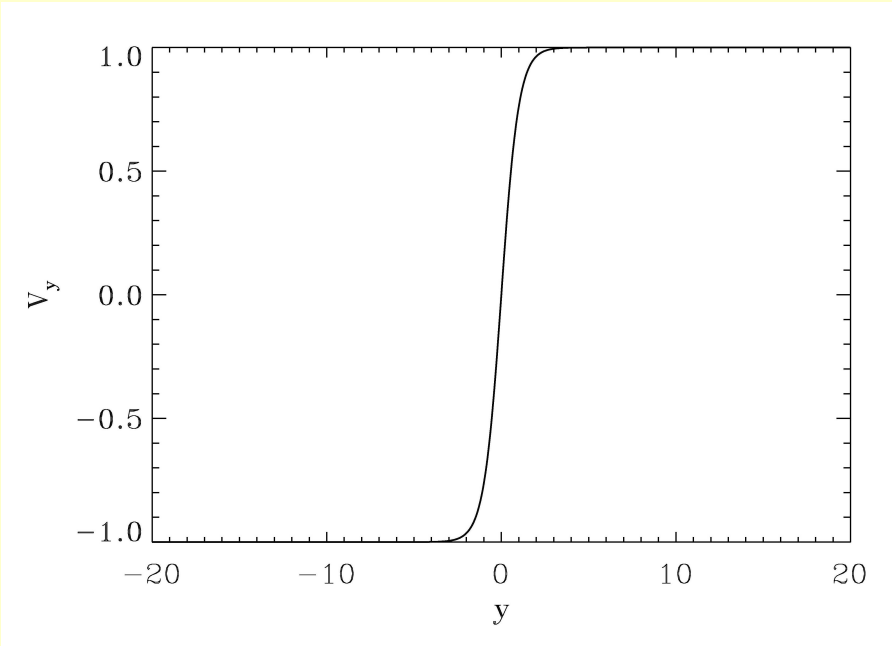

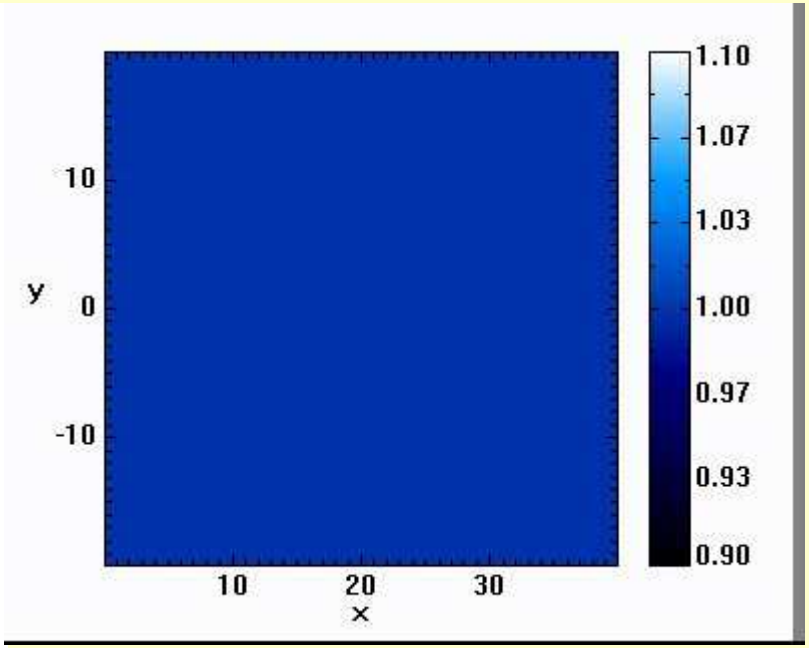

The nonlinear evolution

Reflected (body) modes ($M=3$) in cylindrical geometry:

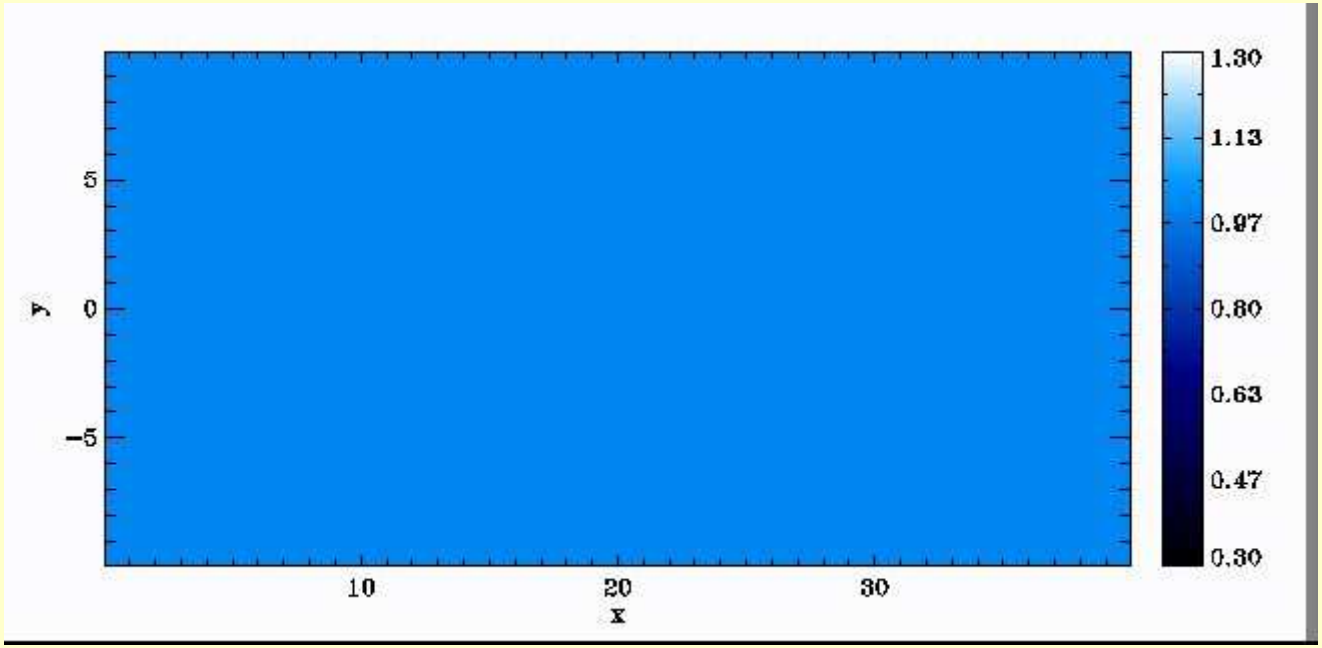

Responsible of the knots along the jets?

Jet instabilities and braking in FRIs

3D nonlinear evolution of Kelvin-Helmholtz instabilities in relativistic hydro jets (Rossi et al. 2008). Relativistic equation set:

$$\frac{\partial}{\partial t}\begin{pmatrix} \rho\gamma \\ w\gamma^2 v_k \\ w\gamma^2 - p \\ \rho\gamma f \end{pmatrix} + \sum_i \frac{\partial}{\partial x_i}\begin{pmatrix} \rho\gamma v_i \\ w\gamma^2 v_k v_i + p\delta_{ki} \\ w\gamma^2 v_i \\ \rho\gamma f v_i \end{pmatrix} = 0$$

p=gas pressure, w=enthalpy, ρ=rest mass density, γ=Lorentz factor, f =tracer

Parameter space:

Case	γ	M	η	pts/beam	$L_x \times L_y \times L_z$	$N_x \times N_y \times N_z$
A	10	3	10^2	20	$50 \times 150 \times 50$	$324 \times 1200 \times 324$
B	10	3	10^4	20	$60 \times 75 \times 60$	$344 \times 600 \times 344$
C	10	3	10^4	12	$50 \times 75 \times 50$	$172 \times 300 \times 172$
D	10	30	10^4	20	$50 \times 150 \times 50$	$324 \times 1050 \times 324$
E	10	30	10^2	12	$24 \times 200 \times 24$	$144 \times 560 \times 144$

η = ambient-to-jet (proper) density ratio

M = Mach number, homogeneous ambient medium

Non-axial perturbation introduced at the jet inlet. The temporal evolution of the system studied numerically with the code PLUTO (Mignone et al. 2007, PPM module)

Numerical simulations: Results

- The dominant parameter in determining the instability evolution and the entrainment properties is the ambient-to-jet density contrast η.
- Lighter jets suffer stronger slowing down in the external layer that in the central part
- Presence of a central spine at high Lorentz factor

$$\frac{\rho_{amb}}{\rho_{jet}} = 10^4, \quad M = \frac{v_j}{c_s} = 3, \quad \gamma = 10$$

Lorentz factor distribution

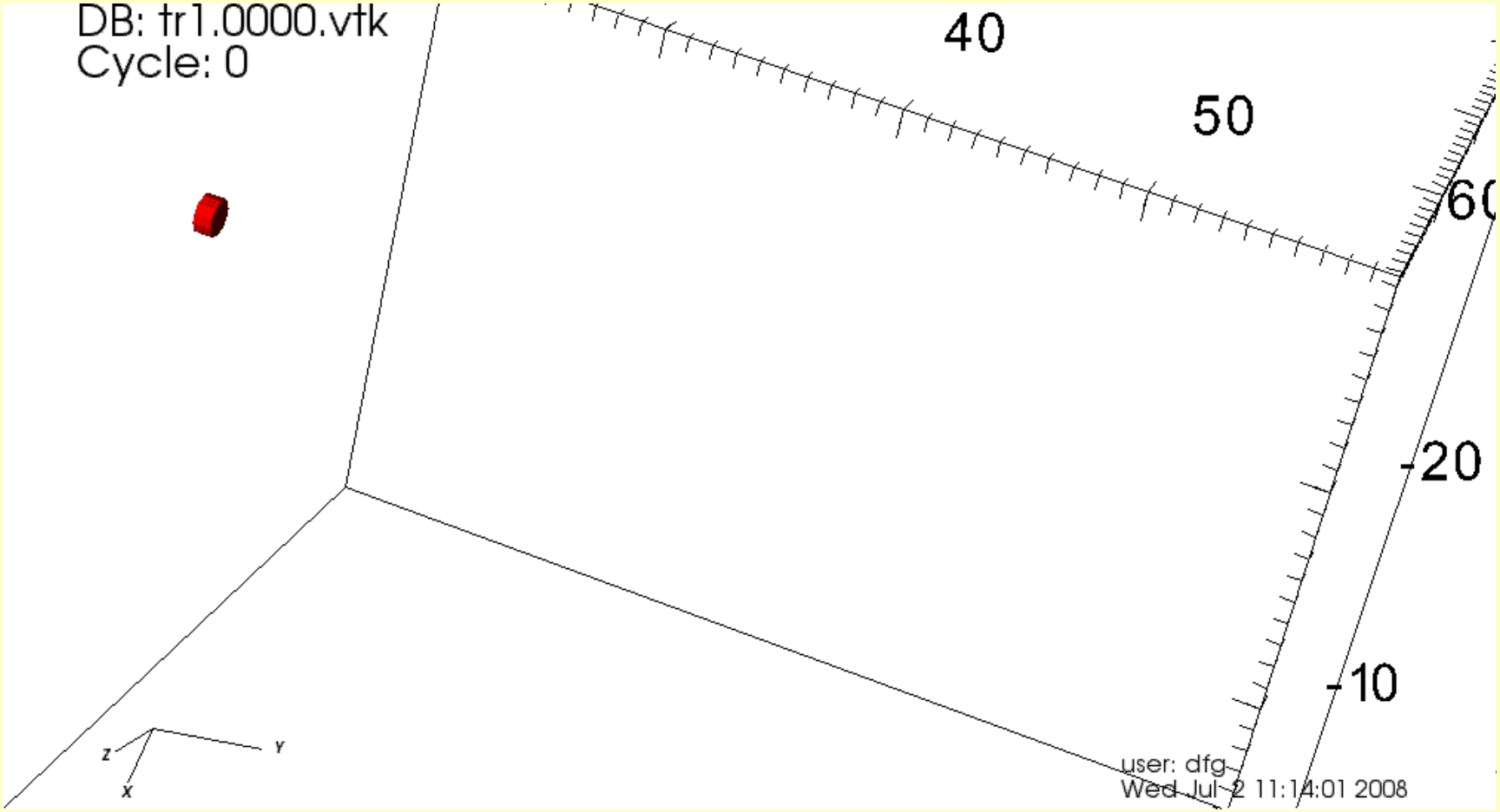

Longitudinal behavior of maximum and averaged Lorentz factor (at VLBI scales) vs distance:

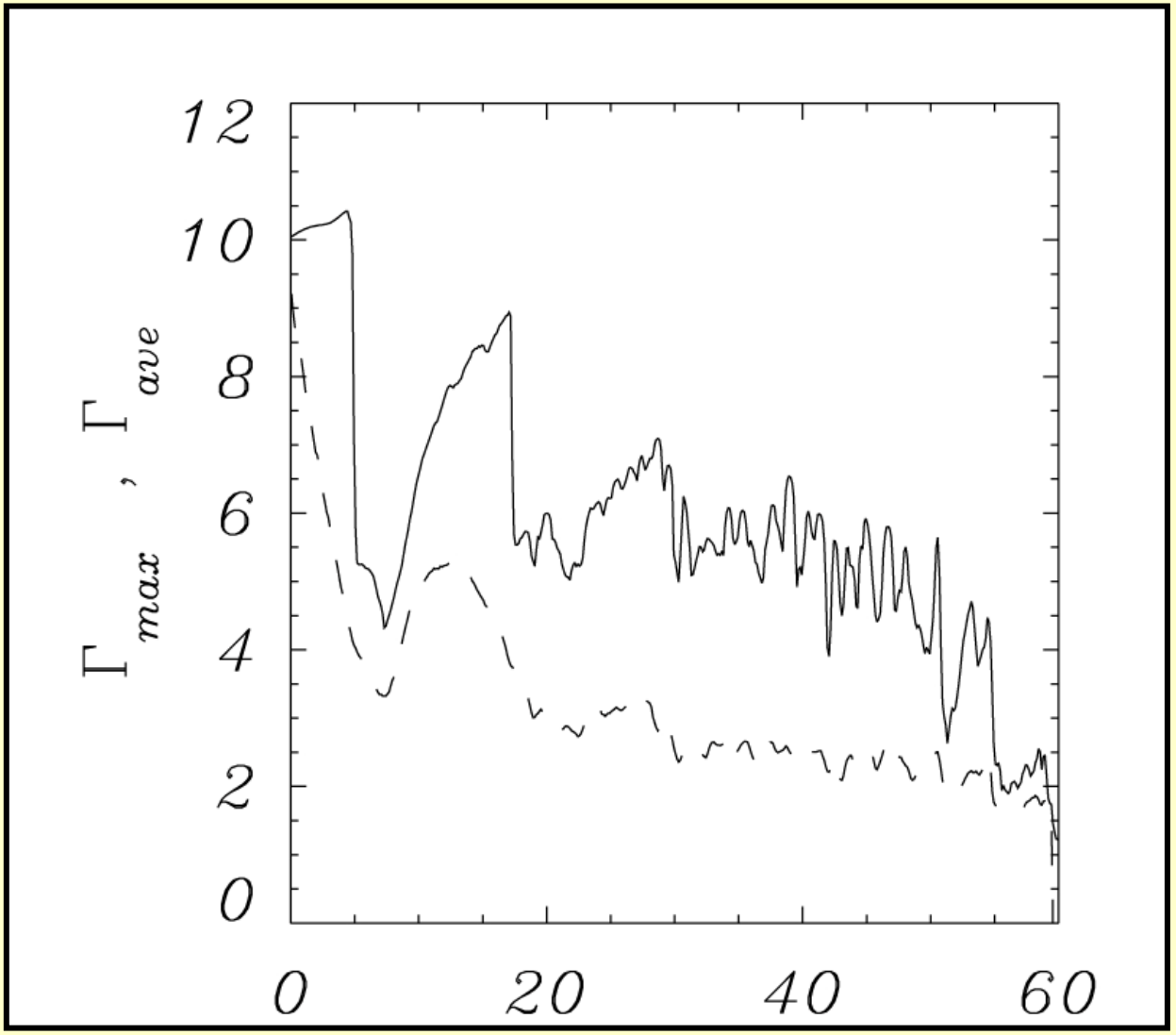

"Spine-layer" structure formation:

Layer: Jet mass at $\gamma\beta \sim 0.2$

Spine: Jet mass at $\gamma\beta \sim 5$

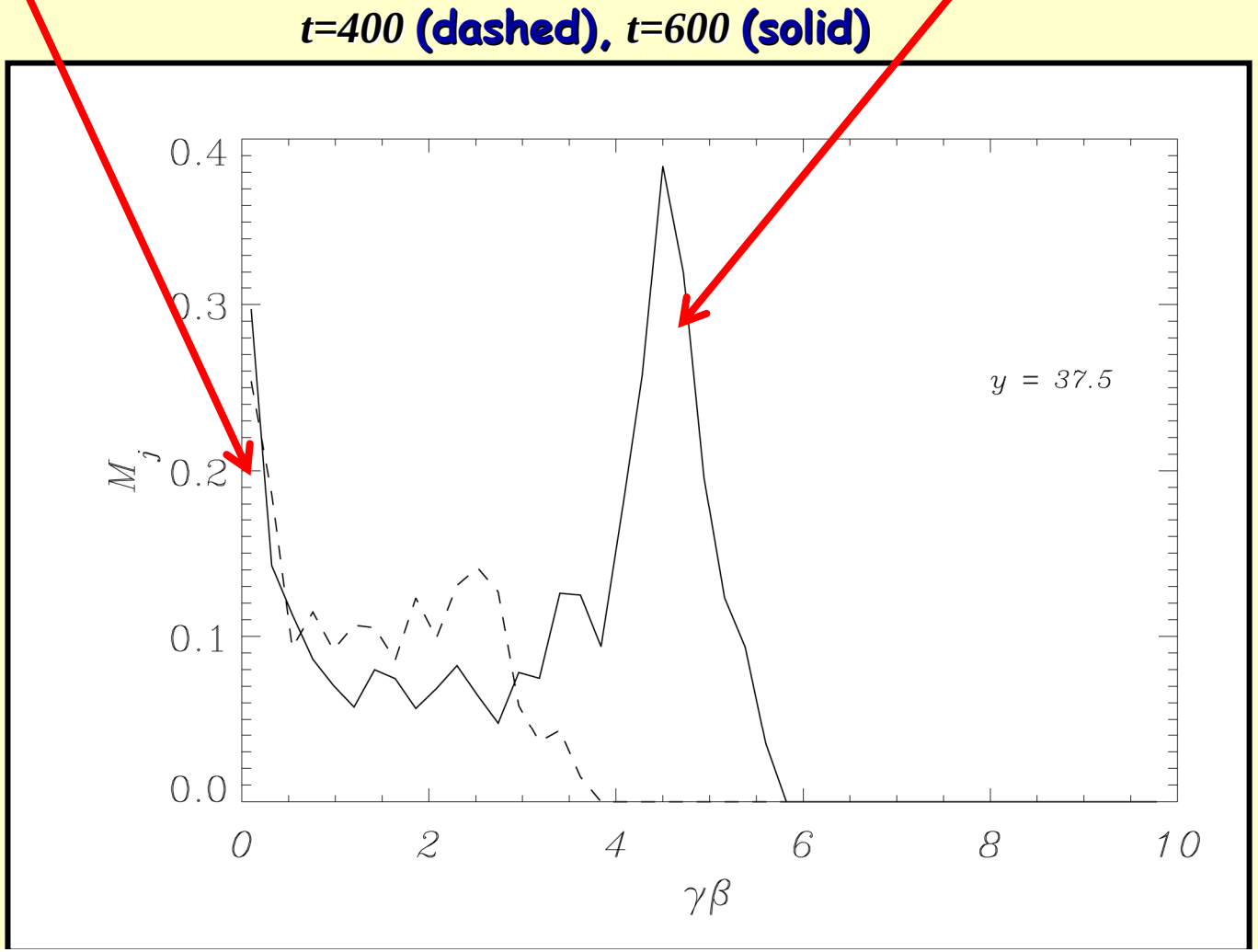

"Spine-layer" structure formation: synthetic VLBI maps = radio emissivity ∝ proper density × $\delta^{-(2+\alpha)}=[\gamma(1-\beta\cos\theta)]^{-(2+\alpha)}$

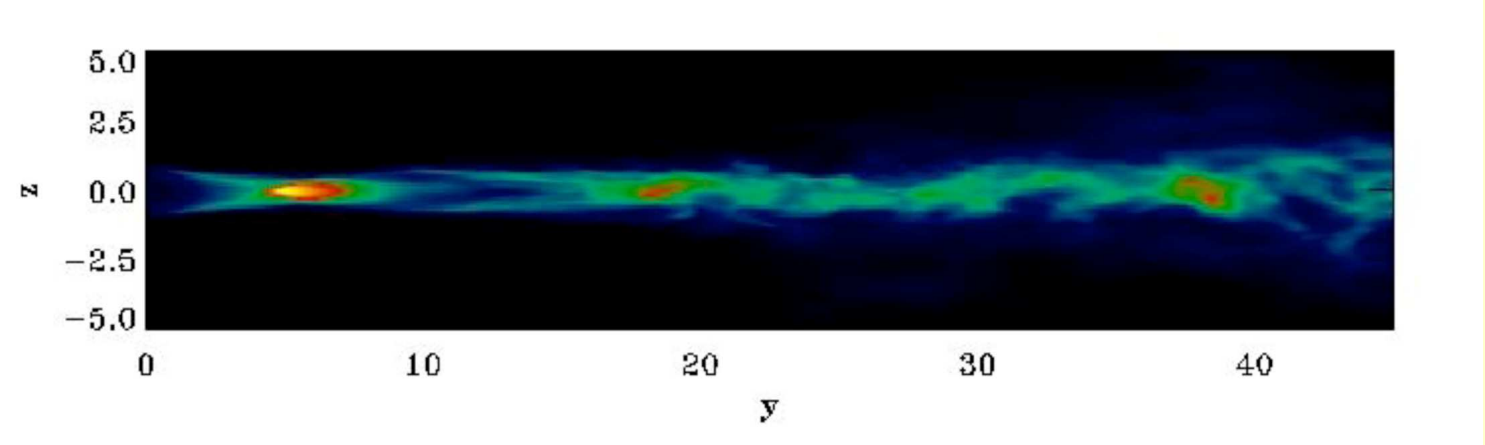

$\theta = 20°$: **Spine boosted**

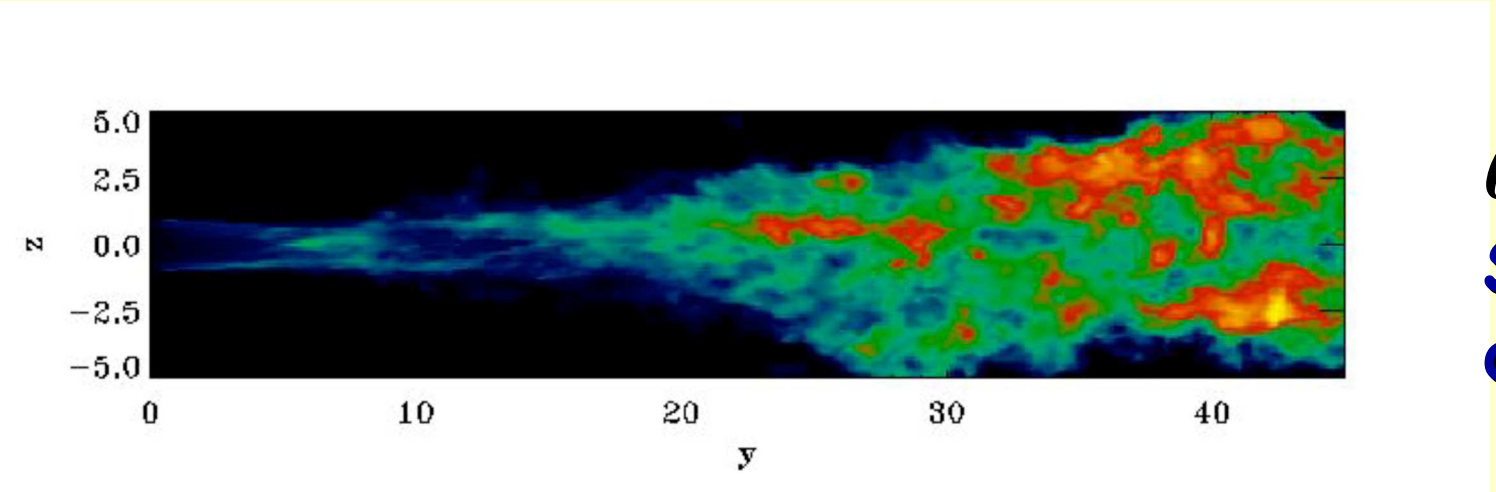

$\theta = 60°$: **Spine deboosted**

- KHI in low density jets would produce jet braking and limb brightening at VLBI scales
- This is consistent with the low kinetic power of FRI sources (e.g. Celotti 2003). The critical kinetic power:

$$P_j^* \approx 10^{44}\left(\frac{r_j}{1pc}\right)^2\left(\frac{\gamma}{10}\right)^2\left(\frac{n_{amb}}{1cm^{-3}}\right)\left(\frac{\eta^*}{10^3}\right)^{-1} \; erg\, s^{-1}$$

- FRI jets would have a density contrast ambient-to-jet exceeding 10^3

Effects of magnetic fields

Purely poloidal field:

- **behaviour similar to the RHD case**

$$M_A = \frac{v_j}{v_A} = 1.67 \rightarrow B \approx 10^{-4}\, G$$

Displacement current not negligible any longer

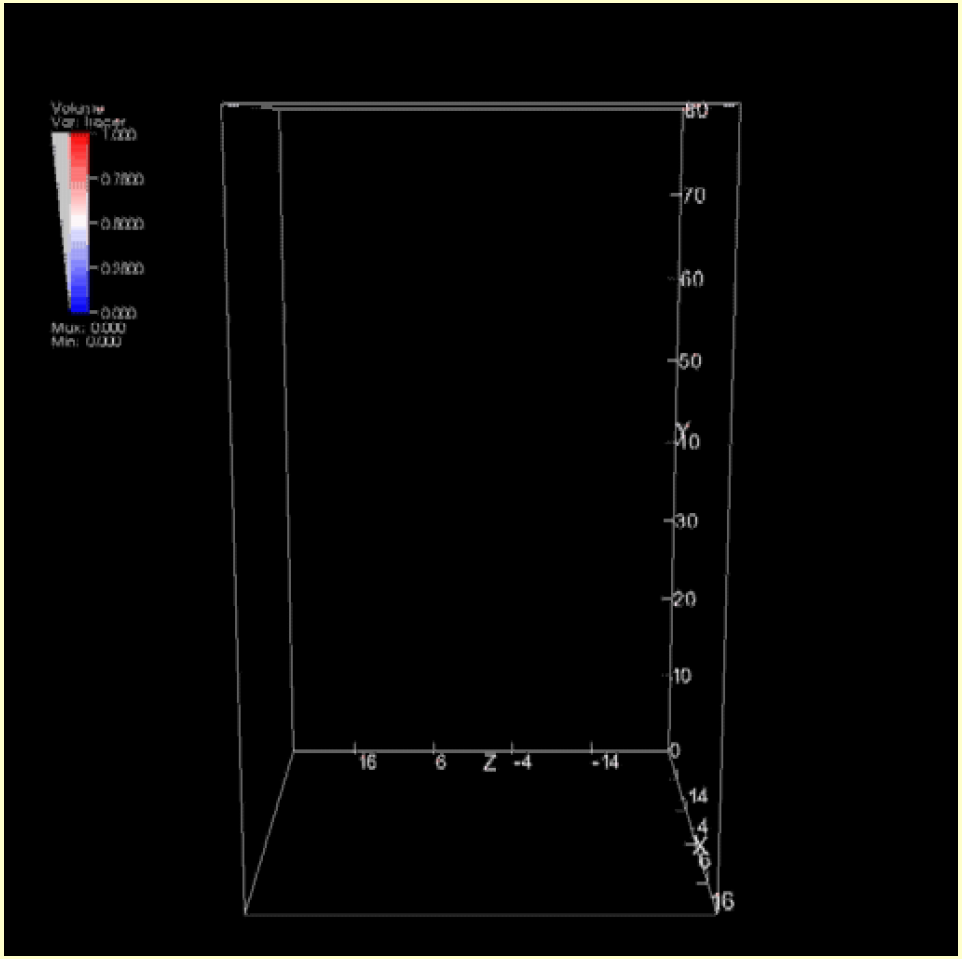

Purely toroidal field:

- kink instability induced wiggling
- shielding of the jet inner core, reducing the jet entrainment and braking

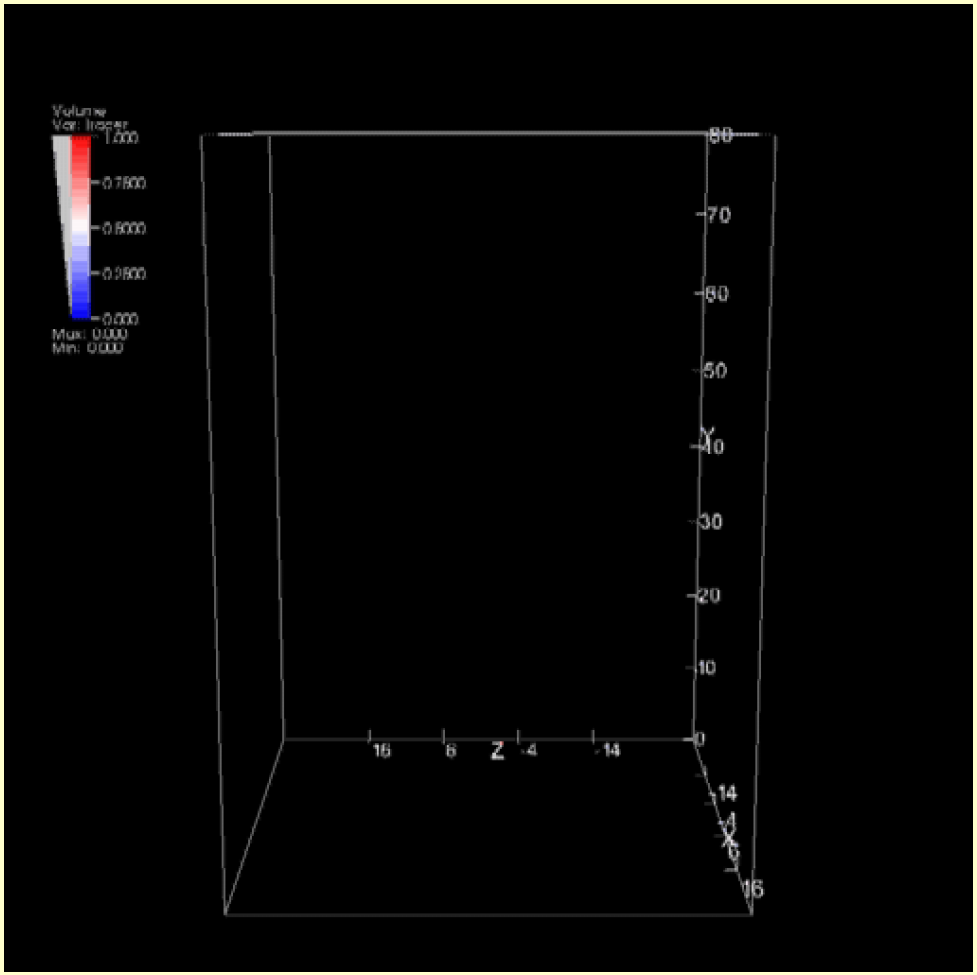

Kink instability

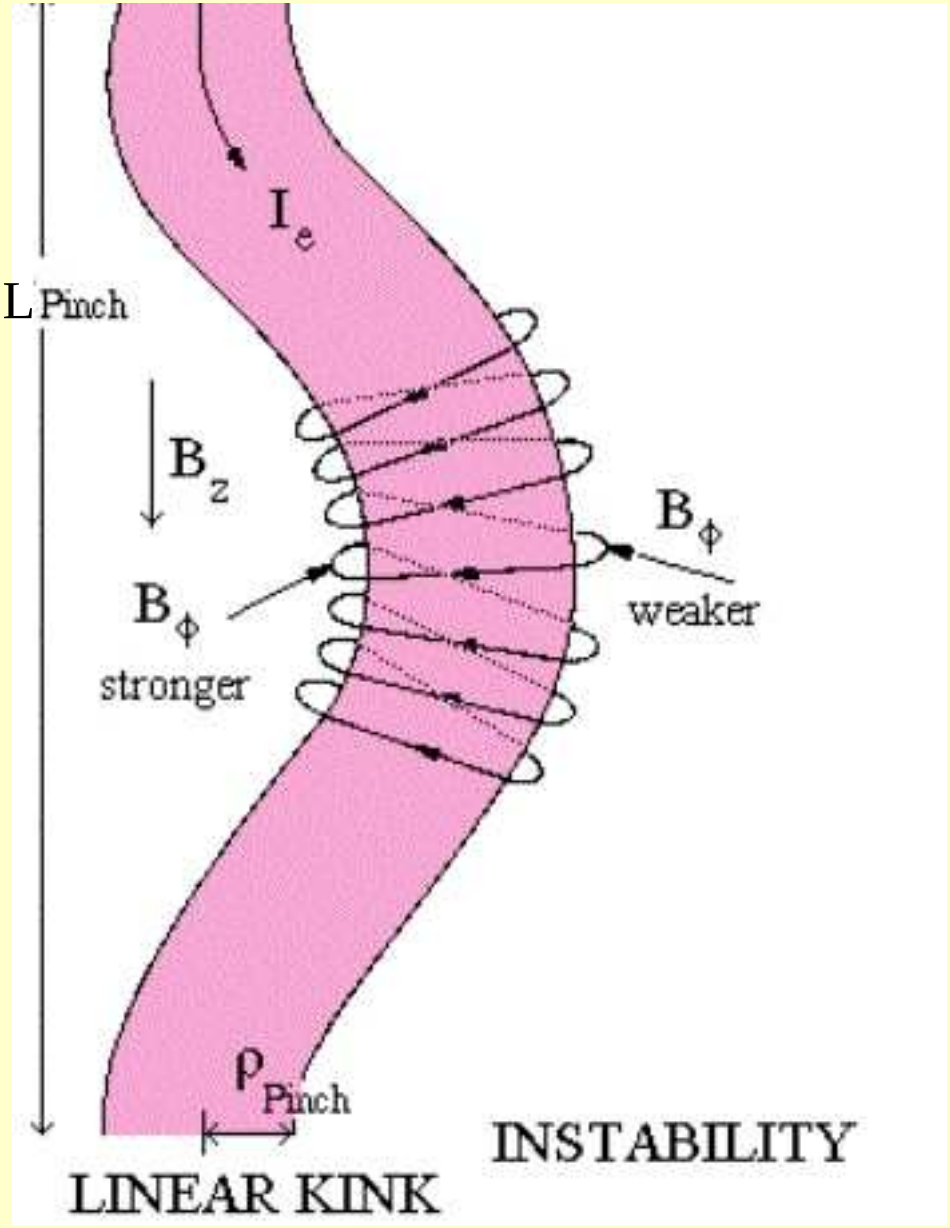

$$P_{B_\phi} \propto B_\phi^2$$

Purely toroidal field:

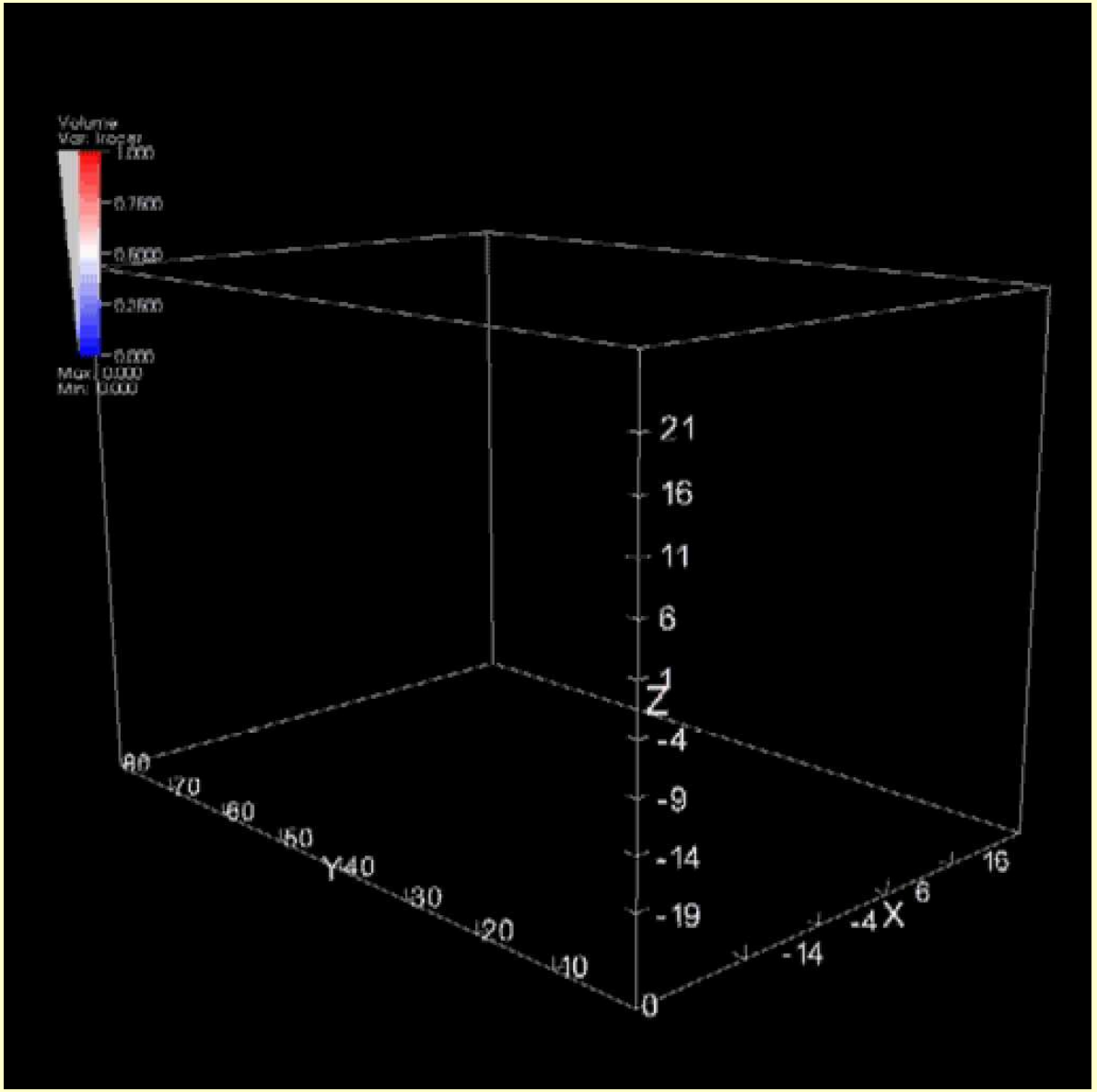

Effect of magnetic fields: jet axis displacement

RMHD

RHD

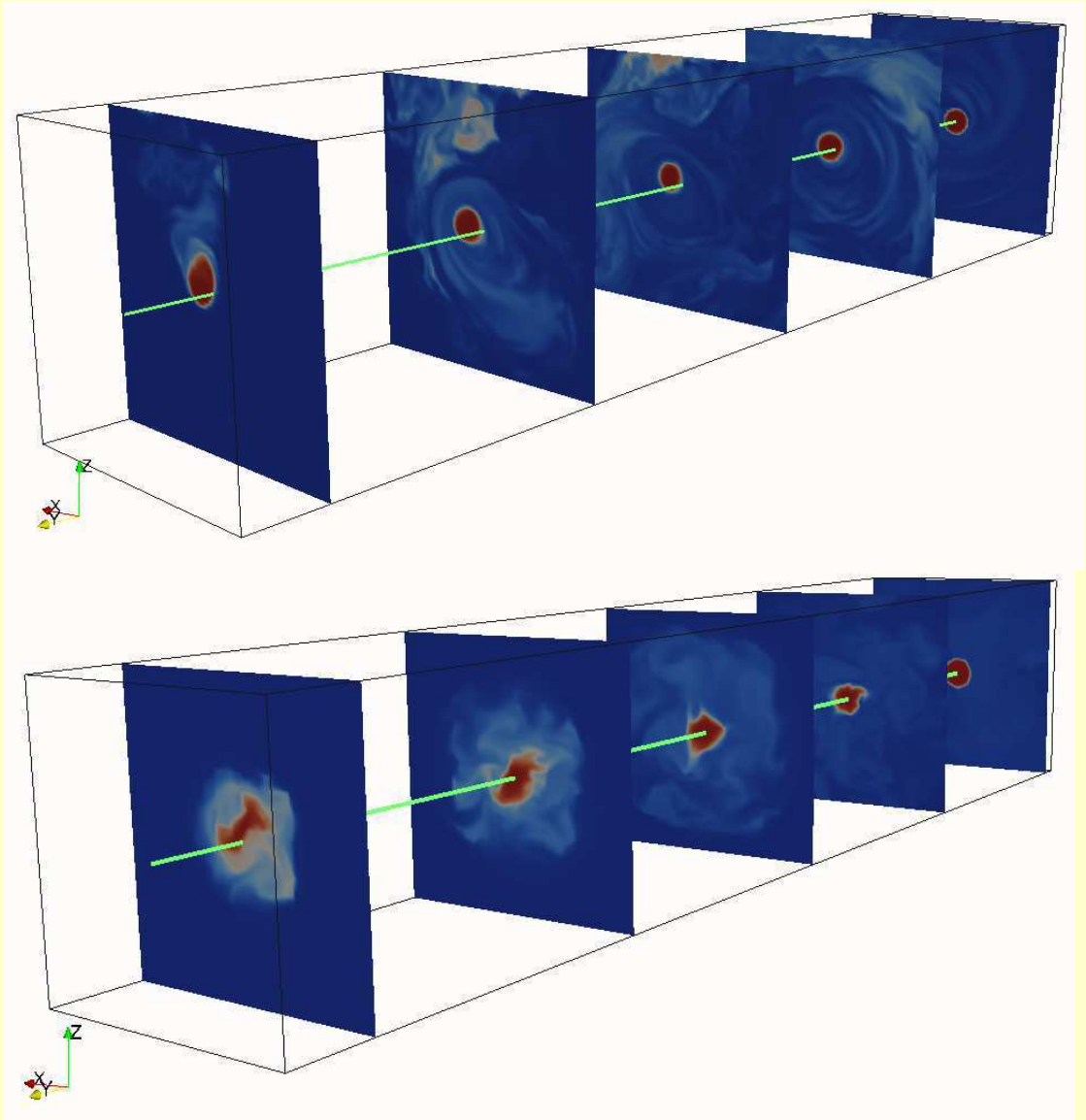

- **MHD acceleration of jets**

Jet acceleration

- Jet energy extracted from the rotating SMBH (Blandford & Znajek 1977), need of a strong magnetic field threading the SMBH;

- Jet kinetic energy originating from the accretion energy (e.g. Blandford & Payne 1982):

MHD-wind acceleration models, driven by the mass accretion rate through a disk

Jet acceleration

1) Jet energy extracted from the rotating SMBH (Blandford & Znajek 1977): need of a strong magnetic field threading the SMBH (Livio et al. 1999), much larger than the inner disk field:

$$\frac{L_{BZ}(\max)}{L_{disk}(\max)} \approx \left(\frac{B_{pH}}{B_{pd}}\right)^2 \left(\frac{R_H}{R_{disk}}\right)^{3/2} a^2$$

$a \approx R_H \Omega_H / c$ BH spin parameter ($a^2 < 1$)

No reason to support this hypothesis.

Acceleration in jets

From the work done to produce cavities (Allen et al. 2006, Heinz et al. 2007):

$$W = \frac{\gamma}{\gamma - 1} PV \rightarrow L_{kin} = \frac{W}{t_{age}}$$

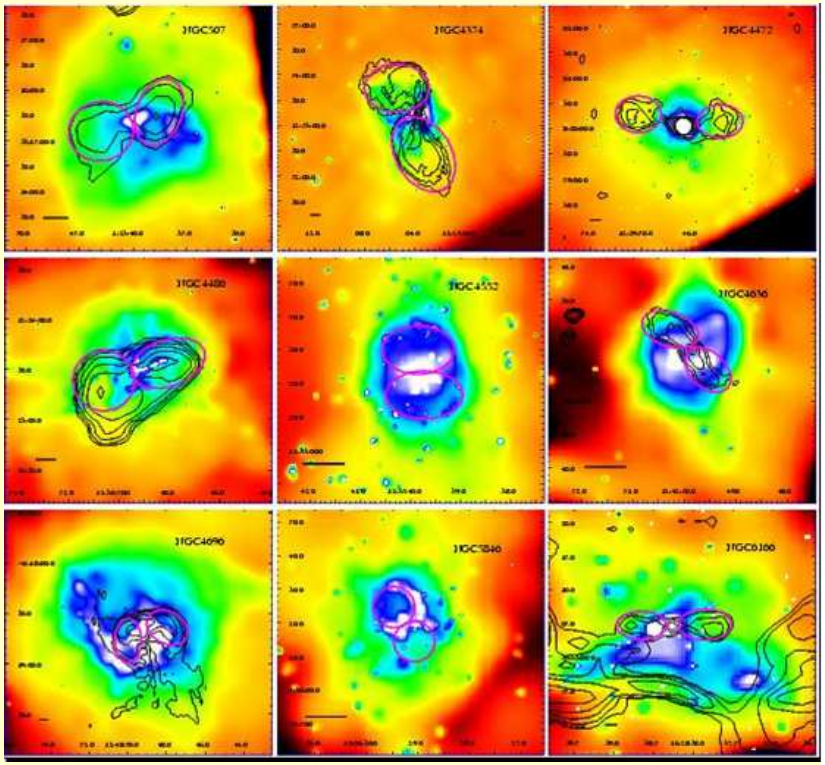

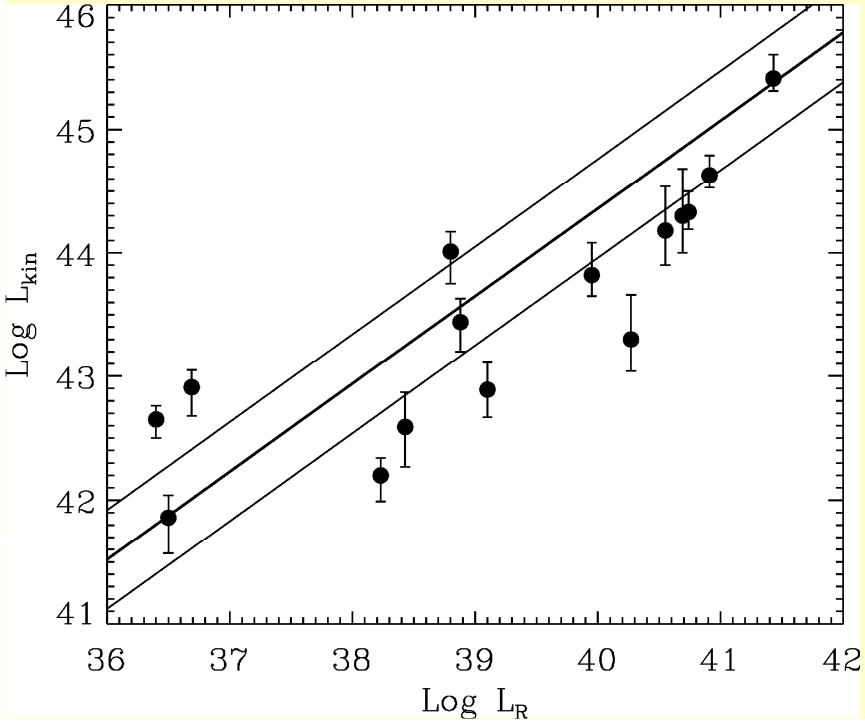

$$L_{kin} = 10^{37} \left(\frac{L_{\nu}^{core}}{7 \times 10^{22}} \right)^{12/17} \text{ W}$$

Accretion and jets

Correlation found between the accretion onto BH and the jet kinetic power (Allen et al. 2006, Heinz et al. 2007, Balmaverde et al. 2008) → Ordinary matter in the jet?

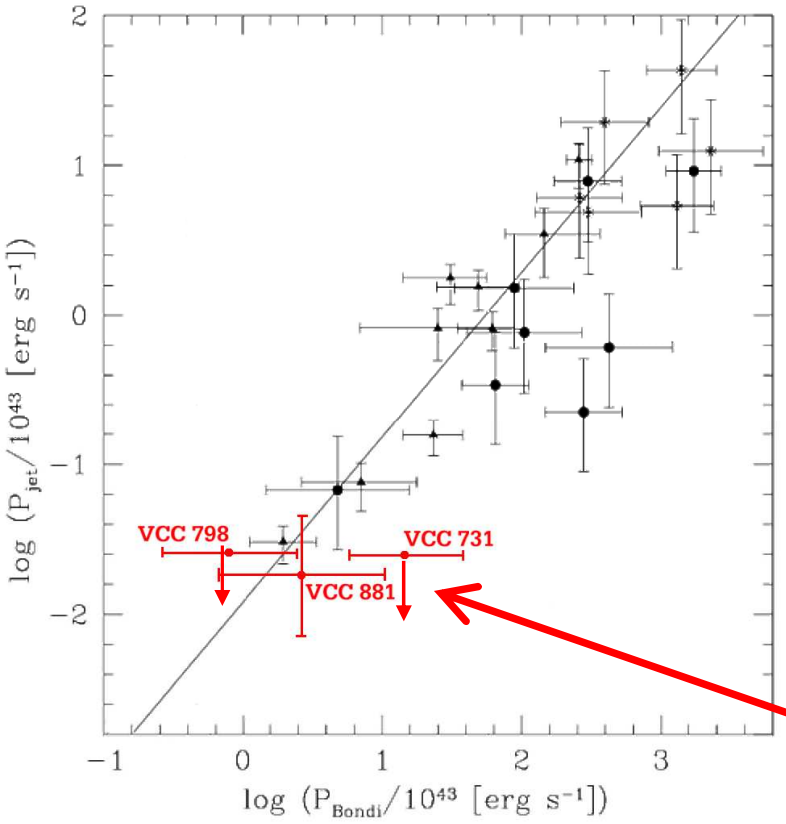

$$1)\ P_B = \dot{M}_B c^2, \quad \dot{M}_B = \frac{\pi G^2 \rho_B M_{BH}^2}{c_s^3}$$

$$2)\ P_j = 8.6\times10^{22} L_{radio\ core}^{12/17}\ erg\ s^{-1}, \quad \alpha_\nu = 0$$

(Jet power from Blandford & Koenigl 1979)

Radio quiet

Jet acceleration: classes of models

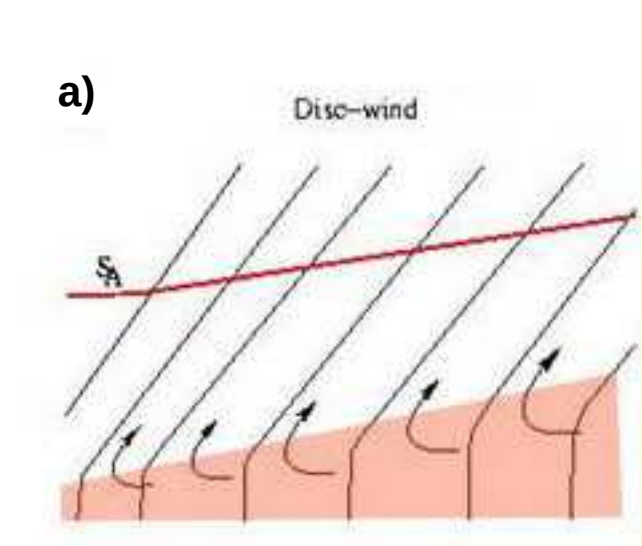

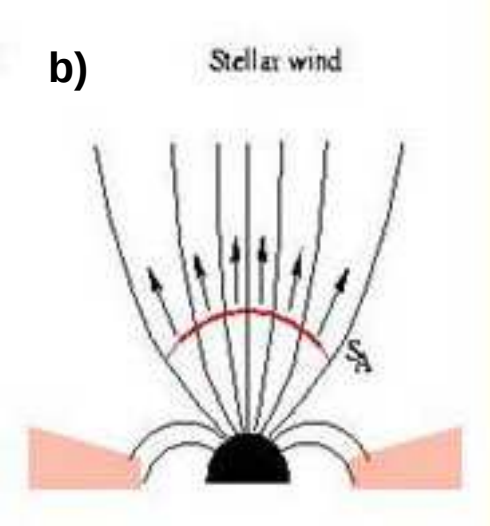

a) Disk-wind models
acceleration: centrifugal below the alfvènic surface, magnetic pressure gradient above
collimation: magnetic tension (hoop-stress)

b) "Stellar" wind models
acceleration: mostly due to pressure gradient
collimation: magnetic tension

Disk-wind jets: stationary models

Blandford & Payne (1982), Camenzind (1996)
Spruit (1996), Ferreira (1997)
Vlahakis et al. (2000)

No corotation

Corotation

Thin disk

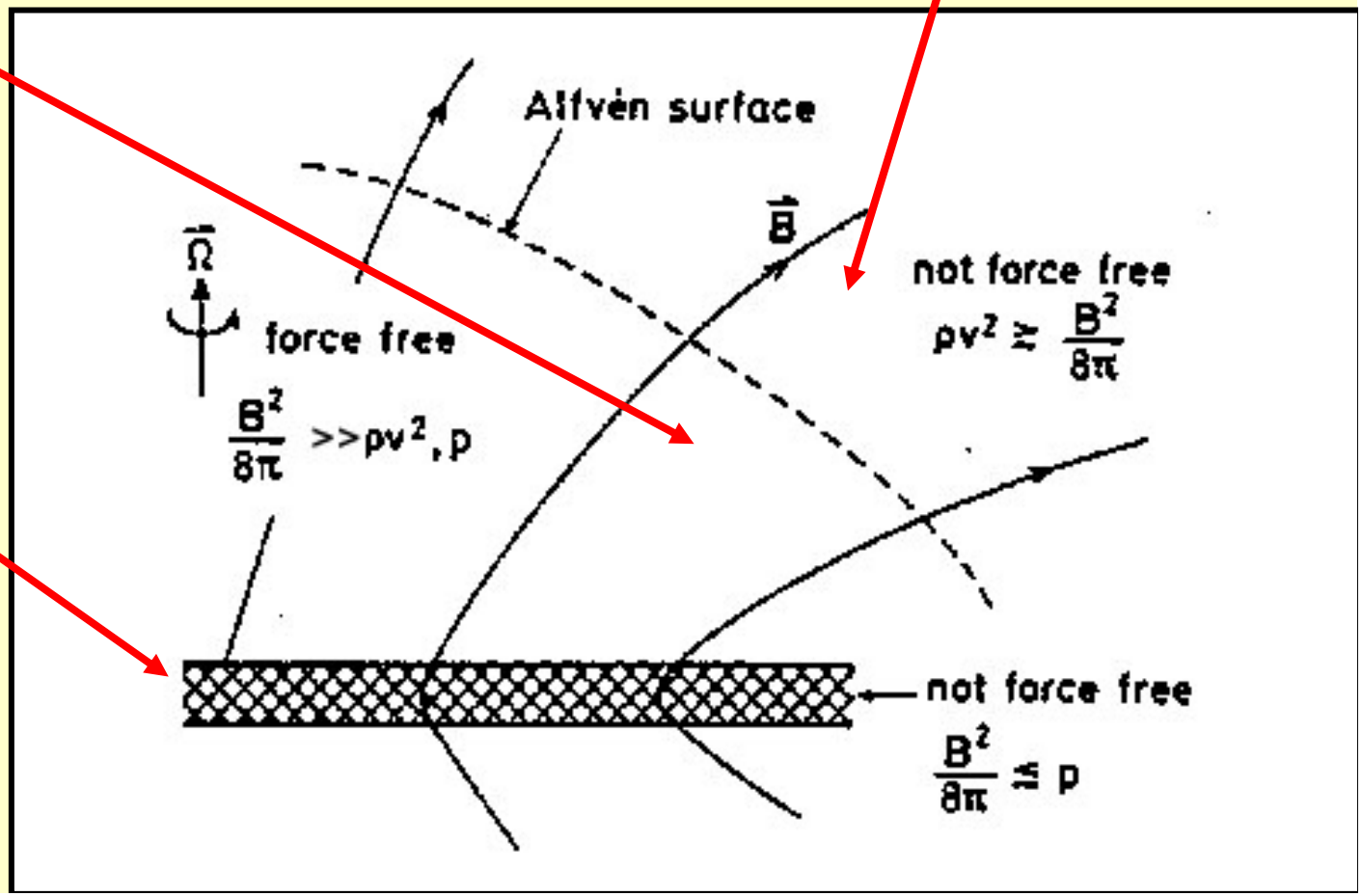

DW jets: launching mechanism

Bead-on-a-wire

Field line

Centrifugal force

1. $\Theta > 60^o$: no flow
2. $\Theta \leq 60^o$: wind
3. $\Theta << 60^o$: slow flow

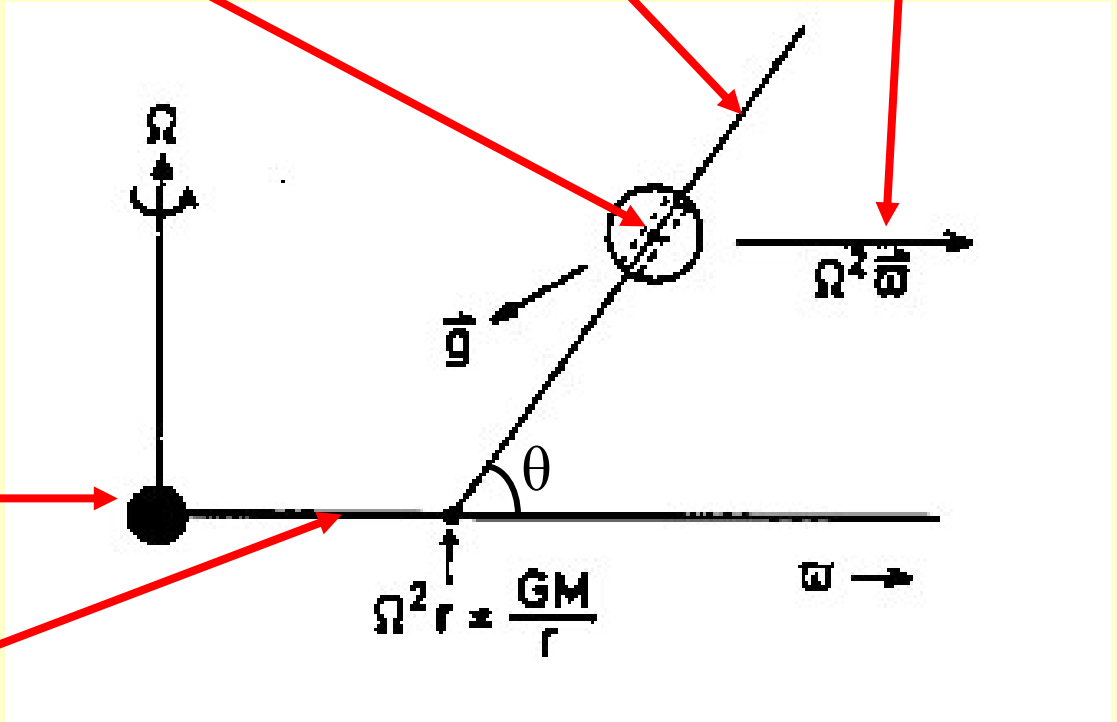

Central object

Disk

DW jets: launching mechanism

Collimation:
Magnetic tension
(Hoop-stress)

Acceleration:
Magnetic pressure
gradient

Acceleration:
centrifugal

Central object

Disk

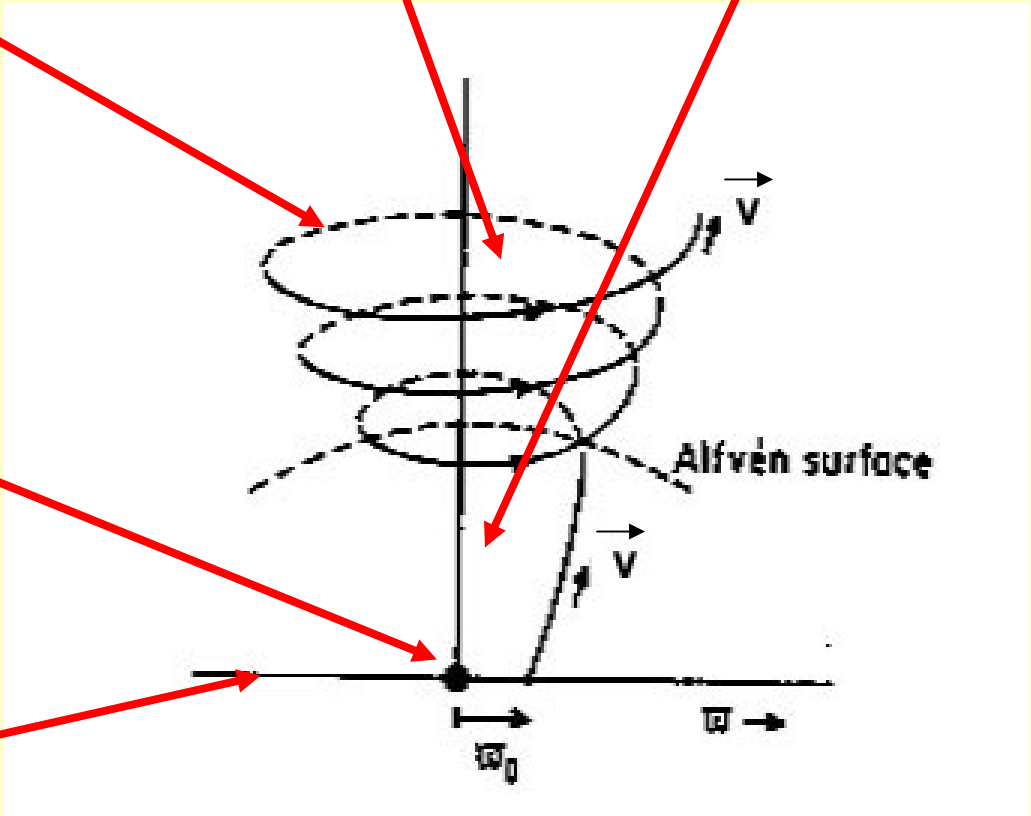

Analytical Approaches

- **The ideal, steady-state axisymmetric MHD equations have been solved by a non-linear separation of the variables**
- **Solutions are obtained by the assumption of self-similarity, which implies the invariance along one direction of the spherical coordinates (r, θ)**
- **The analytical models provide density and the velocity and magnetic field vectors as functions of (r, θ)**

  - Radially Self-Similar (a) ϖ_1 / ϖ_2 the same for any θ
  - Meridionally Self-Similar (b) ϖ_1 / ϖ_2 the same for spherical surfaces

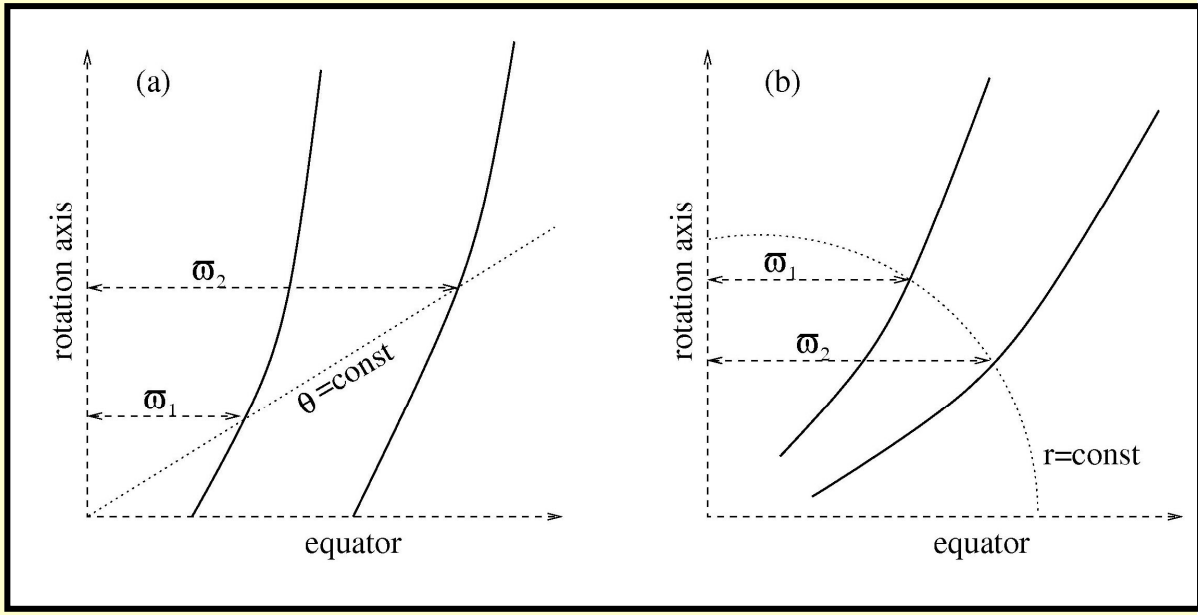

The solutions

The Radially Self Similar Models:

- describe a magneto-centrifugally disk wind
- they have conical critical surfaces (slow, Alfvèn, fast)
- however, they are singular at the axis
- they are derived with the polytropic assumption with a constant polytropic index

(Contopulos & Lovelace 1994, Ferreira 1997, Vlahakis et al. 2000)

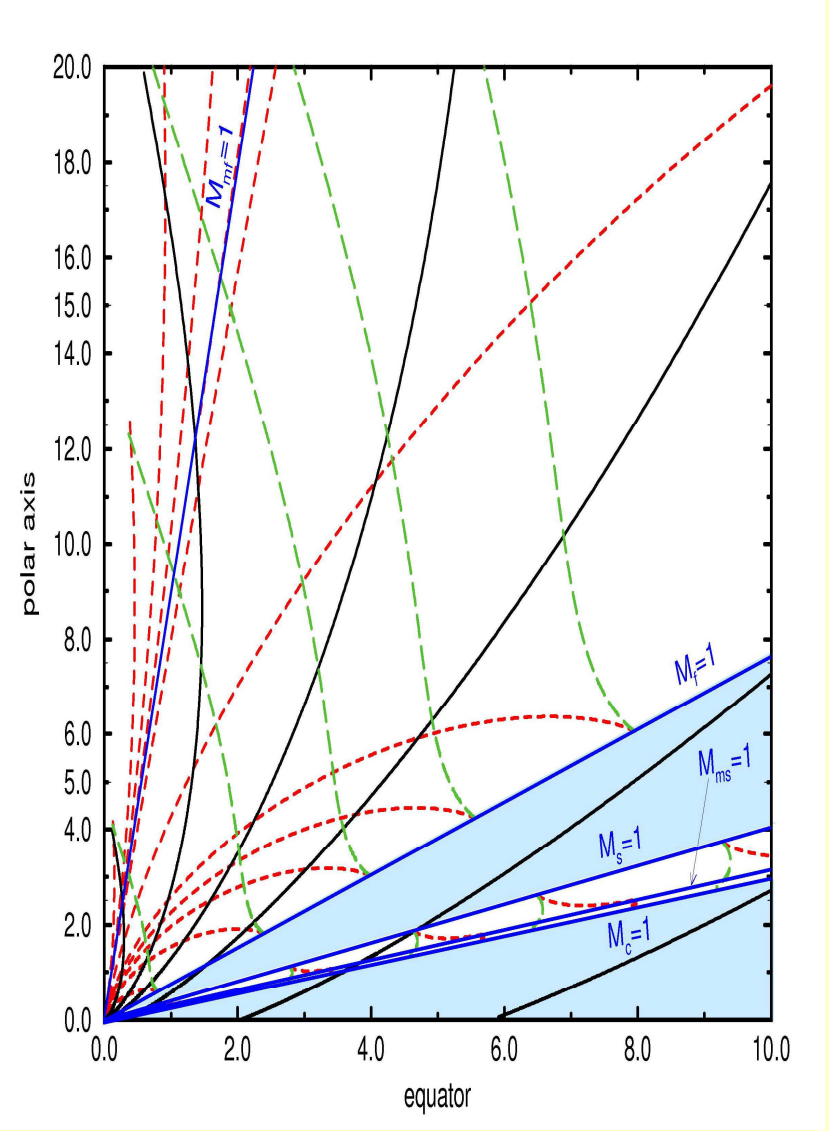

The solutions

Meridionally Self Similar Models:

- describe a thermally driven stellar outflow
- have spherical critical surfaces (slow, Alfvèn, fast)
- there are magnetic fieldlines not connected to the star surface
- they correspond to a variable effective polytropic index

(Sauty & Tsinganos 1994, Trussoni et al. 1997, Sauty et al. 2002)

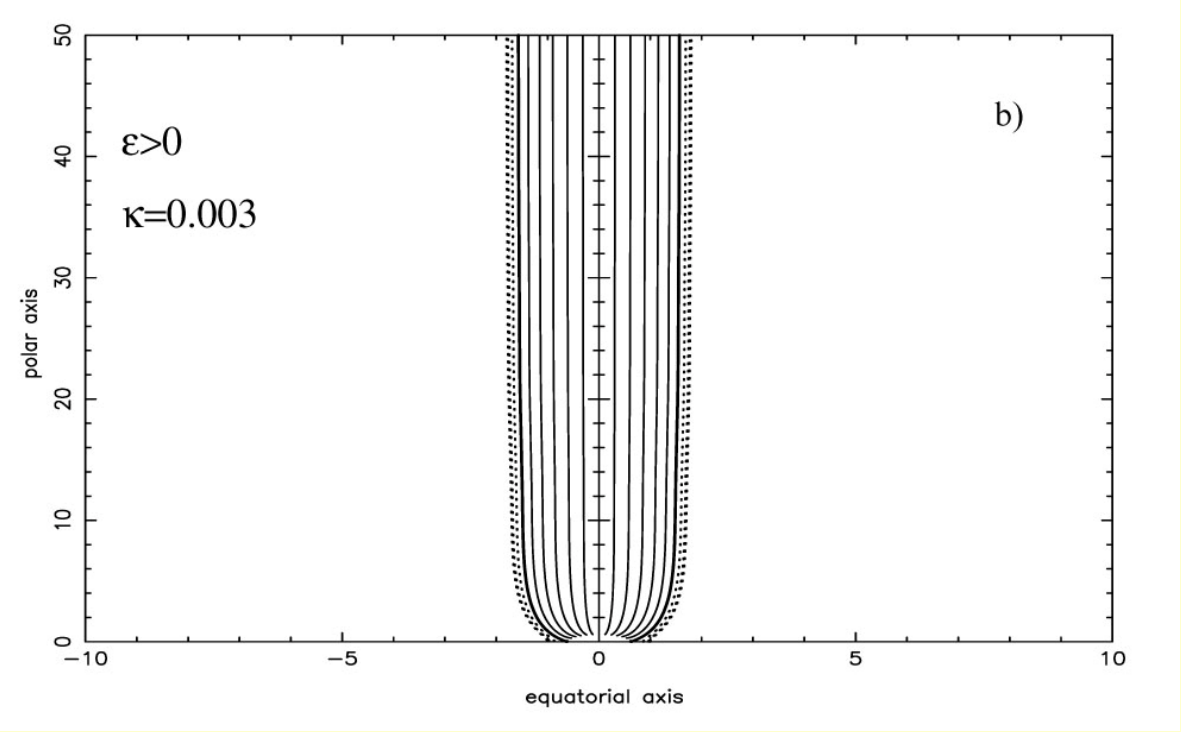

Numerical simulations

MHD jet acceleration studies by numerical means, in 2D axisymmetry:

1. **Considering the disk as a given boundary condition (e.g., Ouyed & Pudritz 1997, Ustyugova et al. 1999, Fendt 2006);**
2. **Producing accretion-ejection flows evolving disk and jet self-consistently (e.g., Casse & Keppens 2002, Kato et al. 2002, Zanni et al. 2007, Tzeferacos et al. 2009)**

Accretion-ejection: initial setup

Self-similar "Keplerian" disk in equilibrium with gravity, thermal pressure gradient and Lorentz force

Disk parameters at $r=r_0$: $\beta = 2P/B^2$, $h = \alpha V_a H \exp[-2(z/H)^2]$

H = **thermal disk heightscale** $=(C_s/\Omega_K)_{z=0}$,

η = **magnetic diffusivity** ("α" **prescription**) (**Rogava and Bodo talks**)

(Shakura & Sunyaev 1973, Ferreira 1997)

Unit of time, r_0 **inner truncation radius:**

$$t_0 = 1.7\left(\frac{M}{M_\Theta}\right)^{-1/2}\left(\frac{r_0}{0.1\,AU}\right)^{3/2} days \quad (YSO)$$

$$= 0.5\left(\frac{M}{10^8 M_\Theta}\right)\left(\frac{r_0}{10\,R_{Schw}}\right)^{3/2} days \quad (AGN)$$

Accretion-ejection: initial setup

Self-similar initial condition for a physical quantity U:

$$U = U_0 \left(\frac{r}{r_0} \right)^{\beta_U} f_U \left(\frac{z}{r} \right)$$

$z=0$ is the disk midplane

• Resistive 2.5D MHD simulations of jet launching. Focus: magnetization

$$\beta = 2P / B^2$$

• From weak (c 1, 2) to strong magnetic fields (c 3, 4), we study the range

$$1/3 \leq \beta \leq 10.0$$

Tzeferacos et al. MNRAS 2009

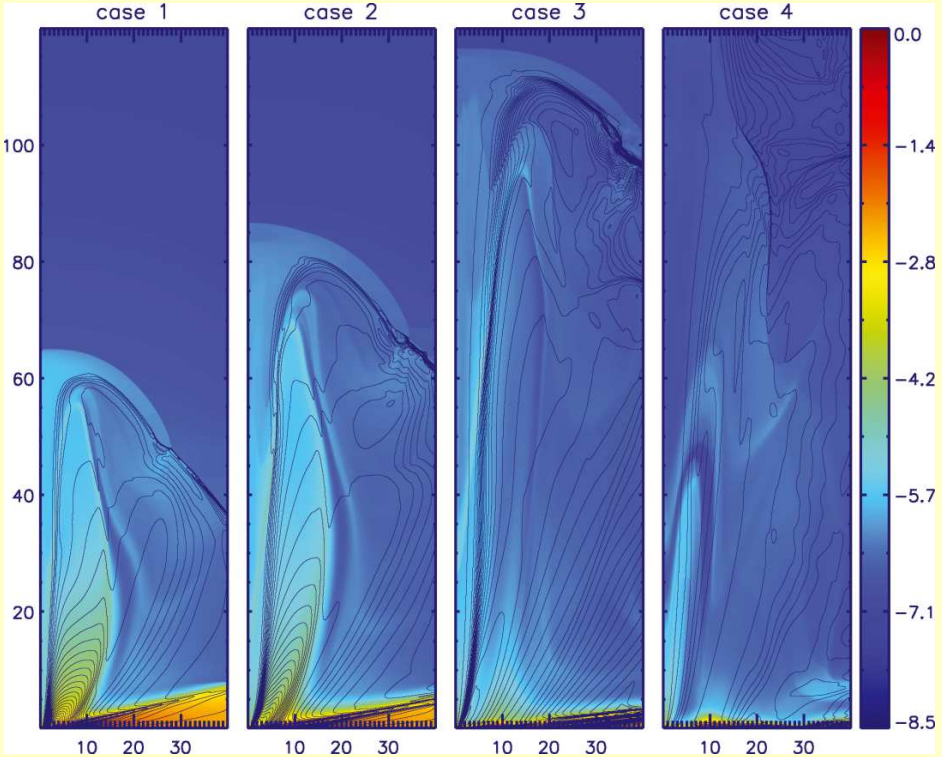

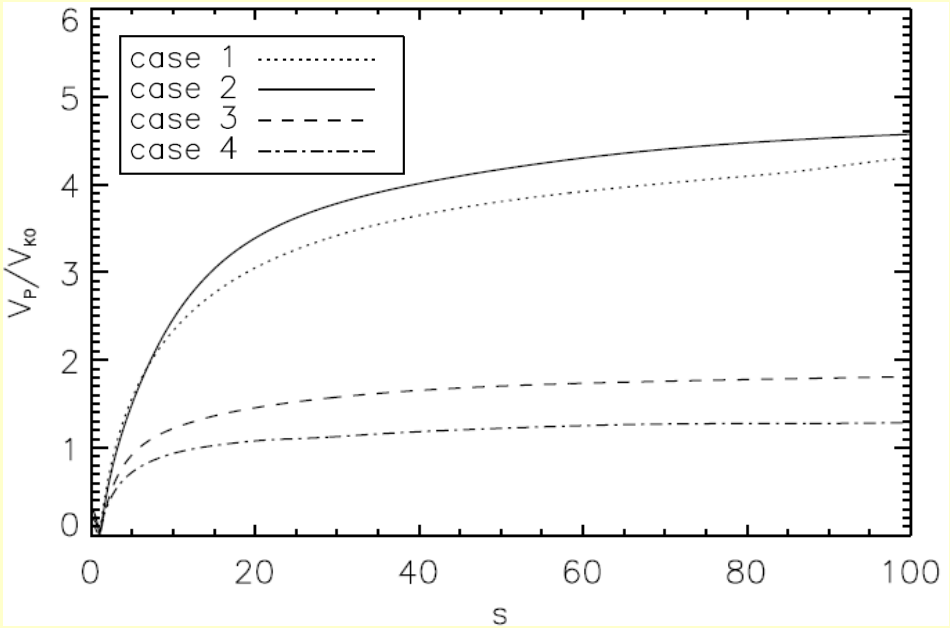

• Self-consistent jet ejection from an accretion disc. Super Alfvènic, super fast magneto-sonic outflows

• Steady state solutions obtained only for above equipartition plasma β (c 1,2)

Initial conditions

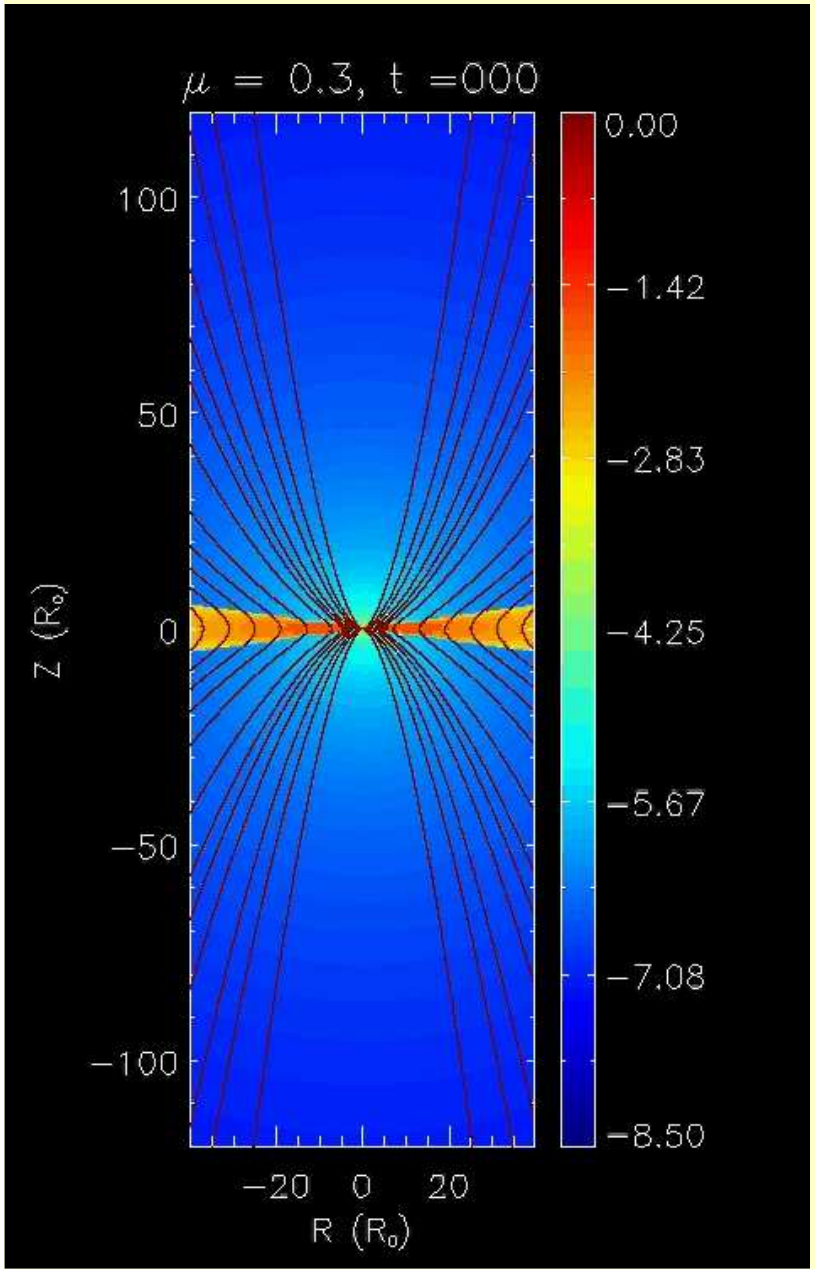

Temporal evolution
Close-up on the ejection region

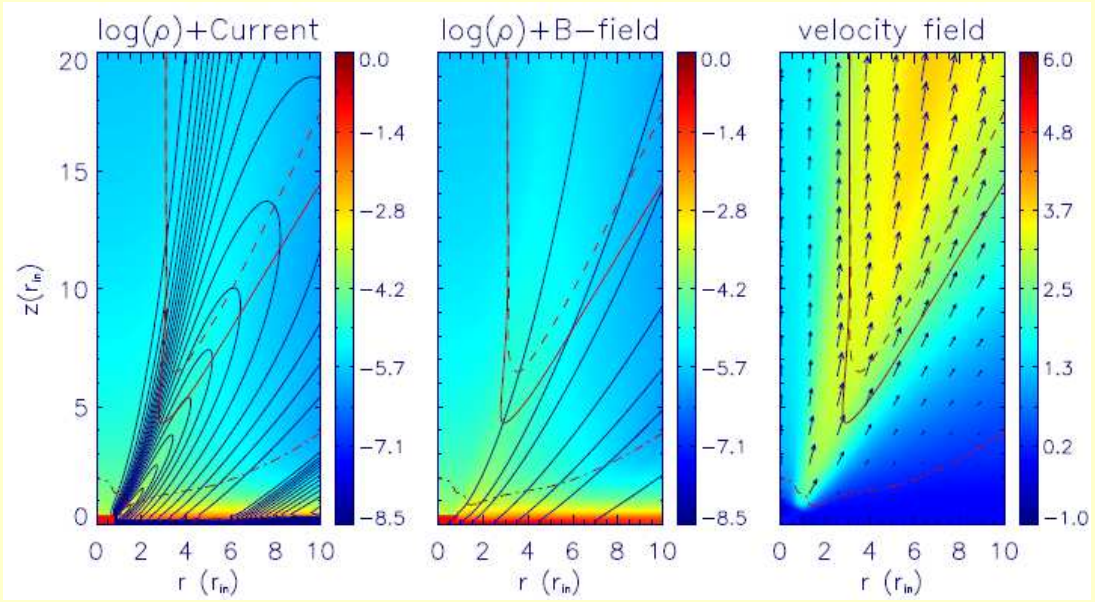

• Viscous and Resistive 2.5D MHD simulations of jet launching.
Focus: Effects of entropy generation due to viscous and Ohmic heating

• Shakura& Sunyaev α prescription for viscosity and resistivity, with a magnetic prandtl number (viscous/ magnetic diffusion rates):

$$P_m = \eta_u / \eta_m \sim 1$$

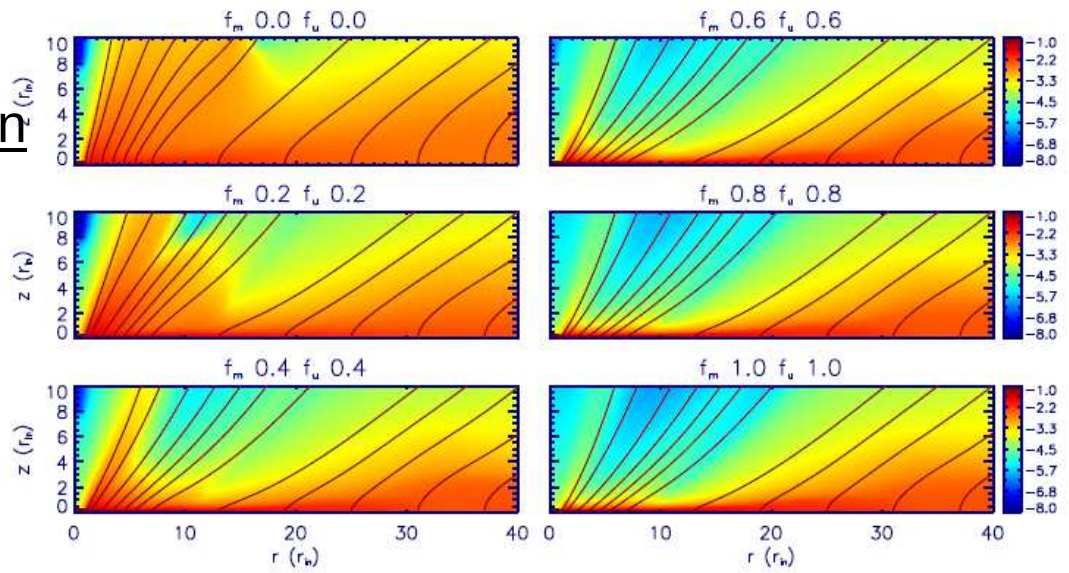

Tzeferacos et al. (TBS to MNRAS)

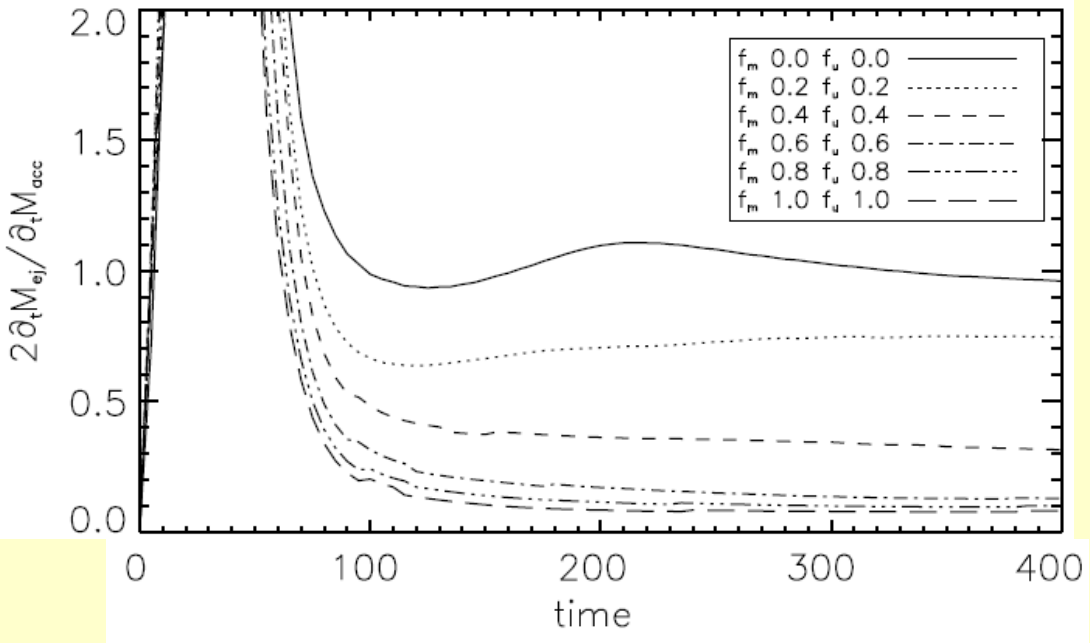

•Strong correlation between disc heating effects and mass loading.

•Efficient acceleration and stationarity is found for mildly warm and cold cases, comparable to slow radio-galaxies and YSO jets

cold

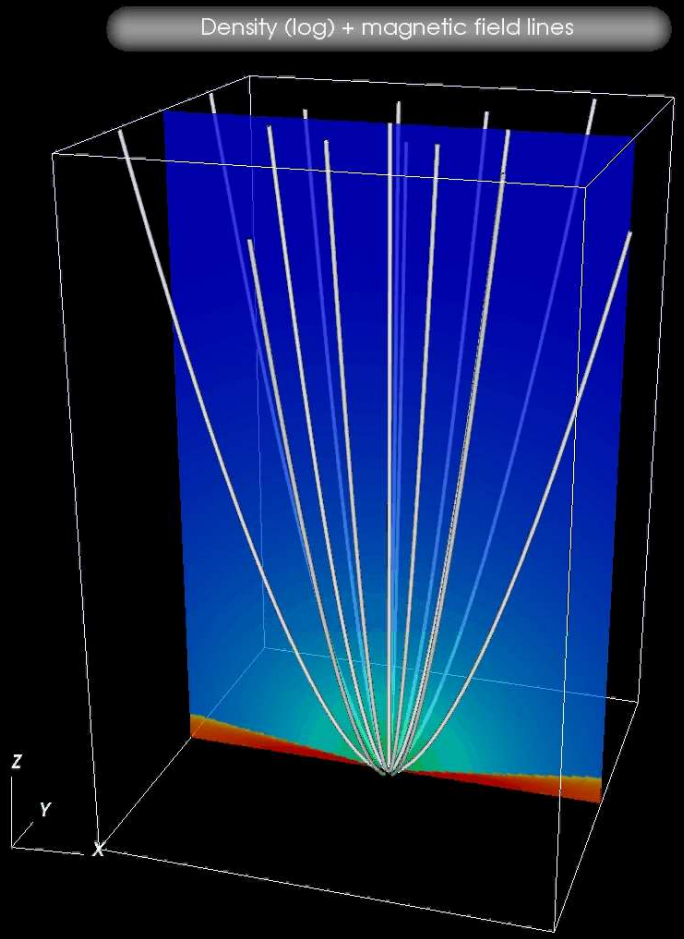
Density (log) + magnetic field lines
Z
Y
X

warm

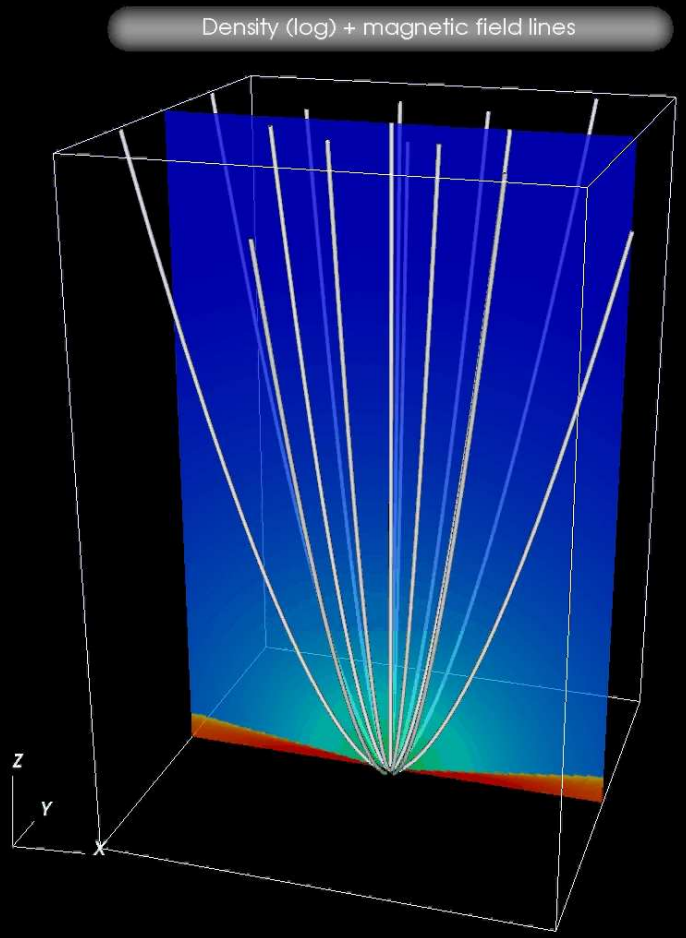
Density (log) + magnetic field lines
Z
Y
X

Conclusions

- AGN jets crucial physical parameters must be indirectly derived from observations
- A fluid description can be reasonably applied to describe the jet phenomenology
- Jet braking and limb-brightening can be intepreted in terms of the evolution of KH instabilities
- Jet power appear to be connected to the accretion power onto the central SMBH $\longrightarrow$ accretion-ejection wind-jet models